DEVELOPMENT OF ENERGY EFFICIENT ELECTRIC DRIVE FOR LOW POWER DRIVE APPLICATION

Thesis

Submitted for the award of
Degree of Doctor of Philosophy
Discipline Electrical Engineering
By

Martand Pratap
Enrollment No: MUIT0117038130

Under the Supervision
of
Dr. Shweta Singh
Assistant Professor
Department of Electrical Engineering,
Maharishi University of Information Technology,
Lucknow

Under the
Maharishi School of Engineering & Technology
Session 2017-2018

Maharishi University of Information Technology
Sitapur Road, P.O. Maharishi Vidya Mandir
Lucknow, 226013
February, 2024

Declaration by the Scholar

I hereby declare that the work presented in this thesis entitled " **DEVELOPMENT OF ENERGY EFFICIENT ELECTRIC DRIVE FOR LOW POWER DRIVE APPLICATION** " in fulfillment of the requirements for the award of Degree of Doctor of Philosophy, submitted in the Maharishi School of Engineering & Technology, Maharishi University of Information Technology, Lucknow is an authentic record of my own research work carried out under the supervision of Dr. Shweta Singh, Assistant Professor, Department of Engineering & Technology. I also declare that the work embodied in the present thesis-

i) is my original work and has not been copied from any journal/ thesis/ book; and
ii) has not been submitted by me for any other Degree or Diploma of any University/ Institution.

Signature of the Scholar

Maharishi University of Information Technology

Lucknow

Supervisor's Certificate

This is to certify that Mr. Martand Pratap has completed the necessary academic turn and the swirl presented by him is a faithful record is a bonafide original work under my guidance and supervision. He has worked on the topic "**DEVELOPMENT OF ENERGY EFFICIENT ELECTRIC DRIVE FOR LOW POWER DRIVE APPLICATION**" under the School of Engineering & Technology, Maharishi University of Information Technology, Lucknow.

Dr. Shweta Singh
Assistant Professor
Department of Electrical Engineering,
Maharishi University of Information Technology,
Lucknow

Date:

ACKNOWLEDGEMENTS

We express our sincere gratitude to Maharishi University of Information Technology, Lucknow for providing the necessary infrastructure and facilities essential for conducting this research. We extend our appreciation to the team at the pharmacy department for their technical assistance and support throughout the experimental procedures.

Our heartfelt thanks go to my supervisor **Dr. Shweta Singh,** Assistant Professor, Department of Electrical Engineering for their valuable contributions to the design and execution of various aspects of this study. Their insights and dedication significantly enriched the project.

We are immensely thankful to the participants and volunteers whose involvement was pivotal in the successful execution of the in vivo experiments. Their cooperation and commitment are greatly appreciated.

We acknowledge the funding support provided by Maharishi University of Information Technology, Lucknow, without which this research would not have been possible. Their financial assistance played a crucial role in facilitating the various stages of this study.

Lastly, we acknowledge the pioneers in the field of herbal medicine whose foundational work continues to inspire and guide our research endeavors.

Martand Pratap

ABSTRACT

Throughout past decade, electric drives have been employed in a variety of applications including industrial, household appliances, medical equipment, and the automobile industry. Machine tools, industrial robots, automated presses, conveyors, elevators, rolling mills, pumps, fans, compressors, electrical vehicles, cranes, the textile sector, and many more uses consume more than two-thirds of all electric energy generated in an industrialised nation. Complicated process and motor control activities are carried out with the assistance of high throughput digital controllers and sub tiny signal processors capable of completing operations per second.

An increase in PWM frequency allows the current and torque control loops to respond faster, improving overall drive performance. In this thesis, the induction motor and BLDC motor drives were examined using different converters such as boost converters, buck boost converters, cuk converters, and SEPIC converters, which were simulated and implemented in hardware prototypes. Matlab/simulink was used to model the boost converter with compound active clamping and FSTPI fed induction motor driving. To reduce the resonance in winding inductance and junction capacitance, the boost converter with compound active clamping supplied IM drive requires an extra diode and inductor. The planned converter was executed with an FSTPI fed induction motor, and results were obtained.

Table of Content

Content Details		Page No.
Title Page		i
Declaration by the Scholar		ii
Certificate by the Supervisor(s)		iii
Acknowledgements		iv
Abstract		v
Table of Content		vi-xi
List of Tables		xii
List of Figures		xiv
Chapter 1	**Introduction**	1-35
1.1	***Introduction***	1-3
1.2	***ADVANTAGES OF ELECTRICAL DRIVES***	3
1.3	***COMPARISON BETWEEN AC AND DC DRIVES***	4-5
	1.3.1 DC DRIVES	4
	1.3.2 AC DRIVES	4-5
1.4	***AC DRIVES – PRINCIPLE OF OPERATION***	5
1.5	***CONTROL OF ELECTRICAL DRIVES***	5-8
	1.5.1 CLOSED LOOP CURRENT LIMIT GOVERNOR	6
	1.5.2 CLOSED LOOP TORQUE GOVERNOR	7
	1.5.3 CLOSED LOOP SPEED GOVERNOR	7-8
1.6	***VECTOR CONTROL***	8-10
1.7	***HARMONIC MITIGATION***	10-11
1.8	***POWER FACTOR CORRECTION***	11-14
1.9	***NEED OF ENERGY EFFICIENT MOTORS & DRIVES***	14
	1.9.1 ELECTRICAL MOTOR DRIVES	16
	1.9.2 ELECTRICAL MOTOR LOSSES	17
	1.9.3 ENERGY EFFICIENT MOTORS	18-20
	1.9.4 FACTORS AFFECTING THE MOTOR EFFICIENCY	20-22
	1.9.4.1 LOAD VARIATION	20
	1.9.4.2 POWER FACTOR	20
	1.9.4.3 EFFECT OF HARMONICS	21
	1.9.4.4 ENERGY EFFICIENCY AND ENVIRONMENT	22
1.10	***ENERGY-EFFICIENCY POLICY OPPORTUNITIES FOR ELECTRIC MOTOR-DRIVEN SYSTEMS***	22-26
1.11	***PERMANENT MAGNET MOTOR DRIVES***	26
1.12	***OPERATION OF BLDC MOTOR***	26-30

1.13	***OBJECTIVES OF THE THESIS***	31
1.14	***ORGANIZATION OF THE THESIS***	31-32
	RFERENCES	33-35
		41
Chapter 2	***LITERATURE REVIEW***	36-81
	RFERENCES	69-81
Chapter 3	***ANALYSIS OF INDUCTION MOTOR DRIVE SYSTEMS***	82-92
3.1	***INDUCTION***	82
3.2	***OPERATION OF INDUCTION MOTOR DRIVE SYSTEM***	82-85
3.3	***BOOST CONVERTER WITH COMPOUND ACTIVE CLAMPING IN FOUR SWITCH THREE PHASE INVERTER FED INDUCTION MOTOR***	85
3.4	***COMPOUND ACTIVE CLAMPING (CAC) BOOST CONVERTER***	86-87
3.5	***SIMULATION RESULTS***	87-92
Chapter 4	***ANALYSIS OF POWER CONVERTERS FOR BLDC DRIVE SYSTEMS***	93
4.1	***INTRODUCTION***	93
4.2	***PFC BUCK-BOOST CONVERTER FED PMBLDC MOTOR***	93-94
4.3	***MATHEMATICAL MODEL OF THE PFC BUCK- BOOST CONVERTER***	94-102
	4.3.1 SIMULATION RESULTS	96-100
	4.3.2 EXPERIMENTAL RESULTS	100-102
4.4	***BRIDGELESS PFC CUK CONVERTER FED PM BLDC MOTOR***	103
	4.4.1 PRINCIPLE OF THE BRIDGELESS CUK CONVERTER TOPOLOGY	104-107
	4.4.2 SIMULATION RESULTS	107-112
	4.4.3 EXPERIMENTAL RESULTS	112-115
4.5	***PFC SEPIC CONVERTER FOR THREE PHASE BLDC MOTOR WITH ELECTRONIC COMMUTATION***	115
	4.5.1 BASIC SEPIC OPERATION	116-122
	4.5.1.1 CONTINUOUS CONDUCTION MODE	117
	4.5.1.2 WHEN SWITCH IS OPENED	119
	4.5.1.3 DISCONTINUOUS CONDUCTION MODE	120-122
	4.5.2 FUZZY LOGIC	122-125

	4.5.2.1 FUZZY LOGIC CONTROL COMPONENTS	122-124
	4.5.2.2 FUZZIFICATION	124
	4.5.2.3 FUZZY INFERENCE	124
	4.5.2.4 DEFUZZIFICATION	125
	4.5.3 PROPOSED FUZZY BASED CONTROLLER IN BLDC MOTOR	126-128
	4.5.3.1.1 MEMBERSHIP FUNCTIONS AND RULE BASE	128-131
	4.5.4 RESULTS AND DISCUSSION	131
	4.5.4.1 CASE 1: BLDC MOTOR UNDER 1500 RPM	132-138
	4.5.4.2 CASE 2: BLDC MOTOR UNDER 2000 RPM	138-145
	4.5.4.3 CASE 3: BLDC MOTOR UNDER 2500 RPM	145-152
	4.5.4.4 CASES 4: BLDC MOTOR UNDER 3000 RPM	152
	4.5.4.5 CASE 5: BLDC MOTOR WITH FUZZY CONTROLLER UNDER DYNAMIC LOAD CONDITIONS	158
Chapter 5	***Conclusion***	168-169
	5.1 CONCLUSION	168
	5.2 SCOPE FOR FUTURE WORK	169

List of Table

Table No.	Table Name	Page No.
TABLE 3.1	Performance Comparison between Existing Converter and Proposed Cac Converter	91
TABLE 4.1	Fuzzy Control Rule Table	129
TABLE 4.2	Comparison between Pi Controller and Fl Controller Based Sepic Converter Fed Bldc Motor	163

List of Figures

Fig No.	Figure Name	Page No.
FIGURE 1.1	Voltage Source Inverter Bldc Drive	26
FIGURE 1.2	Phase Back-EMF and Phase Current	27
FIGURE 3.1	Torque-Speed Curve of Induction Motor	83
FIGURE 3.2	CAC Boost Converter Circuit	85
FIGURE 3.3	Four Switch Three Phase Inverter Fed Induction Motor System with Compound Active Clamping	87
FIGURE 3.4	Power Factor Measurement of Boost Converter with Compound Active Clamping	88
FIGURE 3.5	Driving Pulses for Inverter	89
FIGURE 3.6	Phase Voltage OF Inverter	89
FIGURE 3.7	Output Power vs Efficiency of Boost Converter with Compound Active Clamping FSTPI FED Induction Motor	90
FIGURE 3.8	Output Power vs Efficiency of Soft Switched PFC Boost Converter	90
FIGURE 3.9	THD of Input Current for Boost Converter with Compound Active Clamping FSTPI FED Induction Motor	91
FIGURE 4.1	PFC Buck Boost Converter Topology	94
FIGURE 4.2	Buck-Boost Converter	96
FIGURE 4.3	Closed Loop Speed Control of the PMBLDC Motor with PFC Buck-Boost Converter	97
FIGURE 4.4	Input Voltage and Current Waveforms	97
FIGURE 4.5	Step Change in the Load Torque Applied at T=1 Sec	98
FIGURE 4.6	Speed Response Curve	98
FIGURE 4.7	THD of the Source Current	99
FIGURE 4.8	Top View of the Hardware	100
FIGURE 4.9	Experimental Setup	100
FIGURE 4.10	Voltage and Current Waveforms	101
FIGURE 4.11	Harmonic Spectrum of the Source Voltage	101
FIGURE 4.12	Conventional CUK Topology	104
FIGURE 4.13	Bridgeless CUK Converter Topology	105
FIGURE 4.14	Bridgeless CUK Converter Circuit	107
FIGURE 4.15	Closed Loop Speed Control of the PMBLDC Motor with the Bridgeless PFC CUK Converter	108
FIGURE 4.16	Input Voltage and Current Waveforms	108
FIGURE 4.17	Switching Pulses for the Bridgeless CUK Converter	109
FIGURE 4.18	Step Change in Load Torque Applied at T=1 Sec	110
FIGURE 4.19	Speed Response	110

FIGURE 4.20	FFT Analysis of the Source Current	111
FIGURE 4.21	Experimental Setup	112
FIGURE 4.22	Bridgeless CUK Converter Board	112
FIGURE 4.23	Inverter and BLDC Drive Board	113
FIGURE 4.24	Input Voltage and Input Current Waveforms	113
FIGURE 4.25	Harmonic Spectrum of Source Voltage	114
FIGURE 4.26	Simulink Model of a Sepic Converter	115
FIGURE 4.27	Sepic Converter	116
FIGURE 4.28	Switch on Condition when Switch is Closed	117
FIGURE 4.29	Switch Off Condition	119
FIGURE 4.30	Input Voltage and Input Current Waveforms	120
FIGURE 4.31	Output Voltage and Current Waveforms	120
FIGURE 4.32	FFT Output of Sepic Converter	121
FIGURE 4.33	Fuzzy Logic Controller Operations	122
FIGURE 4.34	Fuzzy Based Proposed Sepic Converter Design with BLDC Motor	126
FIGURE 4.35	Structure of Fuzzy Logic Controller at DC Bus Voltage	126
FIGURE 4.36	Input and Output Membership Functions Of FLC	129
FIGURE 4.37	BLDC Motor Stator Voltage for all the Three Phases for Case 1	132
FIGURE 4.38	BLDC Motor Stator Current for all the Three Phases in Case 1	133
FIGURE 4.39	Electromagnetic Torque of the BLDC Motor For Case 1	134
FIGURE 4.40	Speed of the BLDC Motor for Case 1	134
FIGURE 4.41	DC-Link Voltage of the VSI for Case 1	135
FIGURE 4.42	DC-Link Current of the VSI for Case 1	135
FIGURE 4.43	Source Voltage, Current, Power Factor and Current THD of the AC Source in Case 1	136
FIGURE 4.44	BLDC Motor Stator Voltage for all the Three Phases in Case 2	138
FIGURE 4.45	BLDC Motor Stator Current for all the Three Phases in Case 2	139
FIGURE 4.46	Electromagnetic Torque of the BLDC Motor for Case 2	140
FIGURE 4.47	Speed of the BLDC Motor for Case 2	141
FIGURE 4.48	DC-Link Voltage of the VSI for Case 2	141
FIGURE 4.49	DC-Link Current of the VSI for Case 2	142
FIGURE 4.50	Source Voltage, Current, Power Factor and Current THD of the Ac Source in Case 2	144
FIGURE 4.51	BLDC Motor Stator Voltage for all the Three Phases in Case 3	145

FIGURE 4.52	BLDC Motor Stator Current for all the Three Phases in Case 3	146
FIGURE 4.53	Electromagnetic Torque of the BLDC Motor for Case 3	147
FIGURE 4.54	Speed of the BLDC Motor for Case 3	148
FIGURE 4.55	DC-Link Voltage of the VSI For Case 3	148
FIGURE 4.56	DC-Link Current of the VSI for Case 3	149
FIGURE 4.57	Voltage, Current, Power Factor and Current THD of the AC Source in Case 3	150
FIGURE 4.58	Motor Stator Voltage for all the Three Phases in Case 4	152
FIGURE 4.59	Bldc Motor Stator Current for all the Three Phases in Case 4	153
FIGURE 4.60	Electromagnetic Torque of the BLDC Motor for Case 4	154
FIGURE 4.61	Speed of the BLDC Motor for Case 4	154
FIGURE 4.62	DC-Link Voltage of the VSI for Case 4	155
FIGURE 4.63	DC-Link Current of the VSI For Case 4	156
FIGURE 4.64	Voltage, Current, Power Factor and Current THD of the AC Source in Case 5	156
FIGURE 4.65	BLDC Motor Stator Voltage for all the Three Phases for Case 5	158
FIGURE 4.66	BLDC Motor Stator Current for all the Three Phases for Case 5	159
FIGURE 4.67	Electromagnetic Torque of the BLDC Motor for Case 5	160
FIGURE 4.68	Speed of the BLDC Motor for Case 5	161
FIGURE 4.69	DC-Link Voltage of the VSI for Case 5	161
FIGURE 4.70	DC-Link Current of the VSI for Case 5	162
FIGURE 4.71	Hardware Prototype	166
FIGURE 4.72 (A) & (B)	Current and Voltage of the BLDC Motor	167
FIGURE 4.73 (A) & (B)	DC-Link Voltage and Transient Voltage Waveform	167
FIGURE 4.74	A) SOURCE CURRENT INDUCTOR CURRENT, B) SOURCE VOLTAGE AND CURRENT	167
FIGURE 4.75	PWM Pulses	168

CHAPTER 1
INTRODUCTION

1.1 INTRODUCTION

Throughout the past decade, electric drives have been employed in a variety of applications including industrial, household appliances, medical equipment, and the automobile industry. Machine tools, industrial robots, automated presses, conveyors, elevators, rolling mills, pumps, fans, compressors, electrical vehicles, cranes, the textile sector, and many more uses consume more than two-thirds of all electric energy generated in an industrialised nation. Complicated process and motor control activities are carried out with the assistance of high throughput digital controllers and sub tiny signal processors capable of completing operations per second. An increase in PWM frequency allows the current and torque control loops to respond faster, improving overall drive performance.

An electric motor is described as a device that converts electrical energy into mechanical energy. The electric motor may also transport energy from a power source to a mechanical load. The drive, also known as the electric drive or motor drive, is the device that houses the motor and causes it to spin. The role of the motor drive, which is to extract electrical energy from an electrical source and provide it to the motor, achieves the necessary mechanical output. This is commonly referred to as the motor's speed, torque, and shaft position.

The advancement of strong digital microcontrollers enables full-digital control of electromechanical adaption processes in an electrical drive. Automation made great advances in this process in the 1950s, owing

to the development of Numerical Control (NC). While either flexible or entirely programmable, NC systems have mostly replaced the mechanical timers that were ubiquitous in the industry in the early part of the twentieth century. Because the first dependable and commercially accessible microcontrollers were developed in the 1960s, they were widely employed for the flexible control of electric drives in low-power applications.

Electric drives are currently replacing electrical motors at a rate of 15% each year in an industrialised country. More than 20% of the drives are frequency regulated, whereas the other 80% are constant speed. For varied uses, all industrial, commercial, and other units rely on electrical motors. According to the Electric Power Research Institute (EPRI), motors use 51% of total global energy consumption. Some industries require far less energy. Lighting, for example, contributes for 19%, heating and cooling systems account for 16%, and information technology accounts for 14%. Therefore, there is a need for an efficient and durable controller for motor control, which will result in energy savings.

Electric motors have an impact on practically every element of modern life. Electric motors are used in refrigerators, vacuum cleaners, elevators, air conditioners, washing machines, fans, computer hard disc drives, and industrial operations. In reality, motors consume the majority of energy, regardless of whether the application is domestic, industrial, or commercial. The energy efficiency of a motor is determined by its kind. Some are designed to be more energy efficient than others. In addition, the recent fast growth of motor drives in the vehicle sector with the introduction of new hybrid technologies has produced a significant need for highly efficient variable speed motor drives.

Induction motors are the industry's true workhorses. Because of their inexpensive cost, sturdy construction, and simple control gear, squirrel cage induction motors are employed in the majority of constant speed applications. When one or more of the following considerations are complicated, a wound rotor induction motor is utilised.

1. High starting torque
2. Low starting current
3. Speed control over a limited range

In the case of a constant speed application Everyone can benefit from a synchronous motor. Many adjustable speed drives require accurate and continuous speed control with long-term stability, high transient performance, and improved efficiency. Traditional DC motors are easy to build, have a high linear torque-speed characteristic, and are efficient, but they require periodic maintenance and replacement due to the existence of a commutator and brushes. This restricts the use of direct current motors in commercial applications. Moreover, the supplied torque to motor size ratio is weak, limiting its use in areas where space and weight are critical, particularly in electric cars and aerospace applications. As a result, Brushless DC (BLDC) motors have emerged as a superior alternative to traditional DC motors.

1.2 ADVANTAGES OF ELECTRICAL DRIVES

The advantages are:

1. These drives can be used to manage torque, speed, and power.
2. The controls on these drives are easy to use.
3. Although it is not rational for various prime movers, they are capable of governing in all four quadrants of the speed-torque plane.
4. They do not pollute the environment.

As a result, the above-mentioned advantages of electrical drives are gaining traction and being used on a larger scale.

1.3 COMPARISON BETWEEN AC AND DC DRIVES

AC and DC drives have distinct benefits and features that make them ideal for specific applications.

1.3.1 DC DRIVES

- Normally, DC drives are usable for all power levels.
- Variable speed machines can be powered by DC motors.
- Cooling blowers, intake air flanges, and modules for rising feedback tachometers are examples of DC driving uses.
- Maintenance is reduced when the commutator and brushes are properly applied.
- DC drives are effective in producing the desired torque.

1.3.2 AC DRIVES

- They are ordinary and inexpensive.
- AC motors require no operations and are ideal for drives when the motor is located in an area that is difficult to reach for maintenance or rearrangement.
- AC motors are slightly more frequent, smaller, and less costly than DC motors.
- AC motors are preferable for higher speed functions (i.e., over 2500 rpm) since there are no brushes and commutation is not a problem.
- Several motors in a system must operate at the same frequency / speed.

- It is preferable to use a fixed speed AC motor that is already linked and hooked into a machine.
- Brushes and commutators in DC motors may degrade if used rapidly below this condition.
- A low-cost electronic motor reversal system is required.
- It is critical to create a backup in case the controller fails.

1.4 AC DRIVES – PRINCIPLE OF OPERATION

AC motor drive controllers with variable frequencies are typically easier to operate than DC controllers. To comprehend the working concept of this drive action, three components must be considered: the rectifier, the DC bus, and the inverter unit. The supply potential is applied to the rectifier unit, which converts the alternating supply to a DC supply; the alternating supply is applied to the full wave diode bridge converter. The harmonics created during power conversion are filtered at the DC bus. The constant DC supply is sent into the inverter unit, which converts the DC supply to alternating current.

The AC motor's simple design and inexpensive cost make it appropriate for necessary speed with the assistance of a variable frequency controller, which creates an incredibly high advantage for this drive.

1.5 CONTROL OF ELECTRICAL DRIVES

In general, three types of tasks must be completed: beginning, speed governor, and braking, all of which are mostly accomplished by electrical motors. As a result, it attests to the supremacy of motor in all aspects. Control and monitoring of various parameters using a variety of approaches are required for overall drive control (Leonhard W (2001) (Crowder R. (2006).

There are two types of control structures: open loop and closed loop control systems. In an open loop governing network, the response has no effect on the source, implying that the controlling event is self-governing of the output. The closed loop system is more better and methodical. At this point, the productivity is returned to the contribution terminal, which determines the amount of input to the system. For example, if the output is minimised more than the preset charge, the input is reduced, and vice versa. Closed loop governors of AC drives, such as current governors, torque governors, and speed governors, as explained in sections 1.5.1 to 1.5.3, will suffice to meet the specified requirements (Schröder D. (2007).

Protection: At increased speed, its reaction achieves greater steady-state accuracy. In the following sections, a distinct closed loop architecture is used for electrical drives, regardless of whether the contribution is DC or AC.

1.5.1 CLOSED LOOP CURRENT LIMIT GOVERNOR

Fig.1.1 depicts the current limit control block diagram. It is examined to ensure that preventive estimations are not overlooked. As a result, there is a possibility of huge current flows across the motor route. The current frontier controller is located in order to connect the current and perception of current to a motor. The feedback loop has no effect on the regular driving performance. But, if the current exceeds the predetermined limit, the feedback loop is activated, causing the current to fall below the safe level.

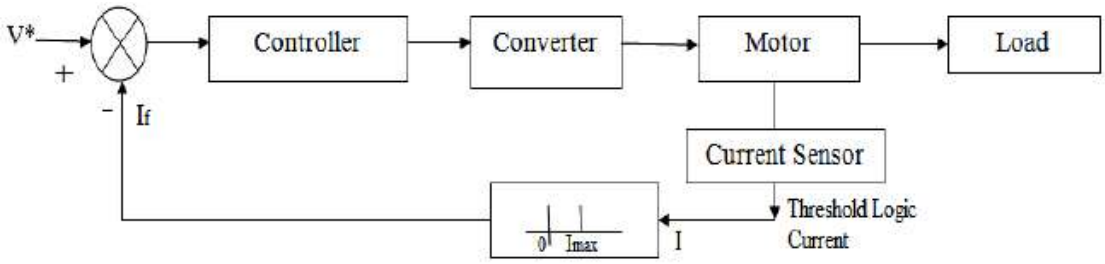

FIG. 1.1 CURRENT LIMIT GOVERNOR

1.5.2 CLOSED LOOP TORQUE GOVERNOR

This sort of torque regulator is commonly used in battery-powered vehicles such as trains and automobiles. The operator compacts the accelerator in the car to locate the indicated torque 'T'. As shown in Fig. 1.2, the actual torque T exceeds the prescribed torque T*, which is disallowed by the operator through accelerator.

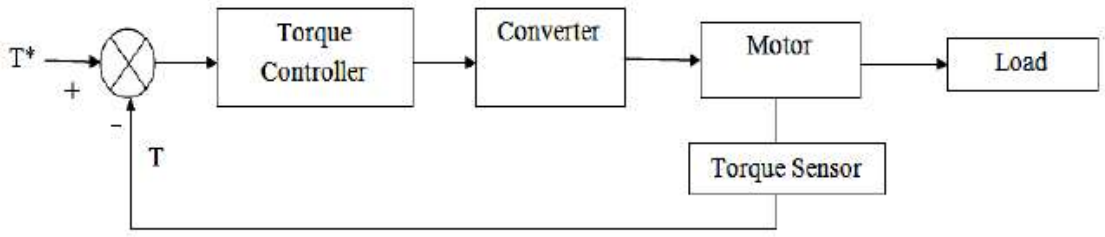

FIG. 1.2 CLOSED LOOP TORQUE GOVERNOR

1.5.3 CLOSED LOOP SPEED GOVERNOR

Speed control loops are most likely employed as drive feedback loops. Fig. 1.3 depicts a closed loop speed governor. Internal and outside loops are the two capable control loops. The inner control loop keeps the converter and motor current or torque within safe limits. Now we can read the control loop portion and drive with appropriate examples. Assuming the indicated speed m* increases and a constructive error m is produced, indicating that the momentum must be improved.

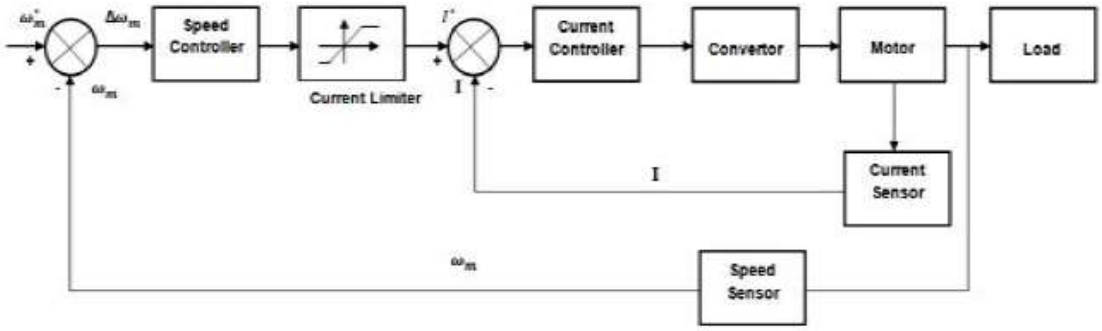

FIG. 1.3 CLOSED LOOP SPEED GOVERNOR

The internal loop will now keep it below the maximum allowable current. The motorist then accelerates. As a result, throughout speed control, the purpose passes from driving to braking and back again, subjecting the motor to heat and sprinting.

Loop closure Control methods are more expensive economically, can improve by reducing loss, and occasionally feedback causes the system to oscillate, resulting in an oscillating response. Vector control is favoured to compensate for all of these limitations since it has good speed regulation, achieves maximum torque at zero speed, is highly responsive, easy to modify, and has a better level of safety.

1.6 VECTOR CONTROL

AC drives have typically been defined using a scalar scheme measured in volts per hertz (V/Hz), in which the drive maintains a constant voltage to frequency ratio in order to provide consistent torque. Nevertheless, the V/Hz organise system does not provide rigid speed regulation and is restricted in its ability to generate torque at low speeds. Vector control, on the other hand, provides for more precise control of speed or torque and is fast gaining ground on V/Hz control in the vast majority of basic AC motor products.

Vector control is a Variable-Frequency Drive (VFD) control in which the stator currents of a three-phase motor are divided into two orthogonal components, one magnetic flux and the other torque, and evaluated using a vector. The drive's control system computes the flux and torque references provided by the drive's speed control. PI controllers are typically used to keep the deliberate current mechanism at its reference values. The adjustable-frequency drive's pulse-width modulation depicts the transistor consistently switching on to the stator voltage input, which is the output of PI controllers. It is sometimes referred to as Field Oriented Control (FOC).

FOC is used to control synchronous and induction motors. FOC was created to provide better motor appliances that are required to regulate over the rated speed, produce full torque while beginning, and have high energetic function including acceleration and deceleration. While the research of AC drive restraint might be technologically justifiable, such investigation generally begins with modelling of the drive motor circuit in question.

Vector control generates a three-phase PWM motor voltage. The production derivative of a composite potential vector is used to regulate a complex current vector generated by the 3-phase stator current excitation of a motor via back and forth rotations and arrangement to synchronise a time invariant system. Such a multidimensional stator current interval vector may be defined in a coordinate structure with right angle components along the direct and quadrature axes, with the field flux linkage constituent of current along the direct axis and the torque component along the quadrature axis. The asynchronous motor

synchronize system can superimpose to the motors instantaneous (a,b,c) three phase sinusoidal system (Bhim Singh 2005),(R.A. Guptha (2008).

There are two vector direct techniques: direct vector control (DFOC) and indirect vector control (IVC) (IFOC). DFOC considers flux magnitude and feedback signal angles directly utilising potential or current. IFOC is more commonly utilised since, in closed loop form, such drives work more simply to velocity ranges ranging from zero momentum to high speed field-weakening. In IFOC, the flux space angle feed forward and flux magnitude signals are used to compute stator currents and rotor velocity before calculating the flux space angle appropriate by summing the rotor angle due to the rotor velocity and the considered reference value of slip angle corresponding to the slip frequency. The current in the stator windings of an alternating current motor has two components: the direct axis magnetising current (id) and the torque-producing quadrature axis current (iq). The magnetising current is 90 degrees behind the voltage, whereas the torque-producing current is in phase with the potential. A vector drive may guide the two currents autonomously after identifying this link. Decoupling the magnetising currents and torque allows for independent torque control. Closed loop vector control is required in processes where errors must be eliminated, such as converting manufacturing.

1.7 HARMONIC MITIGATION

While harmonics are present in the power system, a closed loop monitors the protection in order to improve the reaction speed and steady-state precision of the electrical drive. Since harmonic distortion is still beneficial, its amount is limited. Harmonics are formed under successive loads, which might be dangerous if not analysed, predicted, and regulated. Thyristors are switching devices that are utilised in many applications in

converter circuits to reduce harmonics. According to IEEE Standard 519-1992 advice, discrete harmonic distortion is less than 3% and THD is less than 5% of standard component which allows harmonic acceptance (IEEE) (1992). Additionally, the ripples on the DC side of the AC-DC converter are decreased by filter circuits, and the phase shifting approach is employed to remove harmonics. This technology is known as pulse mitigation, and it is utilised for DC side ripple mitigation, which is being examined and researched.

The harmonic wrap produced by a conventional triple line 6-pulse rectifier study is about 31.1%, however it does not comply with IEEE requirements (IEEE Proceedings 2001, Gary L. Skibinski 2003). Additionally, a 12-pulse rectifier was explored and inspection revealed THD of 15.3% (B. Singh, G. Bhuvaneswari, and V. Garg, 2006) and arranged a vintage opportunity to be used where the grid is expected to perform successfully by lowering harmonic percentage.

For a rectifier to be used without an AC side filter and a DC side filter to reduce THD below the IEEE Standard 519-1992 recommendation and DC ripple below a specific value, a privileged pulse rectifier is required, and additional analysis is required using 18-pulse and 24-pulse phase changing rectifiers.

1.8 POWER FACTOR CORRECTION

Power factor is the most important metric in power electronics since it indicates how effective the system's real power use is. It also represents a measure of line voltage and current distortion, as well as the phase shift between them. In an alternating current circuit, the Power Factor (PF) is defined as the ratio of real power to apparent power, as shown in Eq. 1.1.

Nevertheless, due to the non-linear behaviour of active switching power devices in power electronic systems, the phase-angle description alone is not acceptable. The non-linear load draws typical distorted line current from the line, as shown in Figure 1.4(a).

$$\text{Power factor} = \frac{Real\ Power\ (P)}{Apparent\ Power\ (S)} = \frac{P}{VI} \qquad (1.1)$$

When the load in a linear system draws entirely sinusoidal current and voltage, the PF becomes the cosine of the phase angle between the current and voltage, as shown in eq. 1.2.

$$\text{Power factor} = \frac{\text{Vrms Irms Cos}\phi}{\text{Vrms Irms}} = \text{Cos}\phi \qquad (1.2)$$

$$I = \frac{P}{V \cos\phi} \qquad (1.3)$$

Calculating PF for distorted waveforms is more difficult than for sinusoidal waveforms. The power factor is enhanced by lowering the reactive power and decreasing the power factor angle, as illustrated in Fig. 1.4. (b).

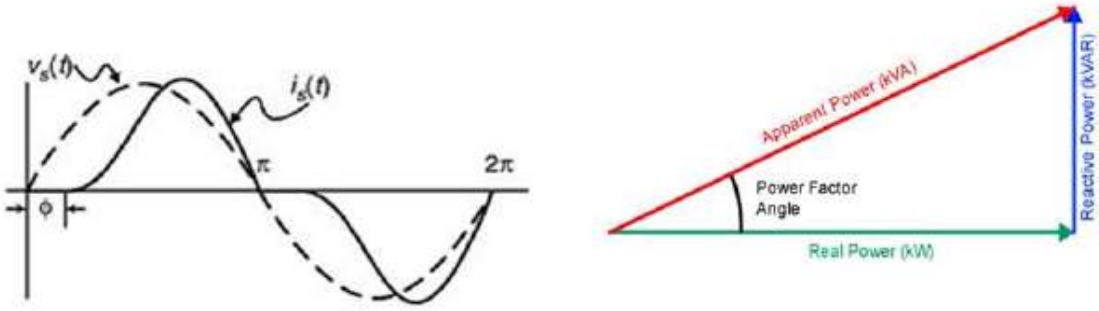

FIG. 1.4 (A) VOLTAGE AND DISTORTED LINE CURRENT WAVE FORM & (B) POWER TRIANGLE

As shown in equation 1.3, for a given power P, the current I taken by the load changes inversely with the load power factor. As a result, a given load draws more current with a low power factor, increasing copper losses and lowering system efficiency. Three-phase induction motors, transformers, and lighting are the loads responsible for the low PF. The active kind of power factor correction circuit depicted in Fig. 1.5 is used to increase the power factor by modifying the waveform of current taken by a load. Active PFCs include synchronous condenser, buck, boost, and buck-boost converters.

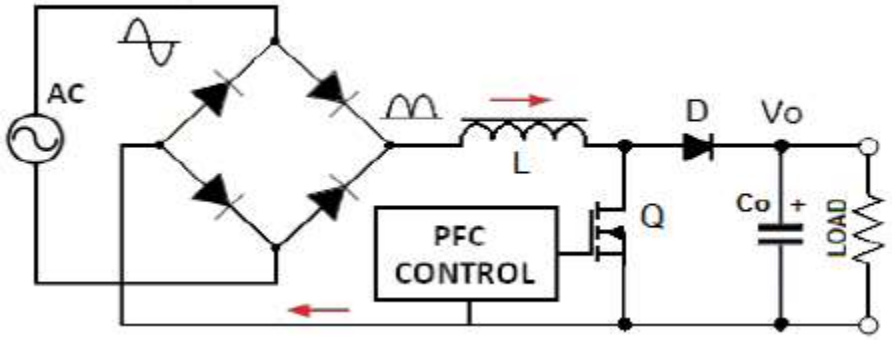

FIG. 1.5 PFC CIRCUIT

A perfect Power Factor Correction (PFC) would be one that follows a resistor on the source side while maintaining a sufficiently synchronised response potential difference. The converter must obtain a sinusoidal current from the service in the case of sinusoidal phase voltage. The primary goal of the PFC procedure is to reduce reactive power and get the power factor closer to one. In this case, the low power factor is caused by inductive loads, which may be remedied by inserting electrical devices such as capacitors into the circuit. Commercially, there are several PFC machines available to collect different types of conditions. Fixed PFC is used when the power factor is low and no single piece of equipment is solely responsible (A. Consoli, 2001, Reinert J, Schroder S. (2002). In this state, the PFC capacitors and capacitor bank terminals are connected to

each three phase wire for power factor correction. At this time, PFC can be connected to the switchgear. Yet, there are other circumstances in which PFC is not so straightforward. When various machines switch on and off repeatedly, the power factor may be modified to account for the changes in the system. In these circumstances, the requisite PFC capacitors must be mechanically regulated, that is, the banks of capacitors must be correctly switched in and out of the power network. To stimulate which form of sluggish power converter is most recommended for a given application, several problems, such as robustness, power compactness, effectiveness, price, and difficulty, must be in use to the point. Under this subject, several converter topologies such as buck, boost, and cuk converter topologies have been proposed in recent years (Najmeh Zamani; 2914-Saijun Zhang; 2014) with the goal of improving the individuality of standard converters used for power factor.

The contemporary power factor correction process with PWM rectifier and Buck- Boost converter is commonly advised to give compensated currents similar to harmonic currents formed by nonlinear loads. These results reduce the filter's value, and no specific dedicated power devices are required for harmonic mitigation. A PI control is used to follow the necessary line current instruction, displaying the single-phase diode rectifier coupled with these converters, which is widely used in active PFC. In addition to the geometric properties mentioned above, the buck-boost topology is too basic and accepts low-distorted source currents with about unity power factor using multiple dedicated governor procedures such as hysteresis control and PI control techniques.

1.9 NEED OF ENERGY EFFICIENT MOTORS & DRIVES

Electric motors have an impact on practically every element of modern life. Electric motors are used in refrigerators, vacuum cleaners, air conditioners, fans, computer hard drives, automated automobile windows, and a variety of other household goods and gadgets to transform electrical energy into useable mechanical energy. Electric motors are responsible for a major amount of industrial activities in addition to driving household gadgets. Electric motors are employed at some stage in the production process of practically every imaginable product manufactured in modern factories. Because electric motors have a practically limitless variety of uses, it is easy to conceive that there are millions of motors of various sizes in operation across the world. Because of the quantity of electricity they use, this massive number of motors and motor drives has a huge influence on the planet.

Before, the systems that controlled electric motors had extremely poor performance, were inefficient, and were highly costly. The quest for higher performance and precision in electric motors, along with the development of superior solid-state electronics and low-cost microprocessors, has resulted in the development of contemporary adjustable speed drives in recent decades. A variable speed drive is a system that consists of an electric motor and the system that drives and regulates it. The power source, the power electronic converter, the electric motor, the controller, and the mechanical load are all different components in any adjustable speed drive.

The power supply can deliver electricity in the form of alternating current (AC) or direct current (DC) at any voltage level. The power electronic converter serves as the link between the power supply and the motor. Almost every form of power source may be utilised with practically

any type of electric motor thanks to this interface. The controller is the circuit that controls the motor output. This is performed by adjusting the frequency, voltage, or current provided to the motor by changing the functioning of the power electronic converter. The controller might be as basic as a relay or as complicated as a microprocessor. The mechanical load is the mechanical system that demands the motor drive's energy. The mechanical load can be fan blades, an air conditioner compressor, conveyor belt rollers, or almost anything else that can be powered by the cyclical motion of a rotating shaft.

1.9.1 ELECTRICAL MOTOR DRIVES

Electric drive systems have improved dramatically as a result of improvements in power electronics, control electronics, microprocessors, microcontrollers, and digital signal processors (DSPs). Power electronic drives are more dependable, efficient, and cost-effective. In reality, a power electronic drive system uses 25% less energy than a traditional motor drive system. Advances in solid-state technology enable the development of power electronic converters for electric drive systems. Motors may now be employed in more accurate applications thanks to power electronic devices. These systems may incorporate extremely accurate speed or position control. Systems that were previously operated pneumatically and hydraulically can now also be controlled electrically.

To improve performance, efficiency, and precision, more modern electric motor drives are now replacing earlier motor drives. Because advanced electric motor drives employ more complex microprocessor or DSP controllers to monitor and regulate motor output, they are more precise. They also provide greater efficiency by employing more efficient converter topologies and electric motors. Modern drives also provide a

performance improvement by adopting improved switching strategies to produce greater output power while using lighter motors and smaller electronics.

1.9.2 ELECTRICAL MOTOR LOSSES

Motor efficiency may be improved by lowering losses. Motor energy losses are classified into several categories, each of which is impacted by the motor's design and construction. The size of the air gap between the rotor and the stator is one design factor. Wide air gaps tend to optimise efficiency at the price of power factor, whereas tiny air gaps marginally reduce efficiency while enhancing power factor greatly. A motor's efficiency is dictated by intrinsic losses, which can only be lowered by modifications in motor design. Intrinsic losses are classified into two types: fixed losses that are independent of motor load and variable losses that are depending on load. Magnetic core losses, as well as friction and windage losses, are examples of fixed losses. Magnetic core losses (also known as iron losses) are eddy current and hysteresis losses in the stator. They differ depending on the core material and shape, as well as the input voltage. Friction and windage losses are created by friction in the motor's bearings, as well as aerodynamic losses from the ventilation fan and other moving elements.

Variable losses include resistance losses in the stator and rotor, as well as stray losses. Variable losses are affected by motor load. Resistance to current flow in the stator and rotor generates heat in proportion to the material resistance and the square of the current (I2R). Where R is the stator winding resistance for stator resistance loss and may be utilised as rotor winding resistance for rotor resistance loss.

Stray losses can occur from a number of causes and are difficult to detect or quantify accurately, although they are normally proportional to the square of the rotor current. No load losses, such as core losses and friction and windage losses, account for approximately 15% of the overall losses that occur in the motor while it is loaded. A motor's part-load performance characteristics are also affected by its design. Under low loads, both and PF collapse to very low values.

1.9.3 ENERGY EFFICIENT MOTORS

Electric motors are critical in both the industrial and agricultural sectors. These motors were used in both constant speed drives with extremely low ratings and variable speed drives with very high ratings. Energy efficiency and energy conservation are inextricably linked. With increased energy consumption and uncertainty in oil supply and changing prices of traditional fuels, energy efficiency and conservation has become an essential part of industrial and rural growth. Induction motors used for irrigation in the rural sector and industrial purposes in the urban sector require a significant quantity of electrical energy. Agriculture and industry are quickly rising in countries such as India, as is electrical energy usage. According to one estimate, a 5% increase in induction motor overall efficiency would save enough energy to equal the energy produced by a new power plant of a few hundred megawatts.

Energy-efficient motors integrate design modifications designed to maximise operational efficiency over standard-design motors. The goal of design enhancements is to reduce intrinsic motor losses. Improvements include the use of lower-loss silicon steel, a longer core (to increase active material), thicker wires (to reduce resistance), thinner laminations, a smaller air gap between stator and rotor, copper bars in the rotor instead of aluminium bars, superior bearings, and a smaller fan, among other things.

Energy-efficient motors, which are currently available in India, have efficiencies that are 3 to 4 percentage points greater than normal motors.

The resistance will be reduced if the copper conductor size is chosen correctly. Lowering motor current is easiest done by lowering the magnetising component of current. Lowering the operational flux density and maybe decreasing the air gap are involved. The rotor I2 R losses are determined by the rotor conductors (often aluminium) and the rotor slip. The use of copper conductors reduces winding resistance. Moving the motor closer to synchronous speed reduces rotor I2 R losses. Core losses are those observed in stator-rotor magnetic steel and are caused by hysterisis and eddy current effects during core material magnetisation at 50 Hz. These losses are load independent and account for 20 to 25% of overall losses. The hysterisis losses, which are proportional to the flux density, have to be decreased by using silicon steel laminations of low loss grade. The flux density is reduced by increasing the core length of the stator and rotor. Circulating current within the core steel laminations causes eddy current losses. Thinner laminations help to decrease this.

Friction and windage losses account for 8 to 12% of overall losses and are caused by bearing friction, windage, and circulating air through the motor. These losses are unaffected by load. Windage losses decrease as fan diameter increases, resulting in lower windage losses. Stray load losses, which account for 4 to 5% of overall losses, fluctuate with the square of the load current and are generated by leakage flux driven by load currents in the laminations. These losses are minimised by selecting slot numbers, tooth/slot geometry, and air gap with care.

Energy efficient motors are available in a wide variety of grades, with full load efficiencies increasing by 3 to 7%. The mounting dimensions are also kept the same to allow for easy replacement. The prices of energy-efficient motors are greater than those of normal motors due to the changes made to increase performance. The extra cost is generally quickly repaid in lower operating expenses, especially in new applications or motor replacements.

1.9.4 FACTORS AFFECTING THE MOTOR EFFICIENCY

1.9.4.1 LOAD VARIATION

Most electric motors are intended to operate at 50% to 100% of rated load, with maximum efficiency often reached near 75% of rated load. Hence, a 10-hp motor has a load range of 5 to 10 hp and a maximum efficiency of 7.5 hp. The efficiency of a motor drops substantially below around 50% of the rated load. Nevertheless, the efficiency range varies with particular motors and tends to be wider with bigger motors. A motor is called underloaded when its efficiency decreases dramatically with decreasing load.

Motor overloading can reduce efficiency. Many motors include a service factor that allows for short-term overloading.

1.9.4.2 POWER FACTOR

Power factor is an essential aspect of AC induction motor efficiency. The magnitude of the active current decreases as the load on the motor decreases. Nevertheless, there is no commensurate drop in magnetising current, which is proportional to supply voltage, resulting in a decrease in motor power factor with a decrease in applied load. Induction motors, particularly those operating at less than their stated capacity, are the

primary cause of poor power factor in electric systems. Motors, like other inductive loads, have power factors that are less than one. As a result, the total current draw required to supply the same actual power is more than that required for a load with a higher PF. Since resistance losses in wiring upstream of the motor are proportional to the square of the current, running with a PF less than one has a significant impact. Consequently, for optimal overall plant functioning, a high PF value near to unity is desirable.

1.9.4.3 EFFECT OF HARMONICS

Harmonics are alternating current voltages and currents whose frequencies are integer multiples of the fundamental frequency. Harmonics were not common in most businesses before owing to balanced linear loads employing three phase induction motors coupled with incandescent lights, resistivity, and so on, but the fast growth of power electronics in industrial applications has made industrial loads non-linear type. Non-sinusoidal current is drawn by these non-linear loads from the sinusoidal voltage waveform. Harmonic disorders are the distortions produced in the voltage and current waveforms as a result of the sinusoidal waveforms.

Harmonics are produced when the number of non-linear loads increases. When the system voltage is linear but the load is non-linear, the current becomes distorted and non-sinusoidal. At the fundamental frequency, the real current will become greater than the current recorded by an ammeter or any other measuring equipment. When the supply system contains harmonics and the voltage is already distorted, the linear loads will respond to such voltage harmonics by drawing harmonic currents against each harmonic in the system and generating the corresponding order of current harmonics. When the system voltage and loads are both non-linear (a more typical circumstance), the voltage harmonics amplify

and new harmonics are formed, corresponding to the load's non-linearity, further distorting an already distorted voltage waveform.

1.9.4.4 ENERGY EFFICIENCY AND ENVIRONMENT

It is commonly understood that the environment and efficiency are inextricably intertwined. Electric drive systems account for the vast majority of power use. As a result, an increase in motor efficiency will result in significant energy savings and a reduction in CO2 emissions into our environment. Throughout the years, machine designers have done their utmost to address the requirement for enhanced induction motor efficiency. The real push for the advancement of greater efficiency motors is the need to save the environment by reducing energy consumption. Energy efficiency improvements will result in lower CO2 emissions. Currently, millions of induction motors are made in India each year, consuming over half of the total energy generated. By boosting efficiency, significant amounts of energy may be saved, as well as the environment, because power producing plants emit millions of tonnes of greenhouse gases into the atmosphere each year to satisfy the load of these equipment. If there is a necessity to support the continually rising demand for energy while also lowering environmental pollution, then the efficiency of energy conversion will have to significantly improve in order to create more power from the same or less material.

1.10 ENERGY-EFFICIENCY POLICY OPPORTUNITIES FOR ELECTRIC MOTOR-DRIVEN SYSTEMS

This research delves into the complicated and hard world of electric motordriven systems (EDMS) and presents policy suggestions to minimise EMDS power usage in a timely and costeffective way. Electric motors are utilised in a broad variety of industrial applications, as well as commercial,

residential, agricultural, and transportation uses. Electric motors are often used as a component in a motor system, transforming electrical power into mechanical power. A motor system's consumption relates to the electricity consumed by its motors plus a minor amount for power system management.

Prior to the study given in this paper, very few attempts had been made to estimate the overall power consumption of electric motors, and no systematic attempt had been made to establish worldwide figures. Yet, "backoftheenvelope" analyses have consistently suggested that motors consume more than 40% of total power (in 2005, more than 6 000 TWh at the global level). In reality, electric motordriven devices tend to be the most common source of power usage, vastly outnumbering lighting, the next most common enduse (approximately 19% of worldwide electricity demand).

It is astonishing how few research have been conducted to quantify the energy consumption of EMDS. This research seeks to offer a more solid foundation for these estimations by employing both topdown and bottomup studies to boost confidence in the findings. It builds upon important regional studies such as the European Union's Lot 11 studies for the Eco-design Directive (De Almeida et al., 2008a [motors]; Falkner, 2008a [pumps]; Falkner, 2008b [circulator pumps]; Radgen, 2008 [fans]), US Department of Energy-sponsored investigations (DOE, 2002), other North American sources (Elliot, 2007; Boteler, 2007; NRCan, 2009), Japanese studies (JWG, 2007), Chinese studies (Zhao, 2007) and other regional data sources.

Electric motors are found in the industrial, commercial, residential, agricultural and transportation sectors.

- Motors are used in the residential sector for compression (in refrigerators and air conditioners), ventilation (to power fans), pumping (to power central heating system circulation and hot and cold water pumps), cooking appliances (food mixers, whisks, oven fans, extractor hoods), laundry, cleaning, ICT (hard discs and fans), and gardening appliances. Motors are also used in certain less common home applications (such as motorised gates and shutters).
- Motors are used in commercial buildings for heating, ventilation, and air conditioning (HVAC), pumping, ICT (hard drives and fans), escalators, lifts (elevators), and hoists, laundry, cleaning, and cooking.
- In the agricultural sector, motors are used for pumping and conveyance activities.
- Motors are used in transportation for motive power for electric trains, trucks, automobiles, and motorcycles, as well as associated cooling; ventilation and auxiliary devices; fluid pumping in vehicles, ships, and aircraft; HVAC applications; servomechanisms in aviation, and a variety of other uses.
- However, electric motors predominate in industry and account for the majority of overall power use. Motors are utilised in industrial applications for pumping, fans, air and liquid compression, transportation, and other sorts of mechanical handling and processing. Electric motordriven systems (EMDS) are by far the most common kind of industrial electric load. They are estimated to account for over 70% of all industrial power usage in the European Union, for example.

The electric motor is merely one component of the overall electromechanical system in each of the applications described above. The sole portion that utilises electricity is the motor (together with the controller), but the quantity of electricity required to perform its job is dictated by the amount of mechanical power required and the degree of the losses that occur in the transmission of that power. These losses occur not just within the motor but, more importantly, within the mechanical system that delivers power from the motor to the final mechanical application.

This paper investigates the markets and applications of electric motordriven systems and estimates their power consumption by industry, application, nation, and globally. It examines the many forms of EDMS and analyses the various technologies in use, as well as the potential for energy savings through better design, setup, and operation. It includes estimates of possible energy savings and CO2 emissions reductions, as well as costefficiency concerns connected with various motorsystem options. It also investigates the hurdles to the adoption and usage of more efficient EMDS, as well as the many standards designed to assess and improve motorsystem electricity demand. It examines existing and forthcoming policy settings for motors and motordriven systems and gives policy suggestions for the future.

The report's conclusions are consistent with and build on the findings of previous regional studies. The research seeks to give forth practical routes to boost energy savings and exploit possibilities more effectively than under present policy settings by paying attention to the vast diversity of measures to increase EMDS efficiency. It suggests governmental initiatives to encourage energyefficiency improvements in motorsystem components, core motor systems, and specific motorsystem

applications, as well as future actions to establish worldwide capability to detect and leverage large EDMS savings.

1.11 PERMANENT MAGNET MOTOR DRIVES

Permanent Magnet materials and power electronic device advancements have resulted in dependable and cost-effective Permanent Magnet-based motor drives for a wide range of applications. The speed-torque characteristics, strong dynamic responsiveness, high power density, suitable torque to inertia ratio, higher efficiency, robustness, extended working life, noiseless operation, and dependability of PMBLDC motor drives make them appealing. A BLDC motor seems identical to a DC motor, with a linear connection between current and torque, voltage and speed. PMBLDC drives use electronic commutation rather than mechanical commutation like traditional brushed DC motors.

1.12 OPERATION OF BLDC MOTOR

Figure 1.1 depicts a typical PMBLDC drive, which consists of a rectifier arrangement for ac to dc conversion, a dc link capacitor for energy storage, a Voltage Source Inverter (VSI) consisting of transistor switches, and finally, the inverter's three-phase output is delivered to the motor. Although not expressly displayed, a Hall position sensor or an optical shutter setup, in conjunction with some form of microcontroller/microprocessor, is utilised for position sensing.

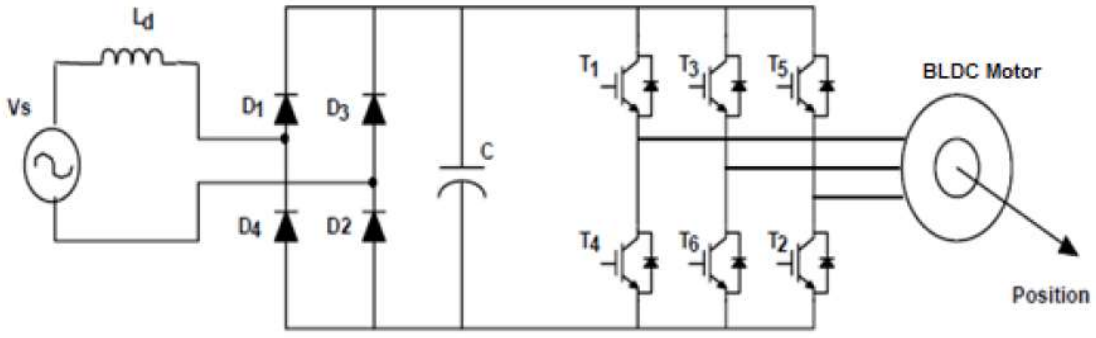

FIGURE 1.1 VOLTAGE SOURCE INVERTER BLDC DRIVE

In order to achieve a constant torque that is ideally free from ripple, the desired current be a rectangular ac wave, 120° broad. Torque is given by expression.

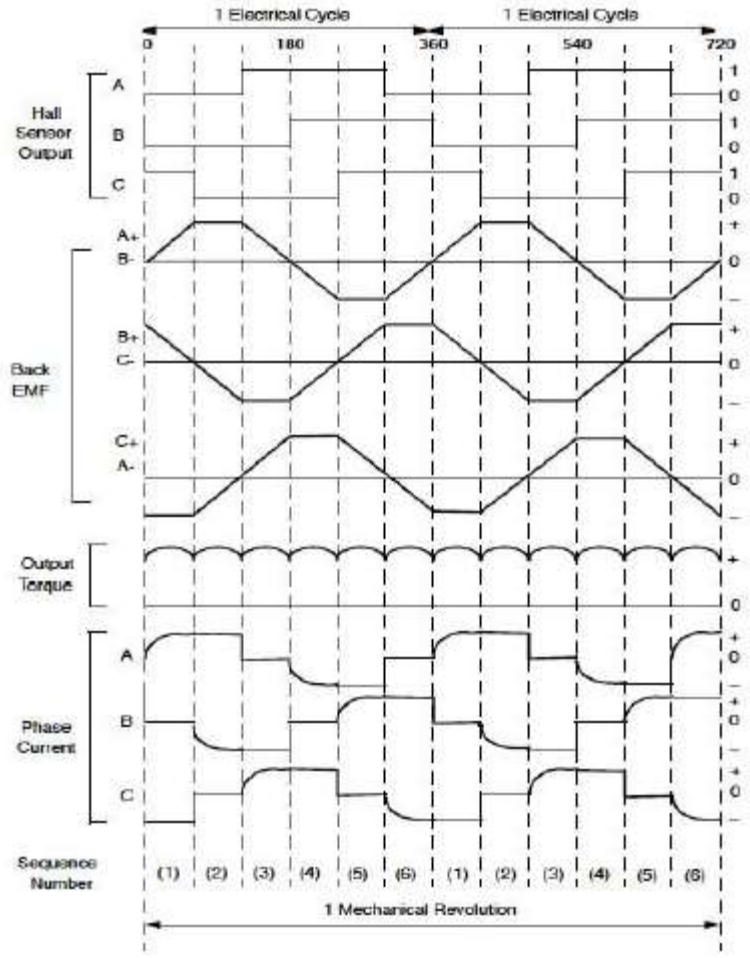

FIGURE 1.2 PHASE BACK-EMF AND PHASE CURRENT

Figure 1.2 depicts the profile of each phase of the motor with respect to their associated back-emfs as a function of rotor position. A constant current multiplies the constant component of the back-emf at each rotor position; hence, the total of the products of a phase back-emf and the corresponding phase current is constant. The required current profile is attained when utilising a VSI by managing the switching of the transistors.

At any one moment, only two of an inverter's six switches are conducting. To ensure proper operation of this motor, the phase currents must be synchronised with the phase back-emfs, which is accomplished through the use of Hall position sensors, which detect the position of the rotor field, and thus the position of the rotor shaft, and then output a combination of binary numbers corresponding to the rotor field.

$$T_{em} = \frac{e_a i_a + e_b i_b + e_c i_c}{\omega_m}$$

ea=phase-to-neutral back-emf of phase A (in volts),
eb= phase-to-neutral back-emf of phase B (in volts),
ec= phase-to-neutral back-emf of phase C (in volts),
ia= current in phase A (in amperes),
ib= current in phase B (in amperes),
ic= current in phase C (in amperes) and
ωm= angular velocity of the rotor shaft (in radians/second).

Figure 1.2 depicts the profile of each phase of the motor with respect to their associated back-emfs as a function of rotor position. A constant current multiplies the constant component of the back-emf at each rotor position; hence, the total of the products of a phase back-emf and the corresponding phase current is constant.

The required current profile is attained when utilising a VSI by managing the switching of the transistors. At any one moment, only two of an inverter's six switches are conducting. To ensure proper operation of this motor, the phase currents must be synchronised with the phase back-emfs, which is accomplished through the use of Hall position sensors, which detect the position of the rotor field, and thus the position of the rotor

shaft, and then output a combination of binary numbers corresponding to the rotor field. Furthermore, the Hall position sensors' rising and falling pulse edges are employed as triggers for timing circuits in the control algorithm. The power factor correction is also known as line current harmonic reduction. The major goal is to fix the power factor. To keep the phase angle between the input voltage and current as little as possible while improving THD, i.e. keeping harmonic content to a minimum. Because of the considerable impact of harmonics and their effects on power systems, electricity regulatory commissions and utilities all over the world are punishing users for harmonic dumping into supply lines. The Central Electricity Regulatory Commission of India has issued guidelines for IEEE Standard 519-92 on allowed limits for harmonics in electrical systems. Both the utility and the users must be aware of and comprehend the standard and the essentials of the restrictions imposed.

Power Factor (PF) is a measure of how efficiently power from the utility grid is used. It has a value between 0 and 1, and it is calculated as the ratio of real power to apparent power, as shown in Equation (1.1).

$$PF = \frac{RealPower}{ApparentPower} \quad (1.1)$$

Real power is measured in watts and is the amount of energy necessary to perform real labour. Assuming that the line voltage is perfect sinusoidal, real power (Preal) is defined as the product of the fundamental of voltage (Vrms), fundamental of current (Irms), and cosine of phase displacement (cos) between these two fundamental values, as shown in Equation (1.2).

$$P_{real} = V_{rms} I_{rms} \cos\phi \quad (1.2)$$

The general equation governing the relationship between the real power and apparent power is given by the Equation (1.3):

$$P_{real} = V_{rms} I_{rms} \cos\phi \cos\theta \quad (1.3)$$

where, cosθ is the distortion factor.

Total Harmonic Distortion (THD) is a measure of harmonic content in a circuit that is defined as the square root of the ratio of the sum of all squared higher-order harmonics to the amplitude of the fundamental harmonic. THD is defined as given in Equation (1.4)

$$THD = \frac{\sqrt{I_{2rms}^2 + I_{3rms}^2 + \ldots\ldots I_{nrms}^2}}{I_{rms}} \quad (1.4)$$

where, n is the order of the nth harmonic current.

Total Harmonic Distortion (THD) is a measure of harmonic content in a circuit that is defined as the square root of the ratio of the sum of all squared higher-order harmonics to the amplitude of the fundamental harmonic.

Electrical drives are used in both residential and industrial applications every day. Because of the world's energy problem, researchers have been pressed to build an efficient loss-less electric powertrain. The goal of this thesis is to create an energy-efficient electric drive for low-power applications. Induction motor and BLDC motor drives are studied and evaluated in the thesis organisation.

1.13 OBJECTIVES OF THE THESIS

The objectives of the work carried out can be summarized as follows:

1. Improving power quality by raising the power factor at the input side of an electric drive, hence lowering losses and boosting efficiency.
2. To simulate a closed-loop controlled power factor correction converter supplied by an IM drive, with an active clamping boost converter.
3. To simulate a closed-loop controlled power factor correction converter feeding a PMBLDC motor drive using buck-boost, Cuk, and SEPIC converters.
4. To compare the PFC converter supplied PMBLDC drives using the converters listed above.
5. Simulation in MATLAB/ SIMULINK and laboratory setup were used to confirm the analysis and design of the aforesaid converters in power factor correction, as well as to check the efficacy of the control approach.

1.14 ORGANIZATION OF THE THESIS

The organization of this thesis is as follows

CHAPTER 1

INTRODUCTION

CHAPTER 2

LITERATURE REVIEW

CHAPTER 3

ANALYSIS OF INDUCTION MOTOR DRIVE SYSTEMS

CHAPTER 4

ANALYSIS OF POWER CONVERTERS FOR BLDC DRIVE SYSTEMS

CHAPTER 5

CONCLUSION

REFERENCES

1. Leonhard W (2001) “Control of Electrical Drives”, 3rd ed., 470 pp., 2001, Springer-Verlag, Berlin, Germany.
2. Crowder R., (2006) Electric Drives and Electromechanical Systems, 308 pp., Elsevier, Oxford, UK, 2006.
3. Schröder D. (2007). Elektrische Antriebe – Grundlagen, “control of electrical drives, and different electrical drive operating regimes” 3rd ed., 750 pp., Springer-Verlag, Berlin, Germany.
4. Bhim Singh (2005)“Eighteen-Pulse AC-DC Converter for Harmonic Mitigation in Vector Controlled Induction Motor Drives” IEEE PEDS 2005, pp 1514-1519.
5. R.A. Guptha (2008) “Performance Analysis of 18-Pulse ac-DC Converter Fed Vector Controlled Induction Motor Drive (Vcimd)” JATIT, 2005 2008, PP 861-873.
6. IEEE (1992) Recommended Practices and Requirements for Harmonics Control in Electric Power Systems, IEEE Std. 519,1992.
7. Sewan Chai “New Pulse Multiplication Technique Based on 6-Pulse Thyristor Converters for High Power Applications” IEEE Proceedings 2001, pp 800-805.

8. Gary L. Skibinski (2003) “Cost effective multi pulse transformer solutions for harmonic mitigation in a.c drives” IEEE Proceedings 2003.
9. B. Singh, G. Bhuvaneswari, and V. Garg, (2006) “Harmonic mitigation using 12-pulse ac– DC converter in vector-controlled induction motor drives,” IEEE Trans. Power Del., vol. 21, no. 3, pp.1483–1492, Jul. 2006.
10. A. Consoli, (2001)“Unipolar converter for Switched reluctance motor drives with power factor Improvement”. Sixteenth annual IEEE applied power electronics conference and exposition, vol.2, pp. 1103 – 1108, 2001.
11. Reinert J, Schroder S. (2002) Power-factor correction for switched reluctance drives. IEEE Transactions on Industrial Electronics. 2002;49(1):54–57. DOI: 10.1109/41.982248.
12. Najmeh Zamani; (2914) “ Bifurcation and chaos control in power-factor-correction boost converter” 2014 22nd Iranian Conference on Electrical Engineering (ICEE), 2014, Pages: 1307 - 1312, DOI: 10.1109/IranianCEE.2014.6999736.
13. Saijun Zhang; (2014)“ Quantification analysis of input/output current of interleaved power factorcorrection (PFC) boost converter” 2014, IEEE Applied Power Electronics Conference and Exposition - APEC 2014, 1902 - 1908, DOI: 10.1109/APEC.2014.6803565.
14. De Almeida A.T., et al. (2008a), Improving the Penetration of Energy-Efficient Motors and Drives, European Commission SAVE Study, Institute of Systems and Robotics, University of Coimbra, Portugal, available at: http://re.jrc.ec.europa.eu/energyefficiency/motorchallenge/pdf/SAVEII- Motors-Final-Report-Mar-2000.pdf.

15. Falkner, H. (2008a), EuP Lot 11: Water Pumps, Technical Study for Eco-design Directive, mandated by European Commission, Didcot, UK, available at: www.ecomotors.org.
16. Falkner, H. (2008b), EuP Lot 11: Circulators, Technical Study for Eco design Directive, mandated by European Commission, Didcot, UK, available at: www.ecomotors.org.
17. Radgen, P., et al. (2008), EuP Lot 11: Fans for Ventilation in Non residential Buildings, Karlsruhe, Germany, available at: www.ecomotors.org.
18. DOE (Department of Energy) (2002), United States Industrial Electric Motor Systems Market Opportunities Assessment, Washington, DC, available at: www1.eere.energy.gov/industry/bestpractices/pdfs/mtrmkt.pdf
19. Elliott, R.N. (2007), Impact of Proposed Increases to Motor Efficiency Performance Standards, Proposed Federal Motor Tax In centives and Suggested New Directions Forward, American Council for an Energy-Efficient Economy, Washington, DC, available at: www.aceee.org/research-report/ie073.
20. Boteler, R. (2007), "NEMA Premium Update", presented at EEMODS 2007, 10-15 June, Beijing.
21. NRCan (Natural Resources Canada) (2009), Canada's Energy Efficiency Regulations – Proposed Regulations Bulletin – Electric Motors, available at: http://oee.nrcan.gc.ca/regulations/bulletin/electric-motors mar2009.cfm?attr=0.
22. JWG (Japanese G8 Working Group on Motors) (2007), "End-Use Assessment on Industrial Electric Motors and Drives: Japanese proposal for Toyko G8 Summit".

23. Zhao, Y. (2007), “General Situation of Energy Conservation Standards for China’s Motor System”, presented at EEMODS 2007, 10-15 June, Beijing.

CHAPTER 2
LITERATURE REVIEW

Lee and Ehsani (2001) demonstrated a sophisticated BLDC motor drive for an electric propulsion system. Power converter topologies and a PWM control approach were used to generate the required dynamic and static torque characteristics. TI TMS320F243 Insulated Gate Bipolar Transistor (IGBT) inverters with high speed DSP were created. Sensor-less control approaches were incorporated directly into several low-cost converter topologies.

Madani et al. (2002) developed a high-performance, low-cost brushless DC (BLDC) motor drive for commercial and household use. The revolutionary drive employs fewer switches than a standard converter and features an active power factor correction function, resulting in a sinusoidal input current with a power factor near to unity. The suggested converter has bidirectional capability, which improves the drive's speed control features. Furthermore, an unique PWM current control system with regenerative braking capacity is shown. As compared to other known strategies, our strategy performed significantly better.

Ottman et al. (2003) proposed an improved method of harvesting vibration energy with a piezoelectric device using a step-down DC-DC converter. The converter directs the power flow from the piezoelectric element to the required electronic load in this design. When the converter is evaluated in discontinuous current conduction mode, an expression including the duty cycle-power relationship is produced. Using the mechanical system, piezoelectric element, and converter parameters, the ideal duty cycle may be determined, where the collected power is enhanced for the degree of mechanical stimulation.

Ma et al. (2003) proposed a single-inductor dual-output boost converter with a combined single-inductor. This converter employs time-multiplexing control to provide two separate supply voltages (3.0 and 3.6 V) while utilising only one 1-H off-chip inductor and a single control loop. This converter is reviewed and compared to its competitors in terms of integration, architecture, control mechanism, and system stability.

Reatti and Kazimierczuk (2003) developed a small-signal circuit model for discontinuous conduction pulse width-modulated DC-DC converters. This model is made up of controlled current sources, a separate voltage source, and resistances. The energy conservation approach is used to take into account the parasitic resistances of the transistor and diode, as well as the diode threshold voltage. The suggested model is ideal for small-signal, frequency-domain converter representation. This model is used to calculate the control-to-output transfer function, input-to-output voltage transfer function, input impedance, and output impedance of a boost converter.

Gopalarathnam and Toliyat (2003) suggested a unique converter for using unipolar currents to power a permanent magnet BLDC (BLDC) motor. A front-end single-ended primary inductance converter (SEPIC) and a switch linked in series with each phase are used. Because all of the switches are ground-referenced, their gate drives are simplified. The available input voltage may be increased for better current control, which is advantageous for low voltage applications. To work with an alternating current supply, the SEPIC converter is designed to operate in the discontinuous conduction mode. In this mode of operation, it approximates a voltage follower, with the line current following the line voltage waveform to some extent. The reduction in low-order harmonics and improved power factor are achieved without the use of any voltage or current sensors.

Chung et al. (2003) showed a new approach for maximising the output power of a solar panel under changing meteorological circumstances. The method relies on connecting a solar panel to a load or battery bus through a pulse-width-modulated (PWM) DC/DC SEPIC or CUK converter. When the input current is continuous, the converter operates in discontinuous capacitor voltage mode.

Kumar et al. (2005) achieved closed loop control of a Permanent Magnet BLDC (PMBLDC) motor using a single current sensor using modelling and DSP. A series circuit is formed by a DC connection and two conducting phases. The DC link current was regulated to control the current in these stages.

Krishnan et al. developed a unique four-quadrant Switched Reluctance Motor (SRM) drive with only one programmable switch (2005). A two-phase machine and a single controlled switch converter were

used for the motor drive. The motor drive was developed, simulated, and tested to ensure that it was suitable for self-starting, speed control, and four quadrant operations.

Fuengwarodsakul et al. (2005) demonstrated a four-quadrant SRM drive for high-dynamic applications. The drive was built on a control method called as Direct Instantaneous Torque Control (DITC). A method for directly creating switching functions via hysteresis torque controllers for SRMs was also presented. The novel controller was designed and tested using a DSP / Field-Programmable Gate Array (FPGA) development platform.

Axelrod et al. (2005) recommended that the notion of adding a switched-capacitor circuit into a typical converter be extended to more advanced power electronics supplies such as UK, ZETA, and SEPIC. Because these DC supplies already have an inner capacitor that serves as an energy transferring element, the solution is simpler than with buck and boost converters: this capacitor is divided into two capacitors, and an internal switched-capacitor circuit is implemented by organising the rectifier diodes in an easy manner. This SC-circuit is not linked to the actual converter; it only serves as the energy transfer capacitor.

Veerachary (2005) created a V2-based MP point tracking (MPPT) technique that employs a buck-boost transformation topology. Despite the availability of several buck-boost transformation topologies, a coupled inductor SEPIC converter was used for experiments. To achieve a practically ripple-free array current, the ripple steering phenomenon was used in conjunction with an integrated inductor.

Urasaki et al. (2005) proposed an adaptive dead-time compensation approach for calculating the basic phase voltage of inverter-fed vector-controlled permanent magnet synchronous motor drives. The amplitude corresponding to the phase dead-time compensation voltage (DTCV) for compensating the disturbance voltage due to unnecessary inverter characteristics such as dead-time, switching device turn-on/off time, and on-voltages of switching devices and diodes is determined adaptively based on a dead-time compensation time (DTCT). On-line detection of DTCT is performed using a -axis disturbance voltage in the current reference frame, which is synchronised with the current vector. The -axis disturbance voltage is estimated with the assistance of a disturbance observer. The correctness of the detected DTCT is experimentally tested by estimating the mean absolute percentage error (MAPE) between a computed and a measured active power.

Iqbal and Levi (2005) investigated alternative space vector PWM (SVPWM) algorithms for a five-phase VSI that may be used to control five-phase motors. First, a thorough model of a five-phase VSI is presented in terms of space vectors. Following that, the possible approach of employing just enormous space vectors is explained. It is demonstrated that this SVPWM approach generates a large number of low-order output voltage harmonics. Finally, a novel SVPWM approach is described that enables operation with pure sinusoidal output voltages until a predetermined reference voltage value that is less than the maximum feasible with the supplied DC link voltage. One SVPWM approach is supplemented with another that unavoidably leads to the creation of a few low order harmonics in order to enable the whole utilisation of the DC bus voltage. However, in compared to the scenario where only big vectors are used, these harmonics have much lower values. An extensive performance

evaluation of existing and newly devised schemes is undertaken, and it is introduced in terms of the quality of the output voltage waveforms.

Kwon et al. (2006) proposed a SEPIC converter with continuous-conduction mode. The newly developed SEPIC converter may reduce diode reverse recovery loss and increase power efficiency. The output diode is turned off at zero current by employing a linked inductor and an additional diode. The connected inductor's leaking inductor reduces the reverse recovery current of the additional diode. In compared to standard PFC circuits employing the SEPIC converter, the newly developed SEPIC converter produces a high power efficiency and power factor.

Sagiroglu et al. (2006) proposed a new approach for line power factor adjustment with differential loads based on artificial neural networks (ANNs). The reactive power of the system was handled by a synchronous motor controlled by the neural compensator. The expanded delta-bar-delta learning approach was then used to train the ANN compensator. The ANN parameters were then entered into a PIC 16F877 controller to obtain a better and faster correction. The results show that the newly introduced innovative method overcomes the problems encountered in traditional compensators, such as over or under compensation, time delay, and step changes in reactive power, and produces an accurate, economical, and rapid compensation when compared to the method with capacitor groups.

Mohamed and El-Saadany (2007) proposed an improved deadbeat current control system for a three-phase pulse-width-modulated (PWM) voltage-source inverter with a novel adaptive self-tuning load model. To begin, an upgraded deadbeat current controller with delay compensation is used to achieve high-bandwidth current control features. The Comparative

analysis findings are used to demonstrate the validity and effectiveness of the newly proposed control mechanism.

Ozturk et al. (2007) investigated a PFC algorithm for direct torque control (DTC) brushless dc motor operation in the constant torque area. In contrast to standard three-phase DTC drives, the innovative DTC technique uses a two-phase conduction mode. Unlike the usual six-step PWM current control, the preferred quasi-square wave current is obtained by selecting the inverter voltage space vectors of the two-phase conduction mode from a simple look-up table at a preset sampling period. As a result, the torque response is substantially faster than with standard current management. Moreover, a pre-saved back-EMF versus position look-up table is built to reduce the low-frequency torque oscillations caused by the non-ideal trapezoidal shape of the original back-EMF waveform of the BLDC motor.

Chen et al. (2007) developed a PMBLDC motor for high-speed embroidery machines. Magnetic field finite-elements analysis was used in the motor design to determine motor characteristics such as air-gap flux, back EMF, and inductance. The self and mutual inductances of the stator windings were calculated using numerical magnetic field solutions and a modified incremental energy approach.

Afjei et al. (2007) described in detail a BLDC motor/generator setup that did not employ a permanent magnet in the rotor. The proposed machine consists of two magnetically dependent stator and rotor sets (layers), with each stator set consisting of nine salient poles with windings wrapped around them and the rotor consisting of six salient poles. A power electronic converter that provided bidirectional current control for each

motor phase independently was presented. This control technique enabled the motor to operate with any number of phases at any moment.

Kim et al. (2007) proposed a BLDC motor control method for motor drive applications that makes use of general-purpose microcontrollers with a single on-chip timer. PWM signals with generic input/output (I/O) ports were used to operate a three-phase permanent magnet BLDC motor using the timer interrupt on the MSP430F1232. An technique was presented that leverages the I/O port to generate PWM signals for BLDC motor control using three Hall sensors.

Hu et al. (2007) investigated a BLDC motor driving mode that employs a cascade bidirectional DC-DC with full-bridge circuit and motor EMF. To regulate the speed, a closed-loop was established using voltage feedback and current positive feedback compensation. A strategy based on inductor current predictive control was presented to overcome capacitor voltage ripples during the motor commutation process. It regulates the duty cycle and compels the inductor current to follow the motor phase current during the commutation process.

Rodriguez et al. (2007) proposed a predictive current control approach for a voltage source inverter. The approach use a discrete-time system model to estimate the future value of the load current for all possible voltage vectors produced by the inverter. The voltage vector with the lowest quality function is picked. In this work, the quality function evaluates the current error throughout the next sample time. The performance of the unique predictive control approach is then compared to that of hysteresis and pulse-width modulation control, demonstrating that

the predictive technique manages the load current extremely efficiently and performs very well in contrast to standard alternatives.

Ye et al. (2008) presented a high power factor SEPIC converter with global input voltages and a dimmable LED light for high brightness LED lighting applications. The discontinuous conduction mode criteria is offered. Because the input inductor current follows the input voltage, the harmonics of the input line current are reduced and the power factor is high. To control the brightness of the LEDs, a current feedback loop is used. The gate drive signal of the switch is generated by comparing the PWM controller's saw-tooth carrier signal to the current feedback signal. This circuit has the advantages of just requiring one stage of power conversion, no need to gauge the input voltage, easy feedback control, voltage step-up and step-down, high power factor, and dimmable LED current. It is especially suitable for offline LED applications.

Han et al. (2008) investigated an average-value modelling of BLDC motor systems with 120o inverter systems. It shown that disregarding the commutation interval can reduce model accuracy, particularly with BLDC motors with low stator resistance (high electrical time constant) and a wide commutation angle. This paper introduces a revolutionary Average Value Modeling (AVM) that includes both commutation and conduction subintervals. The commutation angle has been numerically represented using a nonlinear algebraic function. The novel model was demonstrated in both the time and frequency domains and is applicable to motors with large and small electrical time constants.

Nasiri et al. (2008) described the design parameters and performance assessment of an on-line, low-cost, high-performance single-phase

uninterruptible power supply (UPS) system based on a boost integrated flyback rectifier/energy storage DC/DC (BIFRED) converter. An isolated AC/DC BIFRED converter, a bidirectional DC/DC converter, and a DC/AC inverter compose the system. Input power factor adjustment, electric separation of the input from the output, low battery voltage, and control simplicity are all benefits. Unlike standard UPS topologies, the electrical isolation is achieved by the use of a high frequency transformer, resulting in a decrease in size and expense.

Park et al. (2008) developed an integrated boost SEPIC (IBS) converter by combining a boost converter with a series output module, which may be used to supplement the insufficient step-up ratio. With the help of an isolated SEPIC converter, the new IBS achieves a higher step-up ratio. Because the boost converter and the SEPIC converter share a boost inductor and a switch, their construction is simpler. Moreover, because the transformer leakage inductor mitigates reverse recovery, the newly proposed IBS converter does not require a current snubber for the diodes.

Subudhi et al. (2008) suggested an efficient vector control of induction motor technique for controlling the speed of induction motors utilised in industrial applications. Due to the fluctuation of its properties such as resistance, inductance, and time constant, vector control is a common approach with some problems in generating an accurate model of an Induction Motor (IM). In order to deal with this uncertainty, this research proposes a fuzzy logic-based vector control technique. The paper's main focus is on the real-time implementation utilising dSPACE 1104. In the laboratory, the technique was successfully applied on a 3 HP induction

motor drive. It has been shown to be quite successful in detecting flaws early in the design process.

Man et al. (2008) demonstrated a 0.9-V input discontinuous-conduction-mode (DCM) boost converter with a 2.5-V output and a 100-mA output. We introduce a novel low-voltage pulse-width modulator. Instead of using the 2.5-V output as in traditional modulator designs, the modulator can be supplied straight from the 0.9-V input. Advanced low-voltage analogue blocks, which often use a significant amount of power and chip area, are not required in the modulator. The influence of output-voltage ripple and transient-induced output-voltage disturbances on the operation of the modulator's analogue blocks is eliminated.

Kim et al. (2008) proposed a carrier-based PWM approach for a multilevel four-leg PWM VSI, as well as a novel offset voltage. Three-phase unbalanced loads and many single-phase nonlinear loads in a three-phase four-wire utility system result in neutral line current, which is zero-sequence current. To deal with unbalanced and nonlinear loads in a high power system, this study recommends a multilevel four-leg pulse-width modulation (PWM) voltage-source inverter (VSI) to be used as a topology for high power applications in which a function is required for controlling the zero-sequence component in addition to DC components.

Wang et al. (2009) created an EA-based design optimization tool for a three-phase voltage source inverter with diode front-end rectifier used for industrial motor drive power stage, taking into account all important subsystems such as the front-end rectifier, inverter and thermal management system, and EMI filter. Three optimizers are developed from

analytical connections. The relationships between the subsystems are taken into account in order to achieve universal optimization.

Chiang et al. (2009) investigated the modelling and controller design of a single-ended primary inductance converter-based PV charger system (SEPIC). The developed SEPIC employs peak-current-mode control with the current command generated by the PV voltage regulating loop, where the voltage command is determined by both the PV module maximum power point tracking (MPPT) control loop and the battery charging loop. The control goal is to balance the power flow from the PV module to the battery and the load such that the PV power is used effectively and the battery is charged in three stages. First, this study includes an intricate modelling of the SEPIC, as well as the PV module input and peak-current-mode regulation. In addition to the adaptive MPPT controller, the PV voltage controller is built on this basis.

Miller et al. (2009) discovered that solar power production losses owing to the formation of tiny particles of oily residues on solar PV systems increases soiling concerns in solar farms located near an airport. Such leftovers might be the result of aircraft actions. It conducts research to determine the cause and impact of various sources of soiling on solar power generation. The majority of oily wastes come from car exhaust gas, railroad, power plant, maritime operations, and to a lesser extent airport activities. Ultimately, the study focused on reducing the output power of PV modules.

Bo-Cheng et al. (2009) proposed a mode shift and stability control of a DCM-functioning current mode regulated buck-boost converter. When the current mode controlled DC-DC converter switches from CCM to

DCM, the system trajectory is no longer as chaotic as it was with CCM. Even though the system is universally chaotic, if the current reaches zero during at least one clock period during the period of the current waveform, the orbit tends to become often periodic. The existence of a compensating ramp current can cause the buck-boost converter to switch from DCM to CCM, and this system can be effectively regulated to operate in the stable period-one zone. The current mode regulated buck-boost converter in DCM can exhibit intricate dynamic behaviours when the circuit parameters are modified.

Mishra and Karthikeyan (2009) illustrated the design elements of many passive components as well as the switching dynamics of a voltage source inverter (VSI) for unbalanced and nonlinear load correction. The VSI design approach for tracking the essential reference currents in a smooth manner is demonstrated. The suggested approach has the potential to build the passive components of various VSI topologies used for load correction.

Zhang and Yan (2009) demonstrated a three-phase four-leg inverter with a selective harmonic elimination (SHE) control method. The four legs' control signals are calculated as follows: 1) the control signals of three legs are mathematically expressed on a line-to-line basis using Fourier based equations, as in classical SHE technology, to remove the lower order non-triplen harmonics, and 2) the fourth leg generates the harmonics, which equal the lower triplen harmonics generated by the other legs. Since the fourth leg provides a low-impedance channel for the triplen harmonics, the inverter has nearly symmetric three-phase output voltage with unbalanced load. For a total harmonic distortion of less than 4%, the switching-to-

fundamental frequency ratio in the suggested model is only 13 and 27 (per unit) p.u. for the three legs and the fourth leg, respectively.

Rahimi and Emadi (2010) demonstrated the DCM functioning of DC/DC converters powered by CPLs. If the converter has a resistive load, state-space averaging, circuit averaging, or the average-switch approach is used to get the nonlinear equation of the output voltage. The small-signal control-to-output transfer function of the converter is then obtained using established linearization methods, and the converter's stability with the resistive load is assessed in s-domain. After that, the stability of the open-loop converter in the s-domain when loaded by a CPL was investigated.

Madhusudhana Rao et al. (2010) demonstrated speed control of a BLDC motor drive utilising PWM and the TMS320F240 DSP. The DSP receives input from the Hall signals, phase current sensing signal, and speed command. The PI controller was used in both the outer velocity control loop and the inner current control loop, which was implemented by programming in the TMS320F240 DSP. The performance of the drive was examined for beginning, speed reversal, and load disturbance. For modelling the driving model with the PI speed controller, an algorithm was developed. The numerical integration approach of fourth order Runge-Kutta was used to solve the model's first order differential equations.

Li et al. (2010) demonstrated a BLDC motor Flywheel Energy Storage System (FESS). A buck circuit was designed to reduce motor torque ripple in the charge phase by employing a constant torque control at low speed and a constant power control at high speed. PAM control was first developed using constant torque and constant power control

approaches, which are effective in lowering phase current ripple because to minimal torque ripple.

Chiu et al. (2010) described a method for enhancing the efficiency and torque performance of a single-phase BLDC motor by determining the optimal commutation angle at each speed. The finite element approach was used to simulate the back-EMF voltage and coil current for the single-phase BLDC motor, and the conduction time of switches was then changed by recognising the coil current waveform. When the motor has the ideal shift angle for each speed, it may improve its efficiency, noise, and vibration. The unique design feature in this work was to simply note the smooth degree of the motor current, which can be used to determine the ideal shift angle.

Sue and colleagues (2010) investigated a bi-directional power flow Interior Permanent Magnet BLDC (IPMBLDC) motor drive for electric scooters. For the driving operation, a control mechanism was devised. In addition to the high speed zone, it produced great energy conversion efficiency in the low speed and high torque regions. The basic control concept used the Maximum Torque per Ampere (MTPA) control of an Internal Permanent Magnet Synchronous Motor (IPMSM). A unique switching pattern was developed for the regenerative braking action. It produced a smooth regenerative braking symmetry line current waveform. In order to keep development costs low, the control core was implemented using a DSP.

Demelo et al. (2010) presented a high-power-factor rectifier suitable for universal line base based on a modified single-ended primary inductance converter (SEPIC). The voltage multiplier approach is then

applied to the traditional SEPIC circuit, resulting in unique operation features such as low-switch-voltage functioning and high static gain at low line voltage. This unique arrangement also allows for a reduction in the losses associated with the diode reverse recovery current, and soft commutation is achieved via a simple regenerative snubber circuit.

Singh and Singh (2010) designed and verified a Cuk converter-based PFC topology for a PMBLDC motor drive for an air-conditioner compressor load. The PFC has a high power factor and a wide speed control range. The THD of the alternating current mains current detected fully fulfils international standards. Gopalarathnam and Toliyat (2003) presented a novel converter architecture based on a front-end Single-Ended Primary Inductance Converter (SEPIC) and a switch in series with each phase for driving a PMBLDC utilising unipolar currents. The SEPIC converter is built to work in discontinuous conduction mode.

Rockhill et al. (2011) discussed the design process and performance of an LCL grid filter for a medium-voltage neutral point clamped (NPC) converter intended for usage in a multi-megawatt wind turbine. The incorporation of the medium voltage converter, a lower allowable switching frequency, considerations about the physical size and weight of the component, and severe limits on acceptable injected current harmonics all provide challenges to the particular filter design difficulties in this application. Grid filter design procedures for lower power and higher switching frequency converters do not apply to a multi-megawatt filter that connects a low-frequency switching medium-voltage converter to the electric grid. This study demonstrates a frequency domain model-based approach for obtaining the best filter settings that provide the desired performance under all operating situations while adhering to the design

constraints. Novel notions such as virtual harmonic content and virtual filter losses were presented to achieve this goal.

Zhang and Spencer (2011) developed an A-switching map for a boost PFC converter. The accurate inductor current and capacitor voltage may be calculated using the A-switching map. The input current's fast-scale disruption is visible. This is related to the operation moving from DCM to CCM. The A-switching map is used to calculate the exact numerical border between DCM and CCM under different circuit parameter circumstances. In comparison to the A-switching map result, an analytical condition for DCM operation is derived with high precision. The analytical equations are used to calculate the output power and voltage limits. The output voltage, switching time, and input inductance all limit the maximum output power. The frequency of the output voltage ripple is double that of the line frequency. The magnitude of the voltage ripple is determined by the average output voltage and the RC time constant, with no regard for the input inductance.

Grote et al. (2011) developed a digital control technique for interleaving multi-phase boost power factor correction rectifiers that operates at both DCM and CCM and employs two feed forward algorithms. The first estimates the turn on time to obtain the desired input current, while the second calculates the switching period duration for DCM operation. It is discovered that implementing interleaving characteristics of a converter with variable frequency operation is challenging.

Salah et al. (2011) suggested a BLDC motor control approach based on rotor position sensing. A PIC microcontroller was used to generate PWM signals that powered the power inverter bridge. The efficiency of the

planned motor drive is indicated by the hardware realisation and simulation results. The new motor control and drive's versatility allows for the use of numerous control algorithms for improving the output characteristics of the BLDC motor.

Feyzi et al. (2011) proposed a unified current mechanism for high-performance BLDC motor drivers. It was based on phase current estimate and control, using two single sensors for DC link voltage and current. The phase currents were recreated in two stages, each of which included estimate and regulation. Estimation is based on the dynamic motor model, whereas regulation is based on the states of the inverter switches and the observed DC link current. Particle Swarm Optimization (PSO) was also used to regulate the PID settings of the speed controller in order to get a better dynamic response characteristic of the motor speed.

Mahdavi and Farzanehfard (2011) demonstrated a bridgeless single-ended primary inductance converter power-factor-correction rectifier. The suggested circuit results in lower conduction losses while using fewer components. A voltage loop and a current loop are required for PFC in classic PFC converters (continuous-conduction-mode boost converter). When the converter operates in discontinuous conduction mode, the control circuit of the proposed converter is simplified, and no current loop is required.

Uno and Tanaka (2011) described single-switch cell voltage equalisers that use multi-stacked buck-boost converters such as the single-ended primary inductor converter (SEPIC), ZETA, and UK converters. These equalisers use passive components and a single switch, which reduces the circuit complexity significantly when compared to typical

equalisers. Furthermore, because the suggested equalisers operate in discontinuous conduction mode, feedback control is not required to limit the currents flowing through the cells and circuit parts.

Errabelli and Mutschler (2012) presented a two-level fault-tolerant voltage source inverter (VSI) for permanent magnet drives, which was built and tested methodically. A typical two-level inverter has three legs. In the case of a fault-tolerant inverter, a redundant leg is added to replace the faulty leg. The usage of separate back-to-back-connected thyristors is used to perform faulty leg separation and redundant leg insertion. The suggested inverter can tolerate switching device short-circuit and open-circuit failures. The post-fault performance is comparable to the ordinary pre-fault operation, and fault compensation is sufficiently fast to cause very little distortion in the drive operation. The inverter's fault tolerance is then confirmed using field-oriented control of a permanent magnet synchronous motor.

Hu et al. (2012) developed a resonant Single-Ended Primary Inductor-Converter (SEPIC) converter and control approach for dc-dc power conversion at high and very high frequencies. The newly developed design is distinguished by high efficiency throughout a wide input and output voltage range, up and down voltage conversion, lower size, and exceptional transient performance.

Eke and Senturk (2012) investigated the performance of a dual-axis sun-tracking PV system and a latitude tilt fixed system after one year of operation. At the Mugla University campus in Turkey, two identical 7.9 kWp PV systems with the same modules and inverters were erected. As

compared to the latitude tilt fixed system, the dual-axis sun tracking system is predicted to produce 30.79% more PV power.

Ho et al. (2012) created a brushless DC motor with a high power factor (BLDC). An active power factor controller is used to improve the high input current harmonics created by the power diodes as well as the switching of the inverter to increase the power factor of a BLDC drive. The power factor controller's complete design is analysed and achieved. Also, the BLDC drive is discussed. The experimental findings demonstrate the viability of driving BLDC motors using the newly built APFC controller.

Lodhi and Thakur (2013) devised an accurate method for three-phase induction motor speed control. The Indirect Vector Control Induction Motor Drive (IVCIMD) is designed to offer rapid torque and strong dynamic reactions near zero and high speeds. In this study, several controllers are employed to improve the performance of indirect vector control, and comparative performance is provided and studied.

Samyuktha (2013) suggested a resolver algorithm for a permanent magnet synchronous motor's current-controlled drive system (PMSM). Because the resolver process reduces the angle error to zero, the calculated angle eventually corresponds to the real rotor angle. For detailed modelling and performance calculation of PMSM drive systems, additional control approaches such as constant mutual air gap flux linkages control, optimal torque per ampere control, unity power factor control, and sensor less control may be used.

The complete PMSM control system is mathematically described by Kaushik Jash et al. (2013) by splitting it into many distinct functional

modules such as PMSM body module, inverter module, coordinate transformation module, and Sinusoidal Pulse Width Modulation (SPWM). Even at extremely high speed ranges, the performance of vector control for accomplishing quick reversal of PMSM is good.

According to Lumbreras et al. (2013) studies, the PV panels are positioned in regularly spaced rows at different levels on two slopes to facilitate ventilation and frame expansion. Moreover, the majority of the solar trackers were constructed with a horizontal support attached to the top frame by two crucial connections. Yet, the whole panel and top frame assembly load is divided evenly by these two vital connections, causing stress on the critical points. As a result, the vital points fail in this setup.

Dhamo and Spahiu (2013) suggested a sensor-less technique based on MRAS for controlling a PMSM drive system, the results of which were compared to a vector control scheme based on the IFOC method. A stator current estimator is used by the MRAS to estimate rotor position angle and speed. The suggested approach is extremely basic and uses very little computational resources; it exhibits good adaption even at very low rates. The simulation results of various operation situations demonstrated that the suggested technique is efficient.

Vector control of a BLDC motor using Sinusoidal PWM and Space Vector Modulation was proposed by Jose and Karthikeyan (2013). One of the ways used in variable frequency drives or variable speed drives to regulate the torque of three-phase electric motors by regulating the current is vector control. As a result, when the space vector modulation approach is utilised in the system, the overall performance of the motor drive system improves.

According to Carvalho et al. (2013), this work includes the design and development of a solar tracking system with two axes of movement and photoresistor sensing. The automated system has dependable and simple connections that make component replacement and maintenance easier. In tests conducted around the summer solstice, the tracking panels outperformed the fixed panels by 52.7% in total energy output. This prototype system was difficult to create for large-scale manufacturing.

Li and Ping (2013) offered several converter management approaches to increase power factor and minimise Total Harmonic Distortion (THD). Predictive control approach is described to create duty cycles in order to attain unity power factor in a half line period for boost PFC. Input reference output voltage, voltage, reference current, and inductor current all influence duty cycle. The switching frequency of a boost converter is substantially greater than the line frequency since it operates in continuous conduction mode.

Kessal et al. (2013) developed an AC-DC converter with controlled output voltage and PFC, and this paper proposes a conventional PI regulator with fuzzy logic control. Under load disturbance and uncertainty situations, the fuzzy logic-based controller outperforms the PI equivalent in terms of dynamic responsiveness.

Bridgeless Cuk converter for AC-DC PFC with Fuzzy Logic Controller (FLC) in DCM operation was developed by Nesapriya and Rajalaxmi (2013). By lowering the amount of fuzzy sets and Membership Functions, the study presents a streamlined controller (MFs). The pulsating

output voltage creates common mode noise, which is a significant disadvantage of this converter.

Tibola and Barbi (2013) evaluated and designed a three-phase high power factor rectifier based on a DC-DC single-ended primary-inductance converter (SEPIC) operating in discontinuous conduction mode, as well as output voltage control and high frequency isolation. The operating mode without current sensors and a current control loop is commonly used to obtain the input high power factor. A design example and experimental results for a 4-kW, 380-V line-to-line input voltage, 400-V output voltage, 0.998 power factor, 40-kHz switching frequency, and 4% input current total harmonic distortion laboratory prototype with two unique modulators are presented to validate the theoretical analysis. The switch voltage stress in the boost converter is about the same as the output voltage.

Behera et al. (2014) conducted a comparison study of traditional scalar control closed loop v/f control and Indirect Field Oriented Vector Control (IFOC). The PI controller is utilised in both scalar and vector control of induction motors, and it decreases steady-state error while providing smooth tracking. Uncertainties in the system are impacted by unpredictability in machine parameters and external load disruptions. Several robust control approaches, such as optimum control, variable structure control, adaptive fuzzy and neural control, can be used in place of the PI controller.

Bist and Singh (2014) also created a modified-zeta converter-fed brushless DC (BLDC) motor drive based on power factor (PF). A single-phase supply, followed by a diode bridge rectifier and a modified-zeta converter operating in discontinuous inductor current mode (DICM), is

used to power a BLDC motor via a voltage source inverter (VSI). The modified-zeta converter operating in DICM acts as an intrinsic PF pre-regulator. A single-voltage sensor is used to regulate the DC-link voltage, which is used to control the speed of the BLDC motor. This allows VSI to operate in fundamental frequency switching mode, reducing switching losses in VSI. The newly presented BLDC motor drive is designed, and its performance is then simulated in the MATLAB/ Simulink environment to achieve improved power quality at AC mains for a wide range of speed control. The obtained power quality indices are within the limitations prescribed by the international power quality standard IEC 61000-3-2. Finally, the performance of the suggested drive is validated using test results obtained on a prototype created of the newly introduced BLDC motor drive.

Krishnan and Arjun (2014) created a brushless DC motor control approach that did not need sensors and used the motor's back emf as a commutation parameter. The CUK converter is used as a power factor correction converter for a PMBLDC motor that is powered by a single phase AC mains through a diode bridge rectifier.

Sliding Mode Controller (SMC) for speed control was shown by Hassaine et al. (2014). The suggested study indicates that the SMC controller reduces the Total Harmonic Distortion (THD) value, which is considerably smaller than the traditional (PI) controller achieved result. As a result, one of the Power Quality (PQ) issues (lower THD value) is restricted in this suggested system.

Bist and Singh (2014) developed a low-power brushless dc (BLDC) motor drive with power factor correction (PFC). The speed of the BLDC

motor is controlled in this study by adjusting the dc link voltage of the voltage source inverter (VSI) controlling the BLDC motor. As a result, VSI employs just electronic commutation of the BLDC motor and operates in low frequency switching for reduced switching losses. Using a single voltage sensor, a PFC-based isolated zeta converter operating in discontinuous conduction mode (DCM) is used to regulate the dc link voltage of the VSI with intrinsic PFC at AC mains. The suggested drive is achieved to achieve a unity power factor at AC mains for a wide range of speed control and supply voltage changes. Power quality indices within the restrictions of the IEC 61000-3-2 standard are used to achieve improved power quality.

Ashmore et al. (2015) developed a solar support assembly in which the horizontal frame is coupled to a single pivotal point, resulting in inclination (sag) of the horizontal frame on both frame ends. As a result of the Center's sole support, the seasonal drive arrangement may not operate effectively.

Todd Griffith et al. (2015) offer structural dynamics testing and analysis for heliostat design assessment and monitoring. Vibrations, strain, and displacements under wind loading are the measurement parameters. This data aided in the evaluation and strengthening of structural models that anticipate system deformations owing to static gravity and dynamic wind loadings. It was discovered that optical precision is greatly influenced.

Alexander S. Maklakov et al. (2016) used an 18-pulse connection circuit to create three level neutral point clamped (3L-NPC) Active Front-End (AFE) rectifiers for AC drives. Three power transformers are linked in

parallel in the circuit, and the secondary winding voltages phase shift. For managing the 3L-NPC AFE rectifiers, the authors presented a Pulse Width Modulation Selective Harmonic Elimination (PWMSHE) approach.

Eldin et al. (2016) stated that the employed mathematical model was experimentally confirmed and then applied to many conditions, notably hot and cold locations. In the case of a chilly city like Berlin, Germany, the gain in electrical energy by following the Sun is roughly 39%. Due to overheating of the PV panels, the energy gain does not surpass 8% in such a hot city like Aswan, Egypt. Nevertheless, if the energy necessary to run the monitoring device is included in this study, which varies from 5% to 10% of the energy generated, then tracking the Sun will be impossible in warmer nations. Only real-time implementation results can help you make the best selection.

Singh et al. (2016) demonstrate a dual output PFC converter for driving switching reluctance motors (SRMs). In this case, a modified SEPIC converter is employed for wide-range speed control and power factor correction at the AC mains. A single voltage sensor is utilised to manage the DC link voltage, and its output is used to drive the midpoint converter feed SRM. To lower the overall size of the converter, the switching frequency of the converter is set at 20 kHz. It also discusses the general design and performance of the converter-fed SRM drive. According to the IEC 6100-3-2 standard, the input current THD (Total Harmonic Distortion) is kept below 5%.

Rao et al. (2016) addressed a SEPIC converter-based VSI-fed BLDC drive for low voltage electrical fan applications. Traditionally, BLDC motors do not have current or speed controls, but this study employed a

simplified speed control for BLDC motor. The performance of the SEPIC converter in open loop is simulated, and wave patterns are displayed. The dc-dc SEPIC converter is connected to the commutation circuit's input, and the necessary dc voltage is attained using closed loop controllers. This device also offers speed control so that torque can respond instantly. This method efficiently reduces torque ripples over a wide speed range by utilising a voltage follower approach; a simple control is designed to manage the voltage and hence the speed of the BLDC motor. Speed control and supply voltage fluctuation with power quality indices have yielded good results.

Lodh et al. (2016) employed a SEPIC converter for a high power, high gain application. A single Flyback transformer, in general, cannot handle large power owing to magnetic limitations. As a result, for somewhat higher power applications, interleaved Flyback converter topologies are used. The interleaved Flyback converter, on the other hand, necessitates the usage of two switches. The proposed converter has an intriguing characteristic in that the power management of both Flyback transformers may be done by a single switch with the same voltage rating as the traditional interleaved Flyback converter. As a result, the solution requires fewer components, resulting in a compact and low-cost construction. In an ideal circumstance, the voltage rating of the power electrical equipment employed is substantially lower than the overall output voltage. This leads in minimal conduction loss and excellent voltage step-up conversion efficiency.

Binti et al. (2016) proposed the I-D voltage feedback controller for SEPIC converter, a modified PID. The algorithm is discrete domain modelled and then validated using MATLAB/Simulink simulation. The

findings demonstrate that the proposed controller can adjust for overshoot percentage (%OS) and achieve zero steady-state error in three transient cases: changing the voltage reference, modifying the input voltage for 10V, 12V, and 15V. When the input voltage is 10V, the SEPIC converter functions as a boost converter, with output voltage greater than input voltage. When the input voltage is 15V, the SEPIC converter converts to a buck converter since the output voltage is less than the input value. When the input voltage was 12V, the SEPIC converter produced the same voltage output.

Using a tiny full spectrum simulator, Upamanyu et al. (2016) created current controlled voltage source inverter-based power hardware in loop simulation (mini-FSS). Using the PHIL simulation platform, a synchronous generator with constant frequency and constant excitation feeding a three-phase resistive load was modelled. In mini-FSS, a voltage source inverter is implemented as a three phase current amplifier to amplify the currents simulated by a synchronous generator. A current control method for the voltage source inverter based on a proportional integral (PI) controller has been devised. The performance of the current controller is evaluated for sinusoidal and step responses. The existing controller's performance in tracking the test signals is judged to be sufficient.

Model-based predictive control for PMBLDC drive was developed by Darba et al. (2016). The model predictive control technique regulates the speed of a high bandwidth BLDC drive with disturbance rejection features. The suggested system was developed by the authors using the SPARTAN 3E 1600 field-programmable gate-array FPGA board. The suggested solution has a disadvantage in that the FPGA board is expensive.

Wang et al. (2017) create a SEPIC using a half-bridge LLC resonant converter. This architecture lowers system costs while increasing dependability. Switching losses are minimised because the LLC resonant component retains soft switching characteristics. System bus voltage may be maintained low in high-power LED driving systems by carefully selecting characteristics. To validate theoretical analysis, certain tests with a 100-W prototype are carried out. The obtained power factor was as high as 0.99, and the efficiency is up to 92% at full load due to soft-switching operations.

To alleviate some of the limitations of the standard cascaded boost-SEPIC DC-DC converter, Lee et al. (2017) employed a zero-ripple input current high step-up boost-SEPIC DC-DC converter with decreased switch voltage stress. The auxiliary circuit at the boost stage of the converter considerably reduces input current ripple, and the voltage gain is boosted by employing the turn ratio of a connected inductor. Moreover, the clamping circuit reduces switch voltage stress at the SEPIC stage, and the leakage inductor alleviates the output diode's reverse-recovery difficulty.

Muntasir Alam et al. (2017) suggested a PWM-controlled hybrid resonant bridgeless AC-DC Power Factor Correction (PFC) boost converter. The proposed Paru Co., Ltd Korea 2018, PARU Technology Dual Axis Tracker (PST-2AL) has a surface size of 85 m2 with 49 modules of cells mounted in the surface area. Without modules, the structure weighs 1970 kg. The system's disadvantage is that it is not feasible to raise the longitudinal, and the rated power of the azimuth slewing motor is high.

Junming Zhang (2017) suggested a hybrid PFC converter with low output voltage and continuous input current by merging step-up PFC and

step-down (Buck) PFC converters. The author has designed an improved peak current control technique that enables universal input range; a 150-W prototype has also been created and theoretically validated.

Jayachandran et al. (2017) introduce an air conditioning One Cycle Controlled (OCC) Bridge-less (BL) SEPIC converter fed Brush-Less DC (BLDC) motor drive. Its drive's speed is controlled by a three-phase Voltage Source Inverter using Pulse Amplitude Modulation (PAM) (VSI). The DC bus voltage fluctuation through duty ratio modulation of BL-SEPIC converter switches facilitates pulse amplitude modification. To manage the duty ratio of the BL-SEPIC converter, a nonlinear approach known as One Cycle Control (OCC) is utilised. Auto shaping of supply current is accomplished by constructing a BL-SEPIC converter to operate in Discontinuous Inductor Current Mode (DICM). The Total Harmonic Distortion (THD) of the supply current is kept within the IEC-61000-3-2 limitations.

Bae et al. (2017) describe a design and control of a rail mover system for a wide-area security system. On the rail surface, a geared BLDC (Brushless DC) motor drives the rail mover. The rail mover body's position must be maintained at the right position when operating on the rail surface. The BLDC motor with hall sensor is utilised to regulate the position in this research. Because the hall sensor's speed calculation is inaccurate in the low speed area, precise position control is difficult. Additionally, due to the slip effect on the rail surface and driving roller, the real position and the motor position are not the same. This work proposes an accurate micro-angle control technique in the low speed range and a slip compensator to address these issues. The two sensors attached to the mover's side are utilised to adjust for slip mistake while going forward and backward.

Experiments on the built rail mover system validate this control technique and designed mover.

Kommula et al. (2017) introduce a SEPIC-fed brushless dc motor (BLDCM) with a torque ripple reduction strategy for improving power factor at supply mains and decreasing torque ripples. The speed of BLDCM is controlled by adjusting the dc link voltage. In general, the existence of ripple in commutation torque is caused by current ripple. Ripple in current and commutation torque can be minimised by installing an extra voltage source in the non-commutating phase. The suggested BLDCM drive may be configured to function with a wide speed range control, improved power quality at AC mains, and low torque ripples. The suggested SEPIC with torque ripple reduction approach for BLDCM is developed and simulated in the Matlab/Simulink environment. Lastly, the suggested BLDCM drive's efficacy is confirmed.

V. Viswanathan and Jeevananthan Seenithangom (2018) suggested a SEPIC converter with high static gain and low switching voltage stress; moreover, the converter is employed for torque ripple. In the BLDC drive, the authors employed a three-level NPC inverter. The suggested SEPIC converter is not used to increase power factor.

Zhang et al. (2019) designed and analysed the double-axis gadget (mechanical structure). The Finite Element Method was used to generate the parameterized model (FEM). The static analysis was performed to determine the displacement and stress distributions, as well as the stress evaluation, which was performed under various operating situations. The start-up of fulfilling the stress intensity, the lightweight, was completed, and this served as the foundation for the device's prototype test. This study

covers improved design working procedures that were carried out using a mathematical model, generated the Finite Element Model (FEM), applied the boundary conditions, and calculated and evaluated the stress. The prototype model's tracking precision is a bit greater, and the full load of the moving structure is in two key locations, which may lead to failure at times.

Nasir, Ab-Kadir, and co. (2019) PV panels are particularly susceptible to direct and indirect lightning, as well as other surge overvoltages, and the proper rating of Surge Protection Device (SPD) must be fitted to prevent electrical system damage. The suggested solar tracker system includes a device of type II class (lightning + surge voltage protection).

Lim and co. (2020) Large-scale dual-axis sun tracking device with several row elevation structures and a vertical-axis rotating platform. The installation power is 60 kWp, the diameter is 35 m, the transmission mechanism rotates the entire rotating platform, an AC motor (750 WAC) with a gearbox, 22 DC motors (15 WDC) for elevation movements, cylindrical pins, and a double layer pin-gear, which are the new design concept is implemented in a large-scale dual axis tracking system. The energy converter lessens the need for a front-end diode bridge rectifier. Because the switches share the PWM gating signal, no additional circuitry for sensing positive or negative ac input is necessary. The author created a 650-W prototype with a switching frequency of 70 kHz and a dc output voltage of 400 volts.

Nasib Khadka, Aayush Bista, and colleagues (2020) describe numerous cleaning technologies that have been created and are still in use today. In the suggested method, manual cleaning is performed once a month using water wash.

William Cai et al. (2021) provide a summary of current research and technological advances in electric motor systems and electric powertrains for new energy vehicles. Through the analysis and comparison of direct current motors, induction motors, and synchronous motors, it is discovered that permanent magnet synchronous motors have superior overall performance; when compared to converters with Si-based IGBTs, converters with SiC MOSFETs have significantly higher efficiency and increase driving mileage per charge. Moreover, the advantages and disadvantages of various control schemes and algorithms are presented. Lastly, a technical roadmap for the next 15 years is provided, including the important materials and components at each time frame for the traction motor, power electronic converter, and electric powertrain.

Maksim Sitnikov et al. (2021) study the major techniques of boosting the efficiency of electromechanical converters as well as new types of materials utilised in such devices. The economic ramifications and causes for the shift to extremely energy efficient electrical machines, as well as the introduction of special electrical machines in serial and mass manufacturing, are given specific consideration.

T M Khalina et al. (2022) undertake research on an innovative semiconductor device for starting a three-phase induction motor from a single-phase network. The device simulation model generated in the Matlab Simulink environment allowed researchers to investigate the electromechanical features of an induction motor when powered by a single-phase network. The properties of the motor during operation from a three-phase and a single-phase network are compared. The data gathered from the investigation show that the created device may be utilised to start

and run a squirrel cage induction motor from a single-phase network. Simultaneously, the engine energy characteristics alter somewhat.

REFERENCES

1. Lee, B.K. and Ehsani, M. ―Advanced BLDC motor drive for low cost and high performance propulsion system in electric and hybrid vehicles‖, In Electric Machines and Drives Conference, 2001. IEMDC, pp.246-251, 2001.
2. Madani, S.M., Hao, L. and Toliyat, H.A. ―A low-cost four-switch BLDC motor drive with active power factor correction‖, In IECON 02 , IEEE 2002 28th Annual Conference of the Industrial Electronics Society, Vol.1, pp.579-584.
3. Ottman, G.K., Hofmann, H.F. and Lesieutre, G.A. ―Optimized piezoelectric energy harvesting circuit using step-down converter in discontinuous conduction mode‖, IEEE Transactions on Power Electronics, Vol.18, No.2, pp.696-703, 2003.
4. Ma, D., Ki, W.H., Tsui, C.Y. and Mok, P.K. ―Single-inductor multipleoutput switching converters with time-multiplexing control in discontinuous conduction mode‖, IEEE Journal of Solid-State Circuits, Vol.38, No.1, pp.89-100, 2003.
5. Reatti, A. &Kazimierczuk, M. K. ―Small-signal model of PWM converters for discontinuous conduction mode and its application for boost converter‖, IEEE Transactions on Circuits and Systems I: Fundamental Theory and Applications, Vol.50, No.1, pp.65-73, 2003.

6. Gopalarathnam, T. and Toliyat, H.A. ―A new topology for unipolar brushless DC motor drive with high power factor‖, IEEE Transactions on Power Electronics, Vol.18, No.6, pp.1397-1404, 2003.
7. Chung, H.H., Tse, K.K., Hui, S.R., Mok, C.M. and Ho, M.T. ―A novel maximum power point tracking technique for solar panels using a SEPIC or Cuk converter‖, IEEE Transactions on Power Electronics, Vol.18, No.3, pp.717-724, 2003.
8. Kumar, M., Singh, B. and Singh, B.P. ―Single Current Sensor based speed control of PMBLDC using DSP‖, IE Journal, Vol.86, pp.17-21, 2005.
9. Krishnan, R., Park, S.Y, and Ha, K. ―Theory and Operation of a Four Quadrant Switched Reluctance Motor Drive With a Single Controllable Switch—The Lowest Cost Four-Quadrant Brushless Motor Drive‖, IEEE Transactions on Industry Applications, Vol.41, No.4, pp.1047 -1055, 2005.
10. Fuengwarodsakul, N.H., Menne, M., Inderka, R.B. and De Doncker, R.W. ―High-dynamic four-quadrant switched reluctance drive based on DITC. IEEE Transactions on Industry Applications, Vol.41, No.5, pp.1232-1242, 2005.
11. Axelrod, B., Berkovich, Y. and Ioinovici, A. ―Hybrid switched capacitor-Cuk/Zeta/Sepic converters in step-up mode‖, IEEE International Symposium on Circuits and sytesm, pp. 1310-1313, 2005.
12. Veerachary, M. Power tracking for nonlinear PV sources with coupled inductor SEPIC converter‖, IEEE Transactions on Aerospace and Electronic Systems, Vol.41, No.3, pp.1019-1029, 2005.

13. Urasaki, N., Senjyu, T., Uezato, K. and Funabashi, T. ―An adaptive dead-time compensation strategy for voltage source inverter fed motor drives‖, IEEE Transactions on Power Electronics, Vol.20, No.5, pp.1150-1160, 2005.
14. Iqbal, A. and Levi, E. Space vector modulation schemes for a five phase voltage source inverter‖, In Power Electronics and Applications, 2005 European Conference on, pp. 12-pp, 2005.
15. Kwon, J.M., Choi, W.Y., Lee, J.J., Kim, E.H. and Kwon, B.H. Continuous-conduction-mode SEPIC converter with low reverse recovery loss for power factor correction‖, IEE Proceedings-Electric Power Applications, Vol.153, No.5, pp.673-681, 2006.
16. Sagiroglu, S., Colak, I. and Bayindir, R. ―Power factor correction technique based on artificial neural networks‖, Energy Conversion and Management, Vol.47, No.18, pp.3204-3215, 2006.
17. Mohamed, Y.A.R.I. and Elsaadany, E.F. ―An improved deadbeat current control scheme with a novel adaptive self-tuning load model for a three-phase PWM voltage-source inverter‖, IEEE Transactions on Industrial Electronics, Vol.54, No.2, pp.747-759, 2007.
18. Ozturk, S.B., Yang, O. and Toliyat, H.A. ―Power factor correction of direct torque controlled brushless DC motor drive‖, In Industry Applications Conference, 2007 42nd IAS Annual Meeting. Conference Record, pp. 297-304, 2007.
19. Chen, J., Guo, Y. and Zhu, J. ―Development of a High-Speed Permanent-Magnet Brushless DC Motor for Driving Embroidery Machines‖, IEEE Transactions on Magnetics, Vol.43, No.11, pp. 4004–4009, 2007.
20. Afjei, E., Hashemipour, O., Saati, M.A. and Nezamabadi, M.M. ―A New Hybrid Brushless DC Motor/Generator without Permanent

Magnet‖, IJE Transactions B: Applications, Vol.20, No.1, pp.77-86, 2007.

21. Kim, N., Toliyat, H.A., Panahi, I.M. and Kim, M.H. ―BLDC Motor Control Algorithm for Low-Cost Industrial Applications‖, In Applied Power Electronics Conference, Texas, pp.1400-1405, 2007.
22. Hu, Q., Lu, Z. and Qian, Z. ―Research on a Novel Close-loop Speed Control Technique of Brushless DC Motor‖, In Power Electronics Specialists Conference, pp.2575-2578, 2007.
23. Vazquez, N., Estrada, L., Hernandez, C. and Rodriguez, E. ―The tapped-inductor boost converter‖, IEEE International Symposium on Industrial Electronics (ISIE), pp.538-543, 2007.
24. Ye, Z., Greenfeld, F. and Liang, Z. ―Design considerations of a high power factor SEPIC converter for high brightness white LED lighting applications‖, In Power Electronics Specialists Conference, pp. 2657- 2663, 2008.
25. Han, Q., Samoylenko, N. and Jatskevich, J. ―Average-Value Modeling of Brushless DC Motors With 120º Voltage Source Inverter‖, IEEE Transactions on Energy Conversion, Vol.23, No.2, pp.423-432, 2008.
26. Nasiri, A., Nie, Z., Bekiarov, S.B. and Emadi, A. ―An on-line UPS system with power factor correction and electric isolation using BIFRED converter‖, IEEE Transactions on Industrial Electronics, Vol.55, No.2, pp.722-730, 2008.
27. Park, et al. (2008) "Integrated boost-sepic converter for high step-up applications‖" In Power Electronics Specialists Conference, pp. 944-950, 2008.
28. Subudhi, B, Kumar, A & Jena, D 2008, 'dSPACE implementation of fuzzy logic based vector control of induction motor', Proceedings of IEEE Region 10 Conference, pp.1-6.

29. Man, T.Y., Mok, P.K. and Chan, M.J. A 0.9-V input discontinuousconduction- mode boost converter with CMOS-control rectifier‖, IEEE Journal of Solid-State Circuits, Vol.43, No.9, pp.2036 2046, 2008.
30. Kim, et al. (2008) "Integrated boost-sepic converter for high step-up applications‖" In Power Electronics Specialists Conference, pp. 944-950, 2008.
31. Wang, F., Shen, W., Boroyevich, D., Ragon, S., Stefanovic, V. and Arpilliere, M. Voltage source inverter. IEEE Industry Applications Magazine, Vol.15, No.2, pp.24-33, 2009.
32. Chiang, S.J., Shieh, H.J. and Chen, M.C. ―Modeling and control of PV charger system with SEPIC converter‖, IEEE Transactions on Industrial Electronics, Vol.56, No.11, pp.4344-4353, 2009.
33. Miller et al. (2009) Impact of Soiling and Pollution on PV Generation Performance Loss Due to Pollution", pp 1-5.
34. Bo-cheng, B., Jianping, X. and Zhong, L. ―Mode shift and stability control of a current mode controlled buck-boost converter operating in discontinuous conduction mode with ramp compensation‖, Chinese Physics B, Vol.18, No.11, pp.4742, 2009.
35. Mishra, M.K. and Karthikeyan, K. ―An investigation on design and switching dynamics of a voltage source inverter to compensate unbalanced and nonlinear loads‖, IEEE Transactions on Industrial Electronics, Vol.56, No.8, pp.2802-2810, 2009.
36. Zhang, F. and Yan, Y. ―Selective harmonic elimination PWM control scheme on a three-phase four-leg voltage source inverter‖, IEEE Transactions on Power Electronics, Vol.24, No.7, pp.1682-1689, 2009.
37. Rahimi, A.M. and Emadi, A. Discontinuous-conduction mode DC/DC converters feeding constant-power loads‖, IEEE

Transactions on Industrial Electronics, Vol.57, No.4, pp.1318-1329, 2010.

38. Madhusudhana Rao, G., SankerRam, B.V., Kumar, B.S. and Kumar, K.V. Speed Control of BLDC Motor using DSP‖, International Journal of Engineering Science and Technology, Vol.2, No.3, pp.143- 147, 2010.
39. Li, J., Zhang, H., Wan, Q., Liu, J. and Zhang, H. ―A novel charging control for flywheel energy storage system based on BLDC motor‖, In Power and Energy Engineering Conference (APPEEC), 2010 Asia- Pacific, pp. 1-3, 2010.
40. Chiu, C.L., Chen, Y.T., Liang, Y.L. & Liang, R.H. ―Optimal driving efficiency design for the single phase BLDC fan motor‖, IEEE Transactions on Magnetics, Vol.46, No.4, pp.1123-1130, 2010.
41. Sue, S.M., Huang, Y.S., Syu, J.S. and Sun, C.Y. ―A bi-directional power flow IPM-BLDC motor drive for electrical scooters‖, In Industrial Electronics and Applications, pp.1330-1334, 2010.
42. Demelo, P.F., Gules, R., Romaneli, E.F.R. and Annunziato, R.C. ―A modified SEPIC converter for high-power-factor rectifier and universal input voltage applications‖, IEEE Transactions on Power Electronics, Vol.25, No.2, pp.310-321, 2010.
43. Singh, B. and Singh, S. ―Single-phase power factor controller topologies for permanent magnet brushless DC motor drives‖, IET Power Electronics, Vol.3, No.2, pp.147-175, 2010.
44. Rockhill, A.A., Liserre, M., Teodorescu, R. and Rodriguez, P. Gridfilter design for a multimegawatt medium-voltage voltage-source inverter‖, IEEE Transactions on Industrial Electronics, Vol.58, No.4, pp.1205-1217, 2011.

45. Zhang, X. and Spencer, J.W. ―Analysis of boost PFC converters operating in the discontinuous conduction mode‖, IEEE Transactions on Power Electronics, Vol.26, No.12, Pp.3621-3628, 2011.
46. Grote, T, Figge, H, Frohleke, N, Bocker, J & Schafmeister, F 2011,'Digital control strategy for multi-phase interleaved boundary mode and DCM boost PFC converters', Proceedings of Energy Conversion Congress and Exposition (ECCE), pp. 3186-3192.
47. Salah, W., Ishak, D. and Hammadi, K. PWM Switching Strategy For Torque Ripple minimization in BLDC motor‖, Journal of Electrical Engineering, Vol.62, No.3, pp.141–146, 2011.
48. Feyzi, M.R., Ebadpour, M., Niapour, S.K.M., Feizi, A. and Mousavi, R. A New Single Current Strategy for High-Performance Brushless DC Motor Drives‖, Canadian Conference on Electrical and Computer Engineering, Canada, pp.419 – 424, 2011.
49. Mahdavi, M. and Farzanehfard, H. Bridgeless SEPIC PFC rectifier with reduced components and conduction losses‖, IEEE Transactions on Industrial Electronics, Vol.58, No.9, pp.4153-4160, 2011.
50. Uno, M. and Tanaka, K. ―Single-switch cell voltage equalizer using multistacked buck-boost converters operating in discontinuous conduction mode for series-connected energy storage cells‖, IEEE Transactions on Vehicular Technology, Vol.60, No.8, pp.3635-3645, 2011.
51. Errabelli, R.R. and Mutschler, P. ―Fault-tolerant voltage source inverter for permanent magnet drives‖, IEEE Transactions on Power Electronics, Vol.27, No.2, pp.500-508, 2012.
52. Hu, J., Sagneri, A.D., Rivas, J.M., Han, Y., Davis, S.M. and Perreault, D.J. High-frequency resonant SEPIC converter with wide

input and output voltage ranges‖, IEEE Transactions on Power Electronics, Vol.27, No.1, pp.189-200, 2012.

53. Eke, R & Senturk, A 2012, 'Performance comparison of a double-axis sun tracking versus fixed PV system', Solar Energy, vol. 86, no. 9, pp. 2665-2672.

54. Ho, T.Y., Chen, M.S., Yang, L.H. and Lin, W.L. ―The design of a high power factor brushless DC motor drive‖, In Computer, Consumer and Control (IS3C), 2012 International Symposium , pp.345-348, 2012.

55. Lodhi, R & Thakur, P 2013, 'Performance & Comparison Analysis of Indirect Vector Control of Three Phase Induction Motor', International Journal of Emerging Technology and Advanced Engineering, vol.3,no.10, pp. 716-724.

56. Samyuktha, P 2013, 'Vector Control Drive of Permanent Magnet Synchronous Motor Using Resolver Sensor', International Journal of Computer Science Engineering (IJCSE), vol.2, no.4, pp.81 95.

57. Kaushik, J, Saha, PK & Panda, GK 2013, 'Vector Control of Permanent Magnet Synchronous Motor Based On Sinusoidal Pulse Width Modulated Inverter with Proportional Integral Controller', International Journal of Engineering Research and Applications, vol. 3,no.5, pp.913-917.

58. Lumbreras, RC 2013, Directable solar panel systems, Google Patents.

59. Dhamo, L &Spahiu, A 2013, 'Simulation Based Analysis of Two Different Control Strategies for PMSM', International Journal of Engineering Trends and Technology (IJETT), vol.4, no.4, pp.596-602.

60. Jose, L &Karthikeyan, KB 2013, 'A Comparative Study of Sinusoidal PWM and Space Vector PWM of a Vector Controlled

BLDC Motor', International Journal of Advanced Research in Electrical, Electronics and Instrumentation Engineering, vol.2, no.6, pp.2662-2668.

61. Carvalho, DR, Lacerda Filho, AF, Resende, RC, Possi, MA & Kruckeberg, JP 2013, 'An economical, two axes solar tracking system for implementation in Brazil', Applied Engineering in Agriculture, vol. 29, no. 1, pp. 123-128.
62. Li, L & Ping, L, 'A (2013) predictive digital-controlled algorithm for power factor correction converter', Proceedings of International Conference on Communications, Circuits and Systems, vol.2, pp.390-393.
63. Kessal, A &Rahmani, L 2013, 'Ga-Optimized Parameters of Sliding Mode Controller Based on Both Output voltage and Input Current With an Application in the PFC of AC/DC Converters', IEEE Transactions on Power Electronics, vol.29, pp.3159-3165.
64. Nesapriya, P &Rajalaxmi, S 2013, "Closed Loop Control of Bridgeless Cuk Converter Using Fuzzy Logic Controller for PFC Applications", World Academy of Science, Engineering and Technology. International Journal of Electrical, Robotics, Electronics and Communications Engineering, vol.7, no.11, pp.1042-1047.
65. Tibola, G. and Barbi, I. ―Isolated three-phase high power factor rectifier based on the SEPIC converter operating in discontinuous conduction mode‖, IEEE Transactions on Power Electronics, Vol.28, No.11, pp.4962-4969, 2013.
66. Behera, P, Manoj Kumar Behera & Amit Kumar, S 2014,'Comparative Analysis of scalar & vector control of Induction motor through Modeling& Simulation', International Journal of

Innovative Research in Electrical, Electronics, Instrumentation and Control Engineering, vol. 2, no. 4.pp.1340-1344

67. Bist, V & Singh, B 2014, ‘A Unity Power Factor Bridgeless Isolated Cuk Converter Fed Brushless-DC Motor Drive’, IEEE Transactions on Industrial Electronics, no. 99, pp.1-6.
68. Krishnan, PH &Arjun, M 2014, ‘Control of BLDC motor based on adaptive fuzzy logic PID controller’, Proceedings of IEEE International Conference on Green Computing Communication and Electrical Engineering, pp.1 – 5.
69. Hassaine, S, Moreau, S & Bensmaine, F 2014, ‘Design and hardware implementation of PMSM sliding mode control in SISO and MIMO cases’, Proceedings of IEEE 23rd International Symposium on Industrial Electronics, pp.762-767.
70. Ashmore, E ' Modular solar support assembly', U.S Patent No. 9134045. 15 Sep. 2015.
71. Griffith, DT, Moya, AC, Ho, CK & Hunter, PS 2015, 'Structural dynamics testing and analysis for design evaluation and monitoring of heliostats', Journal of Solar Energy Engineering, Transactions of the ASME, vol. 137, no. 2.
72. Maklakov, A.S., Radionov, A.A. and Gasiyarov, V.R., 2016, October. Power factor correction and minimization THD in industrial grid via reversible medium voltage AC drives based on 3L-NPC AFE rectifiers. In Industrial Electronics Society, IECON 2016-42nd Annual Conference of the IEEE pp. 2551-2556.
73. Eldin, SAS, Abd-Elhady, MS & Kandil, HA 2016, 'Feasibility of solar tracking systems for PV panels in hot and cold regions', Renewable Energy, vol. 85, pp. 228-233.
74. Singh, et al. (2016) "Power Factor Correction in single-ended primary inductance converter fed switched reluctance motor drive‖,

IEEE International Conference on Power Electronics, Intelligent Control and Energy Systems (ICPEICES), pp. 1-6, 2016.

75. Rao, J.V. Sepic converter FED BLDC drive with closed loop speed control‖, IEEE International Conference on Signal Processing, Communication, Power and Embedded System (SCOPES), pp. 1-7, 2016.

76. Lodh, T. and Majumder, T. ―A High Gain High Efficiency and Compact Isolated Sepic DC-DC Converter‖, In presentation at International Conference on Signal Processing, Communication, Power & Embedded Systems (SCOPES), pp. 1-6, 2016.

77. Binti Alias, A., Binti Azri, M. and Bin Jidin, A. ―A modified PID controller of SEPIC converter for excellent dynamic performance‖, IEEE International Conference on Power and Energy (PECon), pp. 423-427, 2016.

78. Upamanyu, K., Chaitanya, M., Narayanan, G. and Gurrala, G. ―Current controlled voltage source inverter based amplifier for power hardware in loop simulation using miniature full spectrum simulator‖, IEEE 7th International Conference on Power India (PIICON), pp. 1-6, 2016.

79. Darba, A., De Belie, F., D'haese, P. and Melkebeek, J.A., 2016. Improved dynamic behavior in BLDC drives using model predictive speed and current control. IEEE Transactions on Industrial Electronics, vol. 63 no.2, pp.728-740.

80. Wang, Y, A single-stage LED driver based on SEPIC and LLC circuits‖, IEEE Transactions on Industrial Electronics, Vol. 64, No. 7, pp. 5766 5776, 2017.

81. Lee, S.W. and Do, H.L. Zero-Ripple Input-Current High-Step-Up Boost–SEPIC DC–DC Converter With Reduced Switch-Voltage

Stress‖, IEEE Transactions on Power Electronics, Vol. 32, No. 8, pp. 6170-6177, 2017.

82. Alam, M., Eberle, W., Gautam, D.S., Botting, C., Dohmeier, N. and Musavi, F., 2017. A hybrid resonant pulse-width modulation bridgeless AC–DC power factor correction converter. IEEE Transactions on Industry Applications, vol. 53 no.2, pp.1406-1415.
83. Zhang, J., Zhao, C., Zhao, S. and Wu, X., 2017. A family of single phase hybrid step-down PFC converters. IEEE Transactions on Power Electronics, vol. 32, no.7, pp.5271-5281.
84. Jayachandran, S. and Vinatha, U. ―One cycle controlled bridge-less SEPIC converter fed BLDC motor drive‖, IEEE International Conference on Signal Processing, Informatics, Communication and Energy Systems (SPICES), pp. 1-6, 2017.
85. Bae, et al. (2017) "A design and control of rail mover with a hall sensor based BLDC motor‖, IEEE Conference and Exp Transportation Electrification Asia-Pacific (ITEC Asia-Pacific), pp. 1 6.
86. Kommula, B.N. and Kota, V.R. ―PFC based SEPIC converter fed BLDC motor with torque ripple minimization approach‖, International Conference on Electrical Engineering Congress (iEECON), pp. 1-4, 2017.
87. Viswanathan, V. and Seenithangom, J., 2018. Commutation Torque Ripple Reduction in the BLDC Motor Using Modified SEPIC and Three-Level NPC Inverter. IEEE Transactions On Power Electronics, vol. 33 no.1, pp.535-546.
88. Zhang, S. Li, C, Zhang, J, Miao, H & Zhang, Y 2019, 'Design and structural analysis of the Sun ray double axis tracking device', Journal of Solar Energy Engineering, vol. 141, ho. 4.

89. Nasir, MSM, Ab-Kadir, MZA, Radzi, MAM, Izadi, M, Ahmad, NI & Zaini, NH 2019, Lightning performance analysis of a rooftop grid-connected solar photovoltaic without external lightning protection system', Plos one, vol. 14, no. 7, pp. e0219326.
90. William Cai et al. (2021) "Review and Development of Electric Motor Systems and Electric Powertrains for New Energy Vehicles" Published: 25 February 2021 valum 4, pages3–22.
91. Maksim Sitnikov et al. (2021) "Trends and New Challenges in the Energy Efficiency of Electric Machines" Advances in Engineering Research, volume 213.
92. T M Khalina et al. (2022) "The development of an energy efficient electric drive for agricultural machines" Volume 1211, IXX International Scientific and Practical DOI 10.1088/1757-899X/1211/1/012018.

CHAPTER 3
ANALYSIS OF INDUCTION MOTOR DRIVE SYSTEMS

3.1 INDUCTION

In industry, the induction machine, particularly the cage rotor type, is most typically employed for variable speed applications. Adjustable speed drives use back-to-back AC to DC and DC to AC conversion to alter the speed. This conversion procedure introduces harmonics and reduces power factor at the supply end. It is now more important than ever to design and build a three-phase induction motor drive with higher power quality. A full report on the converter topologies is used for Power Factor Correction at the input side to eliminate harmonics and enhance power factor at the supply side.

3.2 OPERATION OF INDUCTION MOTOR DRIVE SYSTEM

An induction motor is an alternating current motor that works on the principle of electromagnetic induction. Because of their durability and brushless nature, they are commonly utilised in industrial drives. The squirrel cage induction motor is the most common form of electrical motor used in industry. The squirrel cage motor has many advantages, including.

1. Simple and tough construction. This translates to a low starting cost and great dependability for the consumer.
2. The combination of high efficiency and low maintenance costs leads in lower total operating expenses.

Squirrel cage motors speed depends upon various factors like applied frequency, pole pair number, and load torque. To reverse the machine's direction of rotation, the phase sequence to the motor must be changed. Their speed can be controlled with a variable frequency drive.

For adjustable speed applications, the induction machine, particularly the cage rotor type, is most commonly used in industry. In squirrel cage induction motors the rotor has squirrel cage like structure with shorted end rings and the stator has three-phase winding distributed sinusoidal. When ac voltages are applied to the three-phase stator winding it creates a magnetic field rotating at angular speed

$$\omega s = 4\pi fs/P$$

where
fs is the supply frequency in Hz and
P is the number of stator poles.

When the rotor rotates at an angular speed of ωr the conductors are subjected to a sweeping magnetic field, both voltage and current and mmf in the short-circuited rotor at a frequency (ωs - ωr)P/4π, known as the slip speed.

The interaction of air gap flux and rotor mmf produces torque. The per unit slip ω is defined as

$$S = \frac{\omega_{S-\omega_r}}{\omega_S}$$

Figure 3.1 shows the torque-speed curve. The various operating zones in the figure can be defined as plugging (1.0 < S< 2.0), motoring (0 < S< 1.0), and regenerating (S< 0). During normal motoring region, Te= 0 and S= 0, and as S increases Te also increases as a quasi-linear curve until breakdown, or maximum torque Tem is reached, Te decreases with the increase in S beyond this point.

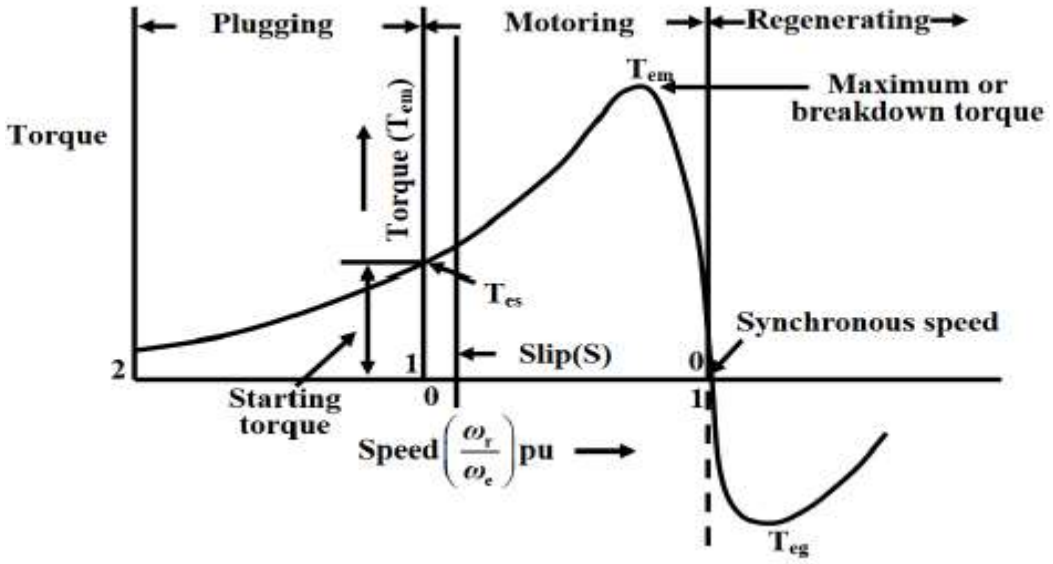

FIGURE 3.1 TORQUE-SPEED CURVE OF INDUCTION MOTOR

As the name implies, the machine functions as a generator in the regenerative zone. The rotor travels at supersynchronous speed in the same direction as the air gap flux, resulting in negative slip and negative or regenerating torque (Teg). Variable-frequency control aids in adjusting the machine stator frequency in order to reduce the rotor speed (ωe<ωr) and achieve regenerative braking. Figure 3.1 shows the torque speed characteristics. It can be observed that the magnitude and/or frequency of

the supply voltage may be changed at any rotor speed to get the appropriate torque.

An input Rectifier unit, an inverter unit, and a DC bus compose the Variable Frequency Drive. The supply voltage is linked to a rectifier unit, which receives AC power, and the three phase supply is supplied into a three phase full wave rectifier, which converts it to DC power. The DC bus has a filter element that filters out harmonics created during the AC to DC conversion. The last portion is an inverter section that includes six IGBTs (Insulated Gate Bipolar Transistors) that convert the filtered DC supply to a quasi sinusoidal wave of AC power that is linked to the induction motor. The input AC power is converted to DC, filtered, and then transformed to variable frequency DC by an inverter in a simple DC-link variable frequency motor controller. Because the synchronous speed of a motor is directly proportional to the supply frequency, the synchronous speed of the motor may be simply varied by adjusting the frequency value. This is the VFD's primary functioning phenomena.

3.3 BOOST CONVERTER WITH COMPOUND ACTIVE CLAMPING IN FOUR SWITCH THREE PHASE INVERTER FED INDUCTION MOTOR

The performance of a four switches three phase inverter (FSTPI) supplied induction motor with boost converter combined with compound active clamping is investigated in this chapter. The suggested converter is executed on a single phase supply, and its performance in terms of power factor, THD, and efficiency are evaluated. The active clamping branch of a converter is self-possessed by a clamping capacitor and an active switch connected in parallel with the resonant inductor. A voltage loop is formed in the circuit by the main switch, auxiliary switch, clamping capacitor,

boost diode, and output filter capacitor. During switching periods, the converter switching devices are expected to be in the ON state. As a result of clamping the voltage across the switch in the off state, a parasitic oscillation between the junction capacitance of the boost diode and the resonant inductor is removed.

3.4 COMPOUND ACTIVE CLAMPING (CAC) BOOST CONVERTER

Figure 3.2 depicts the CAC boost converter circuit. The boost converter circuit uses a bridge rectifier to rectify the alternating current source, two inductors L1 and L2, and two switches S1 and S3. L1 is a boost inductor; L2 and CC are utilised for soft switching S3 with a set duty cycle. The duty cycle of main switch S1 varies with the input voltage and is adjusted to get the desired output voltage. When S1 is activated, inductor L1 is energised, and when S1 is deactivated, the energy stored in L1 is supplied to the capacitor C0.

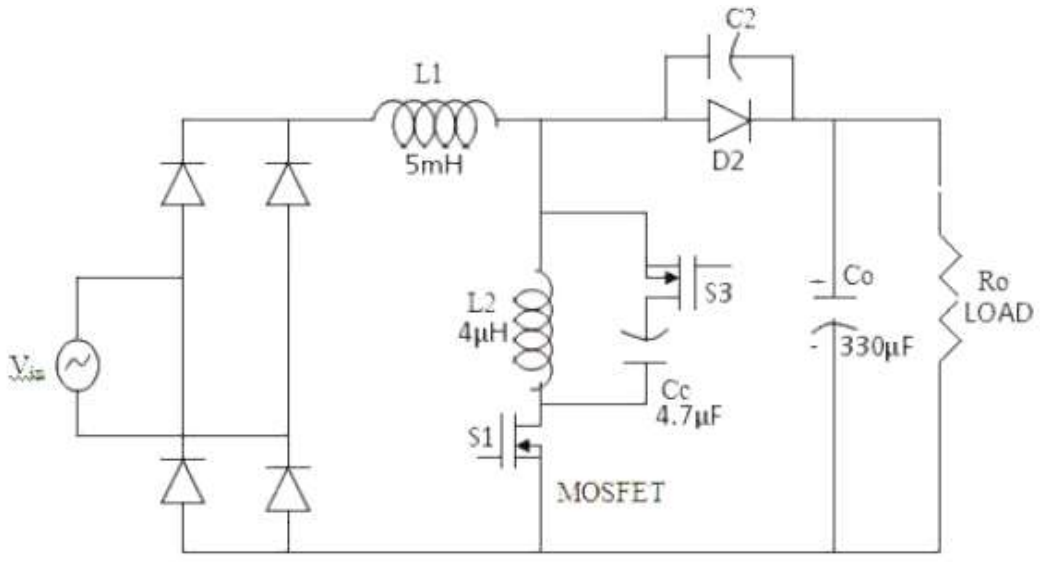

FIGURE 3.2 CAC BOOST CONVERTER CIRCUIT

The bridge rectifier is coupled via inductors L1, L2, and switch S1. When switch S1 is turned on, inductors L1 and L2 store energy, and switch S3, which is linked in parallel with inductor L2, operates as an auxiliary switch. Switch S1 is turned off in the next stage, and voltage across L2 appears across the load. Capacitors Cc and C0 are connected to switches S1 and S3, respectively, while capacitor C2 is connected to boost diode D2.

The input filter inductor L1 is selected to be very big so that the current iL does not change, allowing it to be regarded as a constant current source. When CC is high enough to eliminate voltage ripple, the filter capacitor CO can be represented as constant voltage sources. To a large degree, the resonant frequency of CC and L2 is lower than the working frequency of the converter. The suggested converter's main switch S1 and auxiliary switch S3 do not work in complimentary mode.

To clamp the voltage between main switch S1 and diode D2, auxiliary switch S3 is turned off for a brief period of time when both main switch S1 and diode D2 are commutating circuits; hence, the duty cycle of auxiliary switch S3 is fixed while the duty cycle of main switch S1 varies with input voltage. The entire design of the CAC Boost Converter circuit is provided in the appendix.

3.5 SIMULATION RESULTS

The boost diode is conducting prior to the initial stage, auxiliary switch S3 is switched off, and the current in L1 charges C3 paralleled and C1 paralleled with the main switch S1 discharges. At first, the voltage across S1 falls to zero, and the diode of S1 begins to conduct. Then, under

zero voltage, S1 is switched on. The voltage across S3 is held constant at Vo +Vcc. The current in D2 is falling at this stage, whereas the current in S1 is growing at the same pace as D2. The resonant inductor L1 determines the current changing rate.

Figure 3.3 depicts an FSTPI-fed induction motor circuit with a boost converter and compound active clamping. The boost inductor is inductor L1. S2 is soft switched using inductors L2 and Cc. S1's duty cycle is modified to provide the needed DC voltage at the inverter's three phase four switch input. When S1 is activated, the energy in the inductor L1 is stored, and when S1 is deactivated, the energy in the inductor is provided to the capacitor Co. Switch S2 works as an auxiliary switch when connected in parallel with the inductor. This eliminates resonance between L1 and the diode's internal capacitance D5.

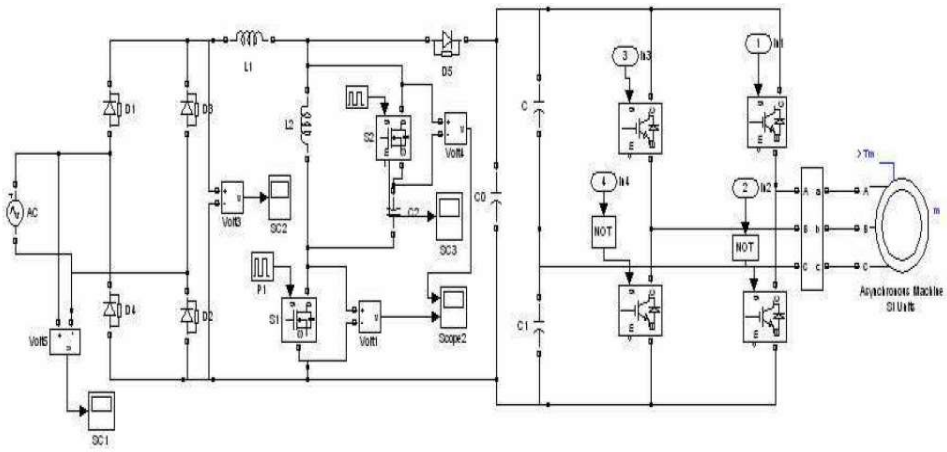

FIGURE 3.3 FOUR SWITCH THREE PHASE INVERTER FED INDUCTION MOTOR SYSTEM WITH COMPOUND ACTIVE CLAMPING

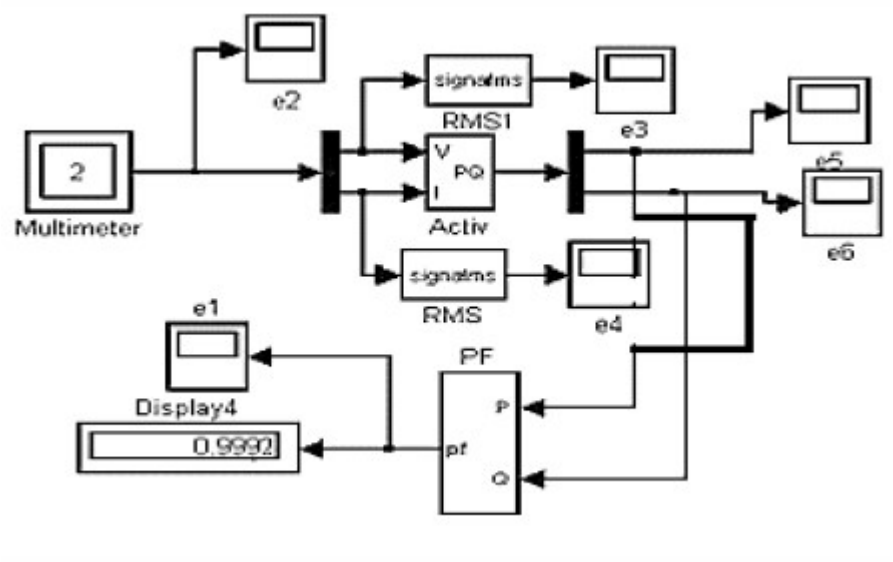

FIGURE 3.4 POWER FACTOR MEASUREMENT OF BOOST CONVERTER WITH COMPOUND ACTIVE CLAMPING

The power factor measuring circuit of a boost PFC converter is seen in Figure 3.4. When compared to the power factor of 0.990 (without active clamping) for the present soft switched PFC boost converter, the power factor attained is 0.999 (with compound active clamping). The power factor is enhanced by clamping the maximum voltage across the primary switch, and voltage ringing across the diode is eliminated. The switching pulses delivered to switches M1 and M2 are depicted in Figure 3.5. The phase voltage delivered to the three-phase induction motor is seen in Figure 3.6.

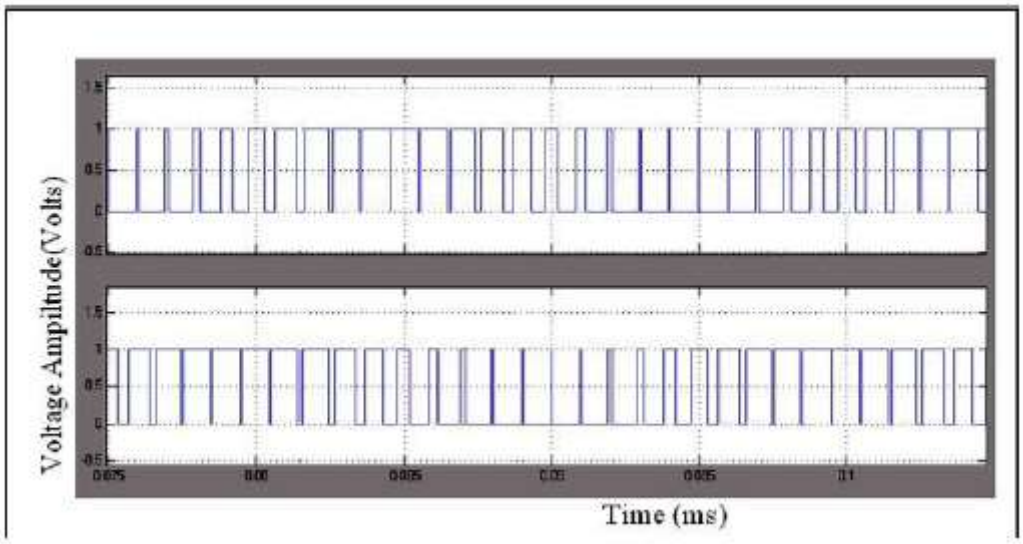

FIGURE 3.5 DRIVING PULSES FOR INVERTER

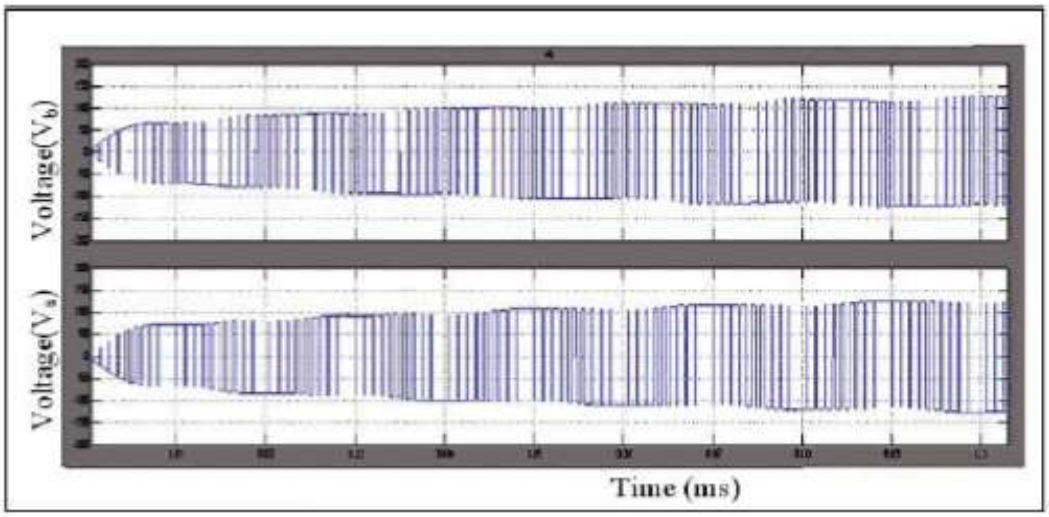

FIGURE 3.6 PHASE VOLTAGE OF INVERTER

Figure 3.7 depicts the efficiency of a three-phase induction motor with a boost converter and compound active clamping FSTPI. It is clear that the efficiency has increased to 95%. Switching losses are decreased in the proposed converter due to the use of a simple active snubber circuit, which provides zero voltage switching conditions for all switches. Because of the decreased number of components, it is more efficient and ideal for practical applications such as AC drive systems, power factor correction, UPS, and induction heating. As shown in Figure 3.8, the performance of

the developed converter outperforms that of the current PFC boost converter.

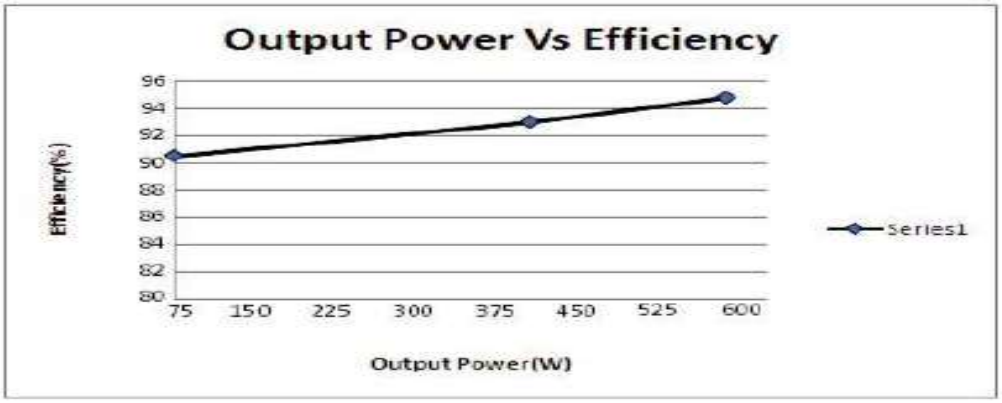

FIGURE 3.7 OUTPUT POWER VS EFFICIENCY OF BOOST CONVERTER WITH COMPOUND ACTIVE CLAMPING FSTPI FED INDUCTION MOTOR

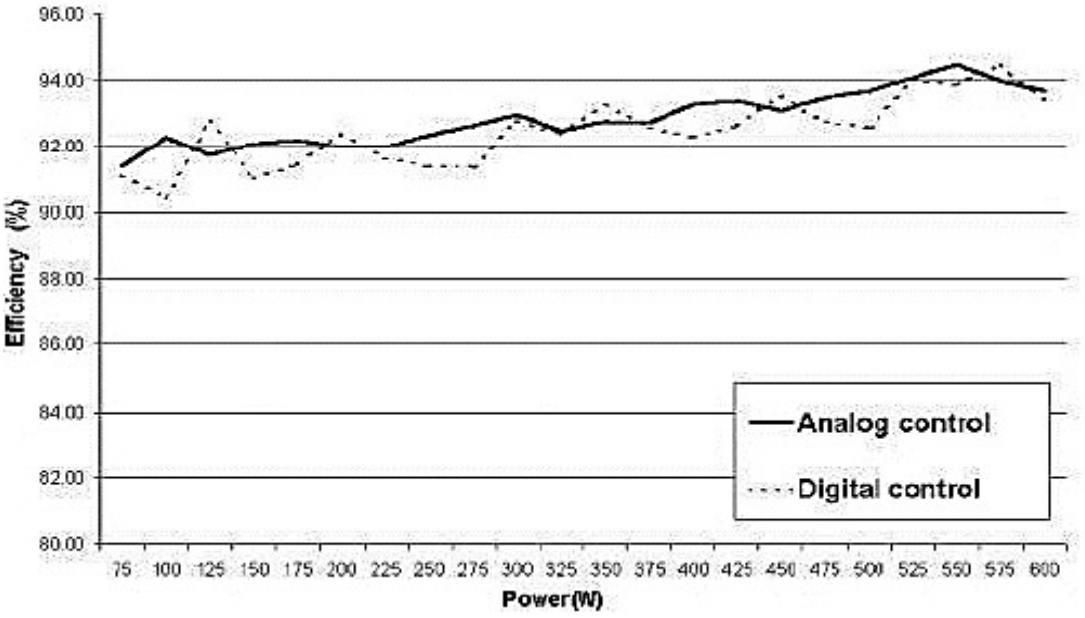

FIGURE 3.8 OUTPUT POWER VS EFFICIENCY OF SOFT SWITCHED PFC BOOST CONVERTER

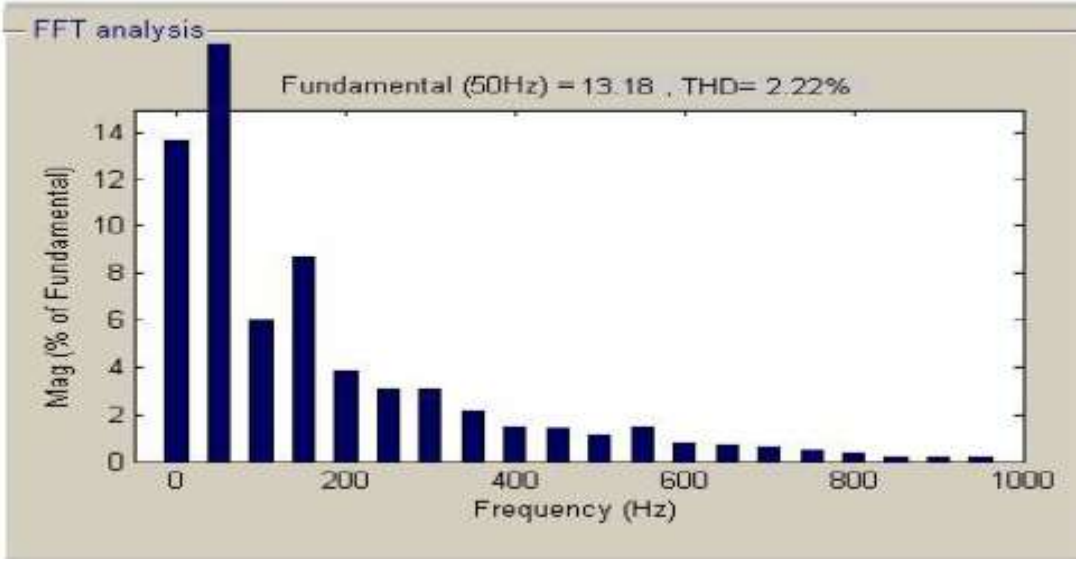

FIGURE 3.9 THD OF INPUT CURRENT FOR BOOST CONVERTER WITH COMPOUND ACTIVE CLAMPING FSTPI FED INDUCTION MOTOR

Figure 3.9 depicts the FFT analysis for the current of a boost converter with a compound active clamping FSTPI supplied induction motor. THD is decreased to 2.22% compared to 4.85% in the case of the previous soft switched PFC boost converter built by Luiz Henrique Silva Colado Barreto (2005). Table 3.1 compares the performance of a planned converter to that of an existing CAC converter.

TABLE 3.1

PERFORMANCE COMPARISON BETWEEN EXISTING CONVERTER AND PROPOSED CAC CONVERTER

PARAMETER	PERFORMANCE OF EXISTING CONVERTER	PERFORMANCE OF PROPOSED CAC CONVERTER
Efficiency	92%	94%
Power Factor	0.94	0.998

THD	4.85%	2.22%

CHAPTER 4
ANALYSIS OF POWER CONVERTERS FOR BLDC DRIVE SYSTEMS

4.1 INTRODUCTION

Brushless DC (BLDC) motor drives have grown in popularity in recent years due to their suitability for a wide range of low and medium power applications such as household appliances, medical equipment, position actuators, Heating, Ventilation, and Air Conditioning (HVAC), motion control, and transportation. These drives have great efficiency, dependability, durability, and outstanding performance across a wide range of speed control. The BLDC motor cannot be connected directly to the supply and must be driven by a drive consisting of VSI controlled by an electronic commutation system. Harmonics are introduced into the main power supply and power factor issue by the electronic commutation system and rectification procedure. Power Factor Correction (PFC) converters are used to improve the power quality and power factor of the alternating current mains.

4.2 PFC BUCK-BOOST CONVERTER FED PMBLDC MOTOR

Single stage PFC circuits are currently experiencing significant hurdles in order to boost output power capabilities with optimal component ratings. A conduction-mode buck-boost PFC converter with anon-inverting dc output has been proposed for wide input voltage range applications. This

chapter is about digitally simulating a Power Factor Correction (PFC) buck boost converter for variable speed driving using a PMBLDC motor. The PFC is used in conjunction with a single-phase AC-DC converter architecture, which is then followed by a buck-boost bridge converter. A PI controller controls the DC link voltage, which is proportional to the desired speed of the PMBLDC motor, to accomplish speed control.

This chapter describes the average current control strategy for the cascaded buck-boost converter using two loops connected to the buck boost converter. The power factor of the circuit is improved by comparing the input current with a sinusoidal current reference in the inner current loop, and the output voltage is controlled by the outer loop. Its drive ensures better power factor, excellent precision, stable operation, and increased efficiency. The PFC converter has non-inverted DC output voltage and can work in both step-up and step-down modes. The suggested topology is capable of working in both continuous and discontinuous conduction modes for high-power applications. A larger power factor may be attained over a wide range of output voltage by employing a buck boost converter. There are two working modes in a buck-boost converter that allow both step-up and step-down voltage conversion based on the operation of the switches, namely buck, boost, and buck-boost modes. The suggested technology, which combines buck and boost modes in a single power stage, provides an easy way to achieve unity power factor for an AC/DC converter.

4.3 MATHEMATICAL MODEL OF THE PFC BUCK- BOOST CONVERTER

Figure 4.1 depicts a proposed buck-boost converter, which is an uncontrolled diode bridge followed by a Buck-Boost Converter (BBC)

with the storage elements Capacitor C with voltage c V, inductor L with current L I output voltage Vo, Supply voltage E, output current Io, magnitude current Im, power switch S, and load resistance R. Based on the duty ratio 'd,' the converter provides an output voltage that is more or less than the input voltage. When switch S is turned on, the inductor current L I rises and diode D fails to conduct. When the switch S is turned off, the inductor current flows through the diode.

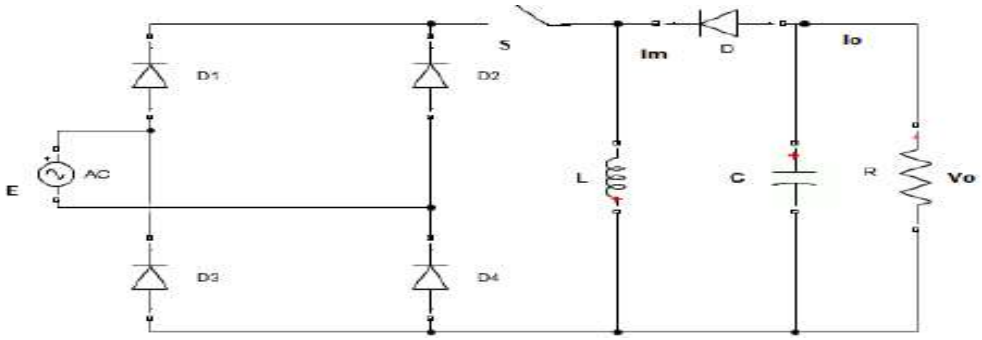

FIGURE 4.1 PFC BUCK BOOST CONVERTER TOPOLOGY

State-space models provide a broad and solid foundation for dynamic modelling of diverse systems, including power converters. State space models may be used to create linear control loops and mimic steady-state and dynamic behaviour using feedback control loops. The buck-boost converter's voltage transfer gain is

$$\frac{V_0}{E} = -\frac{d}{(1-d)} \qquad (4.1)$$

The corresponding current transfer gain is

$$\frac{I_0}{I_m} = \frac{(1-d)}{d} \qquad (4.2)$$

The switch conducts and the diode does not conduct in the on-duration circuit setup. Equations 4.9 exhibit state equations indicating the on-interval circuit setup.

$$\frac{di_L}{dt} = \frac{E}{L} \tag{4.3}$$

$$\frac{dV_c}{dt} = -\frac{1}{RC}V_c \tag{4.4}$$

$$\begin{bmatrix} \frac{di_L}{dt} \\ \frac{dV_c}{dt} \end{bmatrix} = \begin{bmatrix} 0 & 0 \\ 0 & \frac{-1}{RC} \end{bmatrix} \begin{bmatrix} i_L \\ V_c \end{bmatrix} + \begin{bmatrix} \frac{1}{L} \\ 0 \end{bmatrix} E \tag{4.5}$$

The switch opens and the diode conducts in the off-duration circuit setup. The off-circuit topology's state equations are provided as

$$\frac{di_L}{dt} = -\frac{V_c}{L} \tag{4.6}$$

$$\frac{dV_c}{dt} = \frac{1}{C}i_L - \frac{1}{RC}V_c \tag{4.7}$$

$$\begin{bmatrix} \frac{di_L}{dt} \\ \frac{dV_c}{dt} \end{bmatrix} = \begin{bmatrix} 0 & \frac{-1}{L} \\ \frac{1}{C} & \frac{-1}{RC} \end{bmatrix} \begin{bmatrix} i_L \\ V_c \end{bmatrix} \tag{4.8}$$

Using the state space averaging model the system model is written as

$$\begin{bmatrix} \frac{di_L}{dt} \\ \frac{dV_c}{dt} \end{bmatrix} = \begin{bmatrix} 0 & -\frac{1+d}{L} \\ \frac{1-d}{C} & \frac{-1}{RC} \end{bmatrix} \begin{bmatrix} i_L \\ V_C \end{bmatrix} + \begin{bmatrix} \frac{1}{L} \\ 0 \end{bmatrix} E \tag{4.9}$$

4.3.1 SIMULATION RESULTS

MATLAB simulation was performed using the intended circuit parameters, and the results are provided below. The magnitude of the reference speed was set to 1800 rpm, and the load torque was varied at time t=1 sec. Buck-boost converters Figure 4.2 depicts a Simulink model. Figure 4.3 depicts the Simulink model of a closed loop controlled PMBLDC motor with a PFC buck boost converter and a PI controller. To enhance the power factor, a buck boost converter is employed at the input. Figure 4.4 depicts the AC input voltage and current waveforms. Figure 4.5 depicts the step change in load torque.

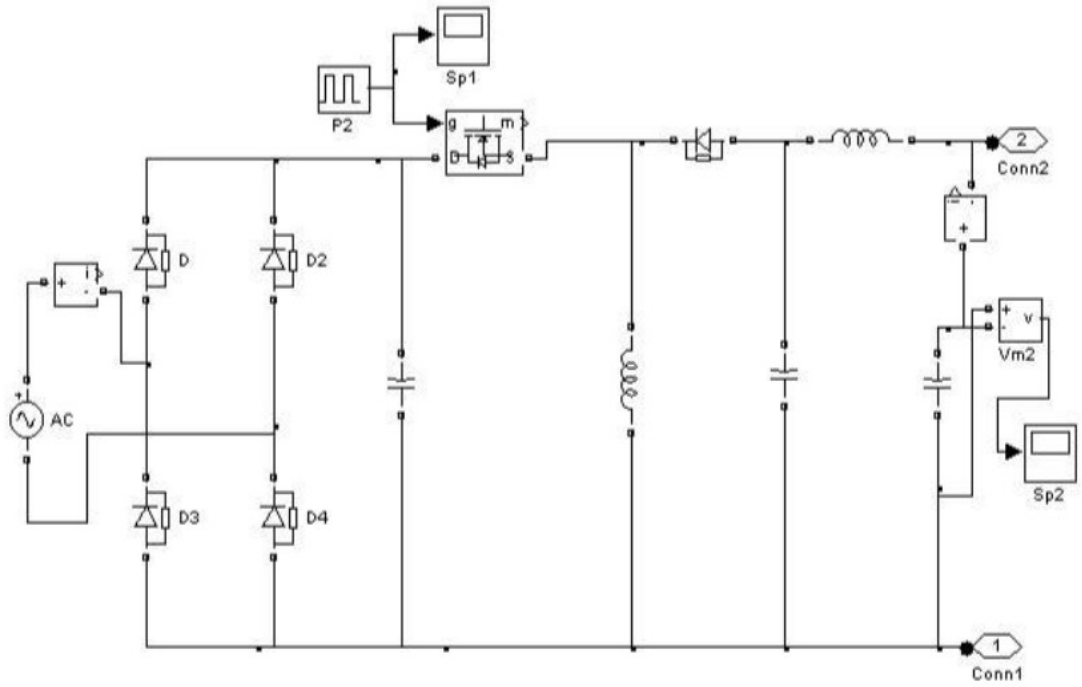

FIGURE 4.2 BUCK-BOOST CONVERTER

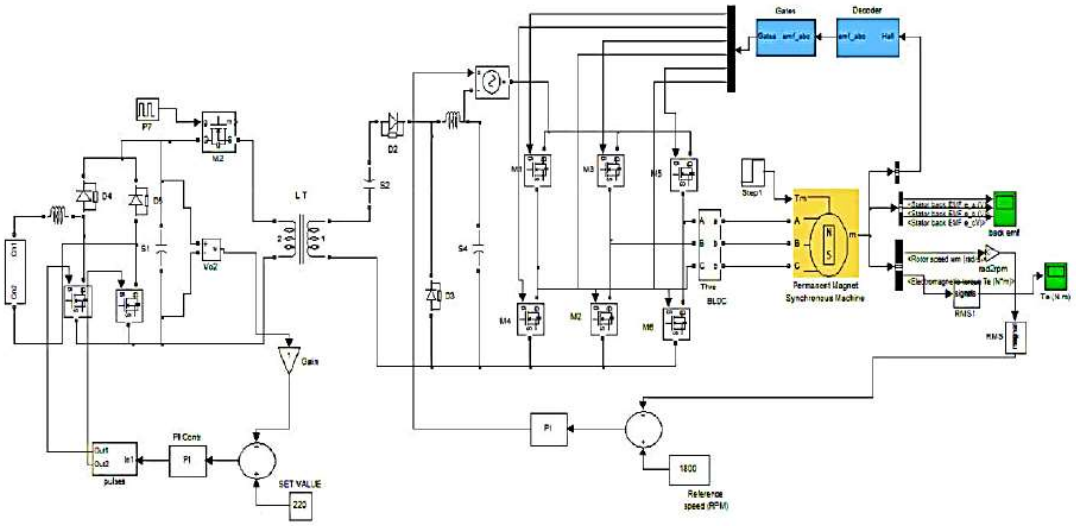

FIGURE 4.3 CLOSED LOOP SPEED CONTROL OF THE PMBLDC MOTOR WITH PFC BUCK-BOOST CONVERTER

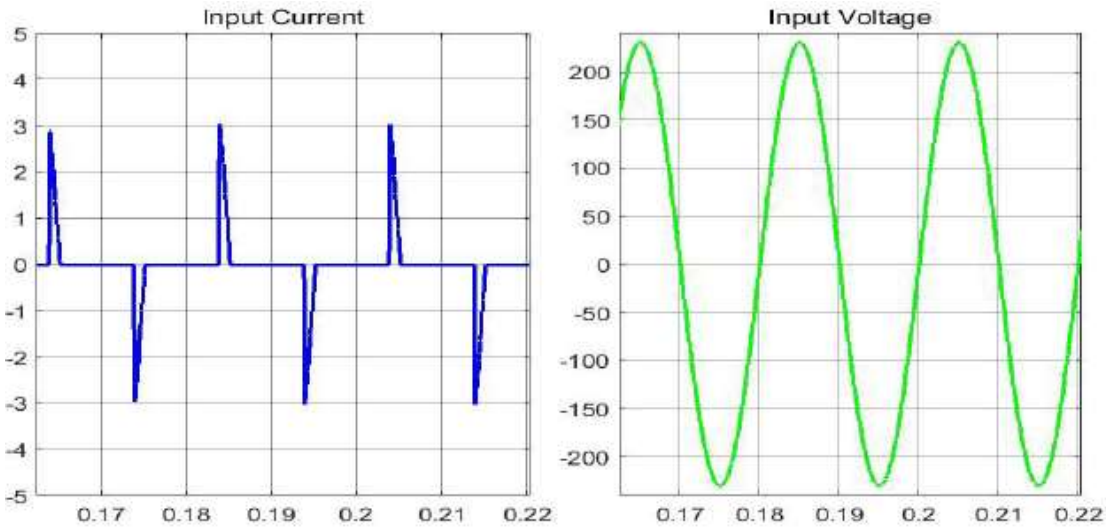

FIGURE 4.4 INPUT VOLTAGE AND CURRENT WAVEFORMS

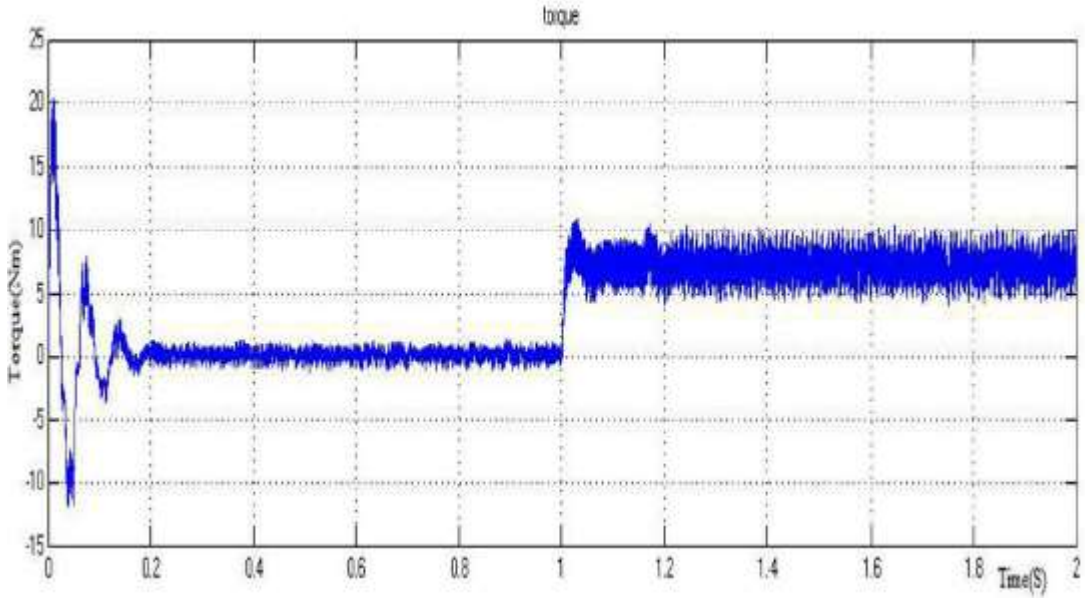

FIGURE 4.5 STEP CHANGE IN THE LOAD TORQUE APPLIED AT T=1 SEC

The closed loop mechanism returns the speed to normal and keeps it steady even throughout the load torque. The speed of the PMBLDC motor is maintained constant, as shown in Figure 4.6. The THD is only 4.71%, according to the FFT analysis in Figure 4.7, but the power factor is greater with the buck-boost converter fed PMBLDC drive, and it is higher than with the PFC bridgeless boost converter fed PMBLDC drive.

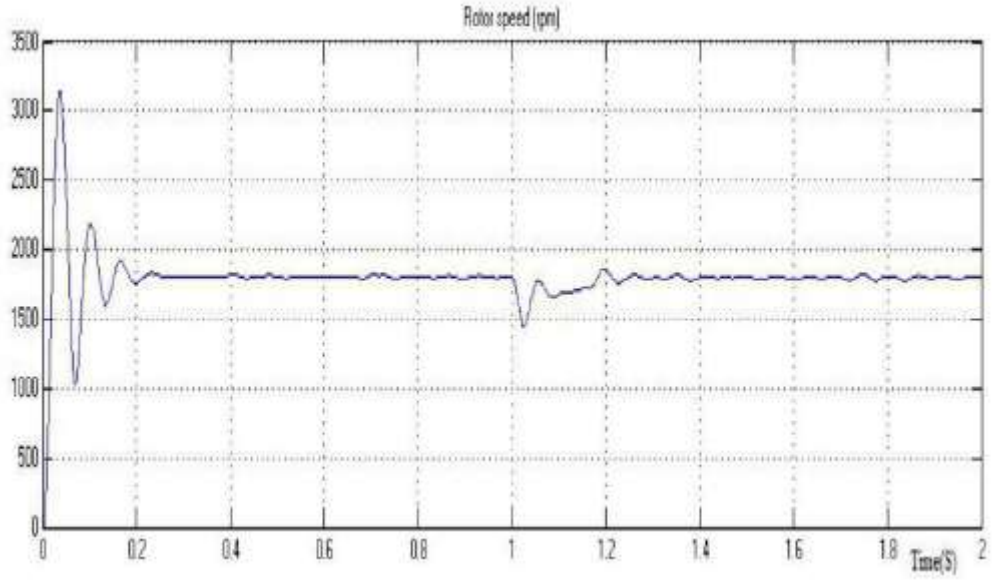

FIGURE 4.6 SPEED RESPONSE CURVE

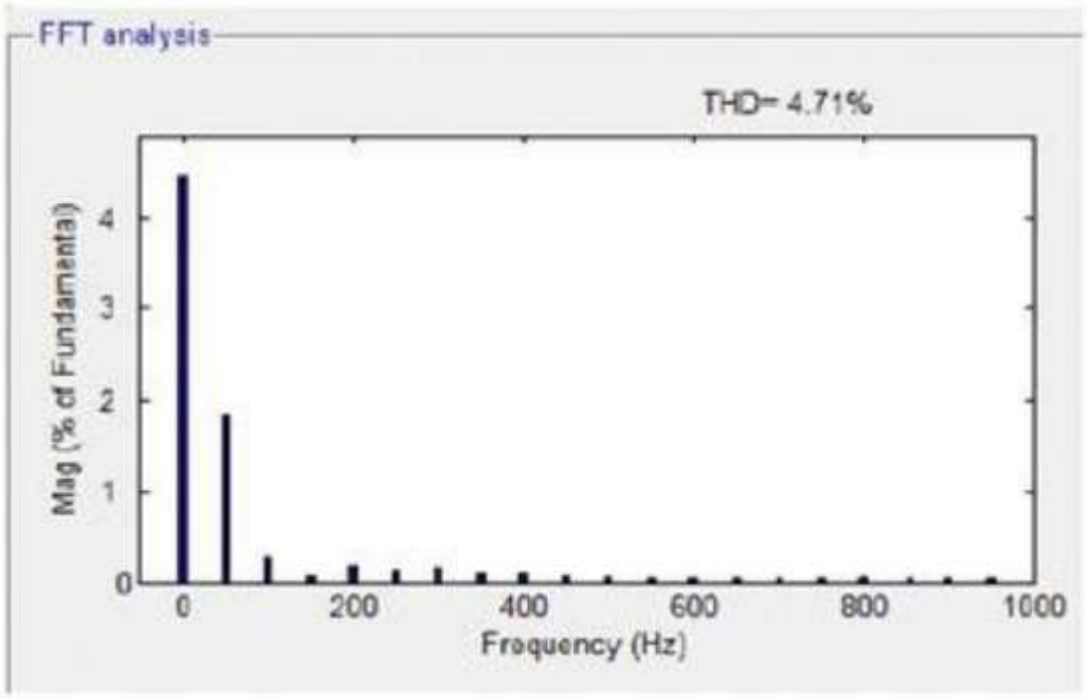

FIGURE 4.7 THD OF THE SOURCE CURRENT

4.3.2 EXPERIMENTAL RESULTS

As a hardware prototype, the buck-boost converter fed PMBLDC motor drive was constructed. Figure 4.8 depicts the hardware from the top. A buck boost converter and inverter circuits, a control circuit, and the PMBLDC motor compose the hardware prototype. Figure 4.9 depicts the experimental setup. Figure 4.10 depicts the input voltage and current waveforms. Figure 4.11 depicts the harmonic spectrum of the source voltage.

The technical specifications of the drive system are as follows: L = 150 mH, C = 220 μF, R= 5 . the bridgeless boost converter fed by 48v dc and the output is 58V .Other components are: Diode IN4007,

Microcontroller AT89C2051, MOSFET IRF840, Driver IR2110, Voltage (0-500V) and Current is 8A.

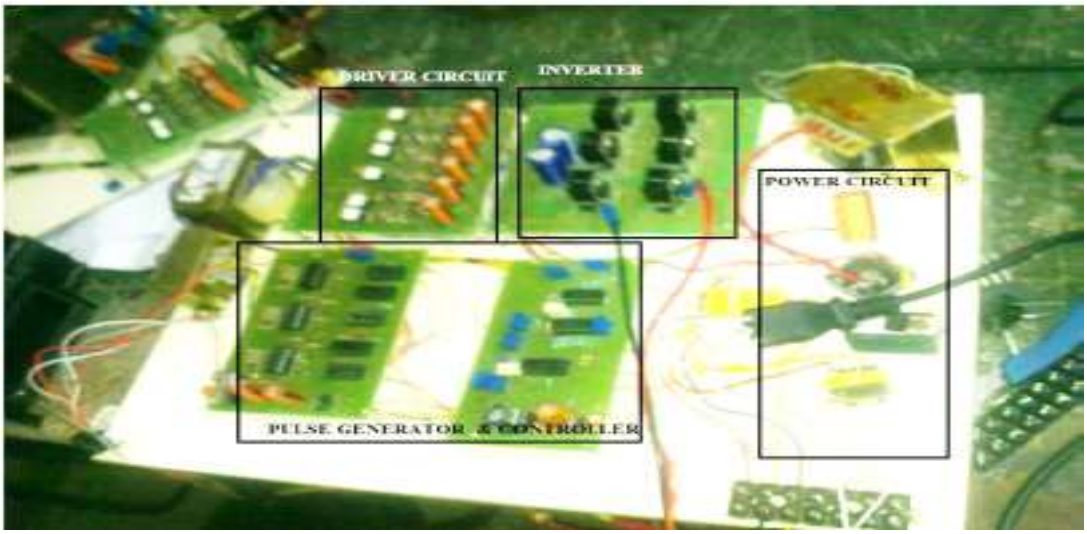

FIGURE 4.8 TOP VIEW OF THE HARDWARE

FIGURE 4.9 EXPERIMENTAL SETUP

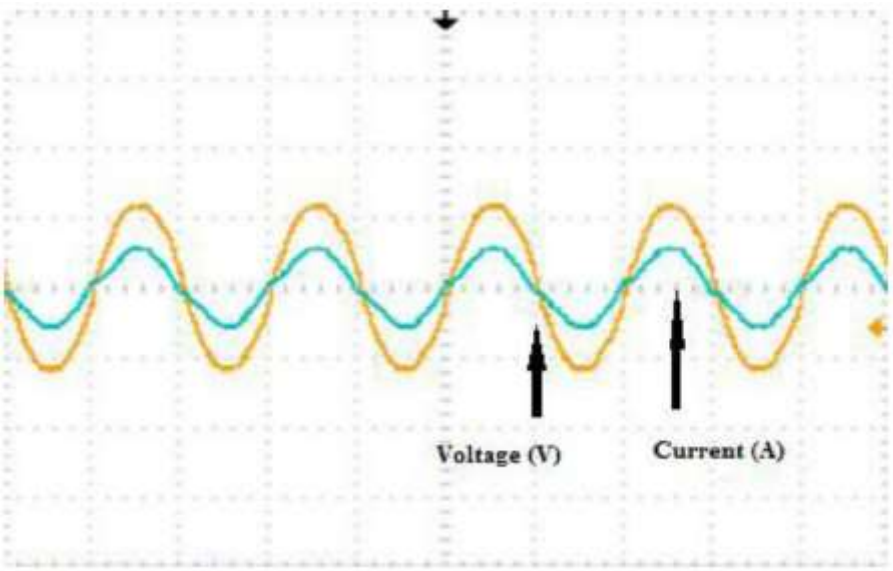

FIGURE 4.10 VOLTAGE AND CURRENT WAVEFORMS

FIGURE 4.11 HARMONIC SPECTRUM OF THE SOURCE VOLTAGE

Because the popular boost converter's main condition is that the output voltage be greater than the input voltage, its uses are restricted. A buck-boost converter can achieve a greater power factor across a wide range of output voltage.

4.4 BRIDGELESS PFC CUK CONVERTER FED PM BLDC MOTOR

The filter capacitor creates peaked pulse current due to the line current drawn by the diode bridge rectifiers, resulting in utility line distortion. Power factor adjustment has become a basic necessity in switching power supply due to the ever-increasing demand for power quality for utilities. PFC converters are used to interface AC to DC conversion in order to ensure unity power factor even when the line voltage is distorted. The boost topology is the most popular because it is simple in terms of both power and control, but it has several limitations, including implementation difficulty in the case of high-frequency insulation, lack of current insulation at start-up and overload conditions, and the requirement of complex control devices. Ripple currents are solely limited by the size of the inductor. Because the boost converter operates in the CCM, a big inductor is necessary. As a result, crossover distortion will rise. The boost converter is located in the DCM and serves as an automated current wave shaper. This, however, necessitates a high conversion gain in order to reduce distortion. Because the ripple currents in the DCM are strong, line harmonics must be filtered, and the Cuk converter is favoured to overcome them.

The Cuk converter is chosen to overcome these. The Cuk converter adjusts the voltage at the DC link to achieve the appropriate speed of the PMBLDC motor in addition to increasing the power quality in the AC mains.

Only by lowering the inductor size in boost converters can ripples be decreased. Because the boost converter runs in Continuous Conduction Mode (CCM), the inductor required is greater, increasing crossover distortion. Inductor coupling helps lessen input current ripples in the Cuk converter. Depending on the switching duty cycle, the Cuk converter may also step up or step down voltage. The Cuk converter features decreased current ripple due to series inductors at both the input and output. These ripples can also be eliminated in the input or output by carefully adjusting the inductor settings. Even with a basic control, these converters function in DCM. There is no need for duty-cycle modulation to obtain unity power factor. The DCM is best suited for low-power applications, whereas the CCM is best suited for medium and high-power applications.

This chapter proposes speed control based on a digital simulation of a Bridgeless Power Factor Correction (BLPFC) Cuk converter fed PMBLDC motor. The MATLAB-Simulink framework is used to simulate the cuk-based PFC converter fed PMBLDC motor drive, and a hardware prototype is also constructed. The speed is controlled with a PI controller. The suggested power converter has the following advantages: a unity power factor, reduced harmonic content, less switching loss, a simpler control stage, better power density, and unidirectional power flow.

4.4.1 PRINCIPLE OF THE BRIDGELESS CUK CONVERTER TOPOLOGY

Figure 4.12 depicts a standard PFC Cuk converter. During the switch turn-on time, current flows through the two rectifier diodes, the power switch S, and the output diode D0. During the switch turn-off period, current flows through the other two rectifier bridge diodes and the output diode D0. As a result, three semiconductor devices conduct current during

each switching cycle. While this configuration is appropriate for low power applications, large conduction losses limit system efficiency when employed for high power applications. This mandates the use of a bridge rectifier with a larger current handling capability, but also increases the size and expense of the power supply in the long run.

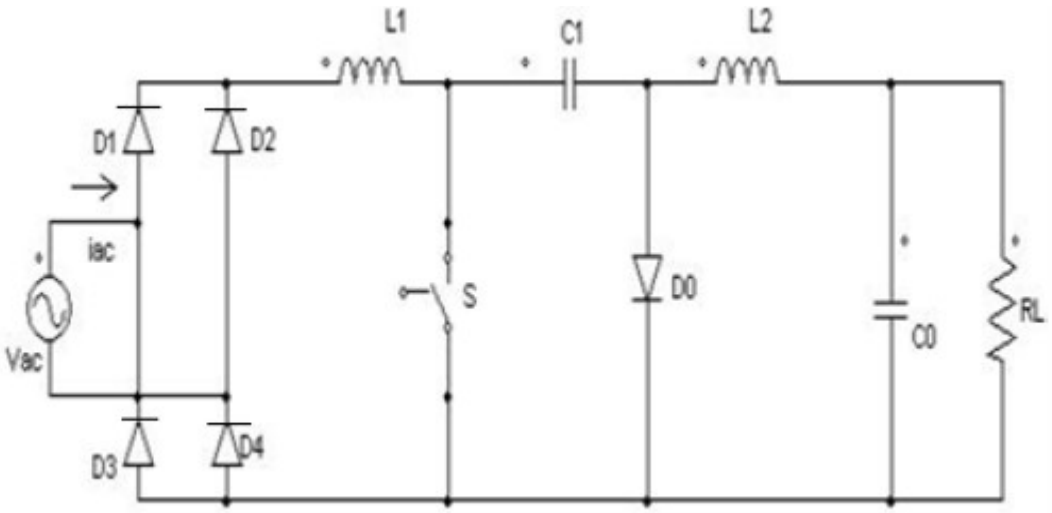

FIGURE 4.12 CONVENTIONAL CUK TOPOLOGY

However, BLPFC is characterised by a limited number of power switches, allowing for little power loss. Moreover, in typical active PFC, the power switches are in the on and off positions throughout the power supply duration. They must withstand high voltage and current strains, which result in significant switching and conduction losses, reducing their efficiency. The common-mode noise of a bridgeless PFC boost rectifier is significantly higher than that of a typical PFC boost rectifier. To avoid the limitations of bridgeless PFC boost rectifiers, the bridgeless topologies of the Cuk converter depicted in Figure 4.13 have been developed, however they need an isolated gate-drive.

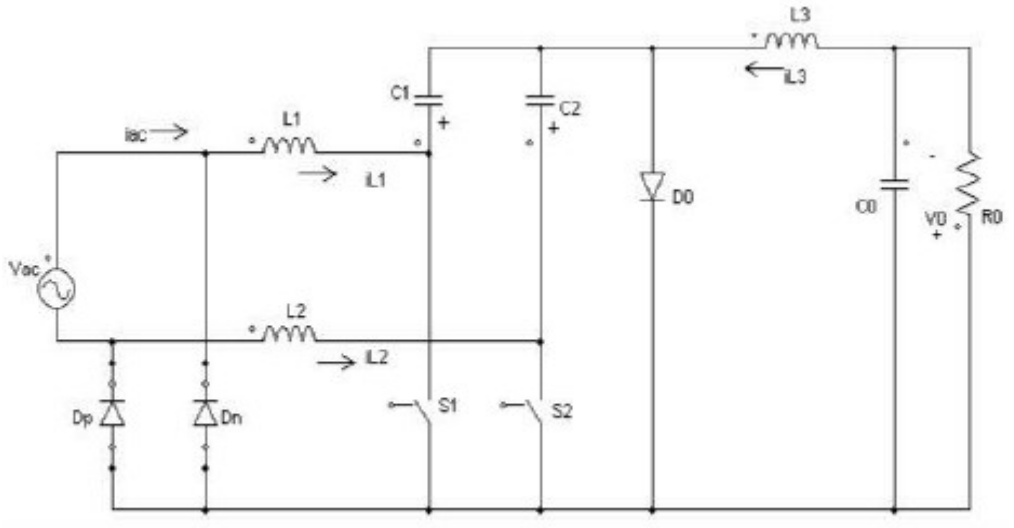

FIGURE 4.13 BRIDGELESS CUK CONVERTER TOPOLOGY

The cuk topology offers various advantages in PFC applications, such as lower input current ripple, transformer isolation, inherent inrush current limitations during start-up, overload condition and less EMI associated with the DCM topology. It can be seen from a scrutiny of Figure 4.13, that there are one or two semiconductors in the current path, reducing the conduction losses as well thermal stresses on the switching devices. The supply line is always connected to the output ground, through the slow-recovery diodes Dn and Dp. Two power switches S1 and S2, two low-recovery diodes Dp and Dn, and a fast diode Do are used in the bridgeless Cuk converter. The control circuitry is straightforward since two of the power switches are driven by the same control signal, but the third inductor is frequently considered as a negative in terms of size and cost. To decrease the size and expense of the suggested topology, the three inductors can be linked to the same magnetic core. Since each power switch functions during the half-line time, the stress on the switches is lessened.

Cuk converters are mostly employed in regulated power supplies, where negative polarity output is not a concern in relation to the common terminals of the input voltage and where the average output is either greater

or lower than the input DC voltage. The PFC converter's DC link voltage is as follows:

$$V_0 = V_{\propto} \frac{D}{(1-D)} \qquad (4.1)$$

Vac is the diode bridge rectifier output for a given AC input voltage (Vs).

$$V_{\propto} = \sqrt[2]{2} \frac{V_S}{\pi} \qquad (4.2)$$

A ripple filter has been created for ripple-free voltage at the Cuk converter's DC connection. At a switching frequency of, the ripple filter's inductor (L3) limits the inductor peak to peak ripple current (iL3) within set limits (fs). C0 is used to account for the allowable ripple in the DC link voltage (V0). The inductance and capacitance of the ripple filter are given as

$$L_3 = \frac{(1-D)V_{dc}}{F_S(\Delta i L_3} \qquad (4.3)$$

$$C_0 = \frac{iL_3}{2\omega\Delta V_0} \qquad (4.4)$$

The PFC Cuk converter is designed for a supply voltage of 230V, L3 = .5mH, Co = 2200μF and shown in appendix

4.4.2 SIMULATION RESULTS

The technical specifications of the drive system are as follows:

C= 2200 μF.TON= 5.88 μsecs. TOFF= 5.88μsecs.T= 11.76 μsecs. Stator Resistance is 2.875 ohms, Stator Inductance is 8.5mH, and the Motor inertia is 0.8mJ.The MATLAB simulation was done for the proposed cuk based PMBLDC drive and the results are presented a set speed at 1800 rpm and load change applied at time t=1 sec.

The Simulink model of a bridgeless Cuk Converter is shown in Figure 4.14. Figure 4.15 depicts a Simulink model PMBLDC drive with a bridgeless PFC Cuk converter PI controller closed loop control. To increase the power factor, a bridgeless PFC Cuk converter was employed at the input. Figure 4.16 depicts the AC input voltage and current waveforms of a closed loop regulated PMBLDC drive supplied by a bridgeless PFC Cuk converter.

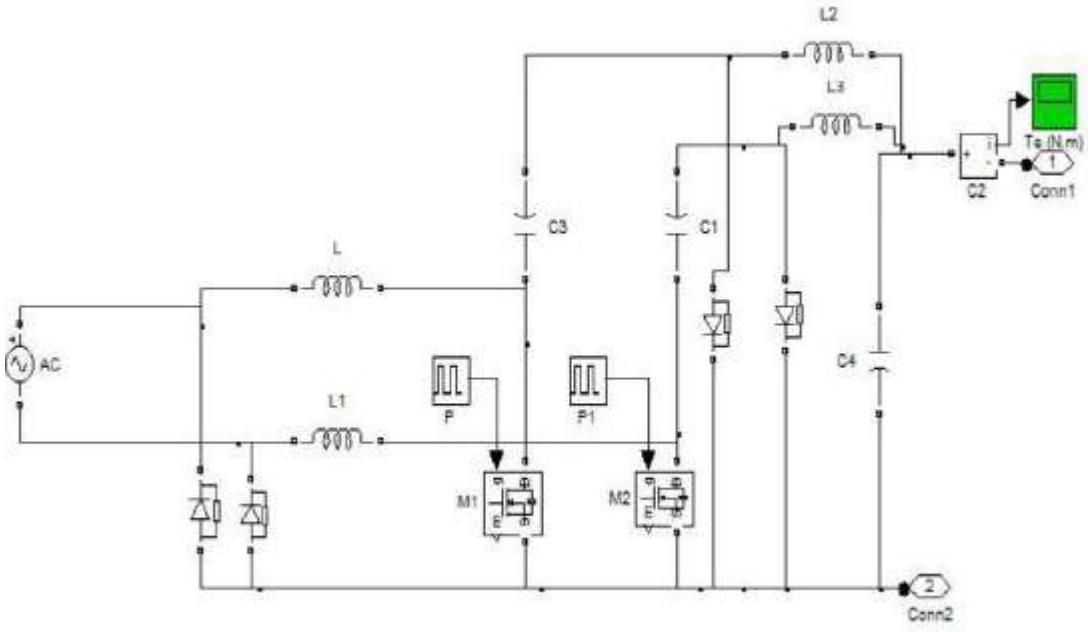

FIGURE 4.14 BRIDGELESS CUK CONVERTER CIRCUIT

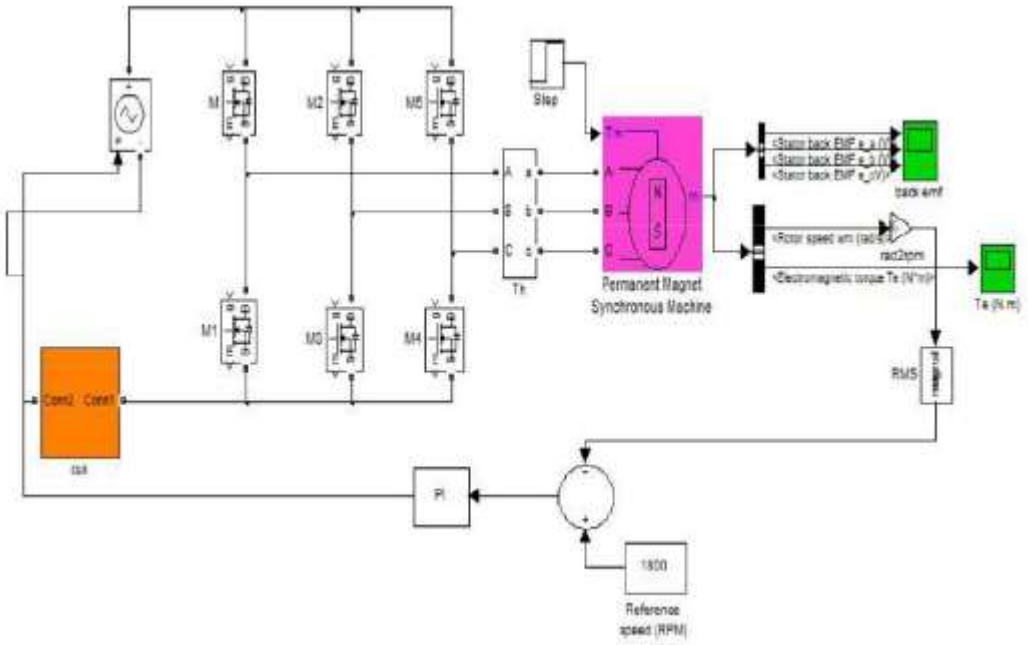

FIGURE 4.15 CLOSED LOOP SPEED CONTROL OF THE PMBLDC MOTOR WITH THE BRIDGELESS PFC CUK CONVERTER

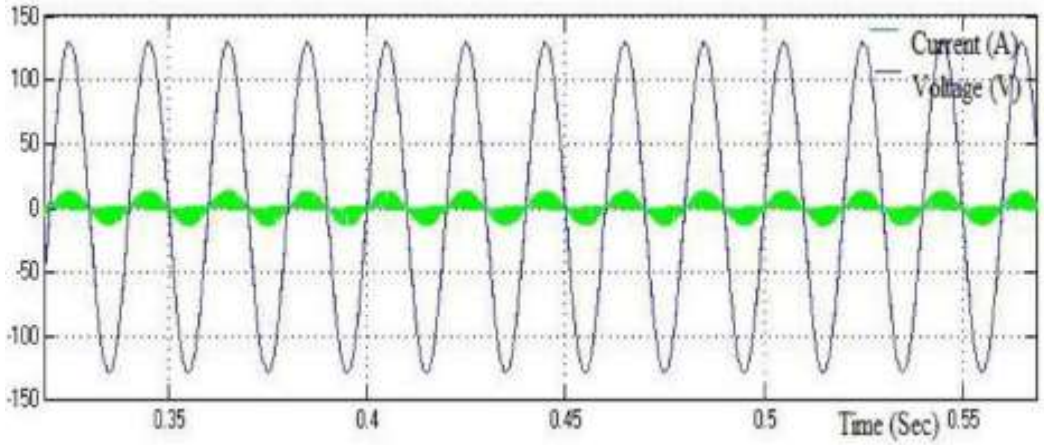

FIGURE 4.16 INPUT VOLTAGE AND CURRENT WAVEFORMS

A close examination of the figure reveals that the phase gap between the input voltage and current has been decreased. As a result, using a bridgeless Cuk converter as the PFC converter for a PMBLDC drive

enhances the power factor, and the power factor has been shown to be greater than that of a PFC Zeta converter fed PMBLDC motor. Figure 4.17 depicts the switching pulses for the bridgeless Cuk Converter. Figure 4.18 depicts the step change that is implemented at t=1 sec of load torque.

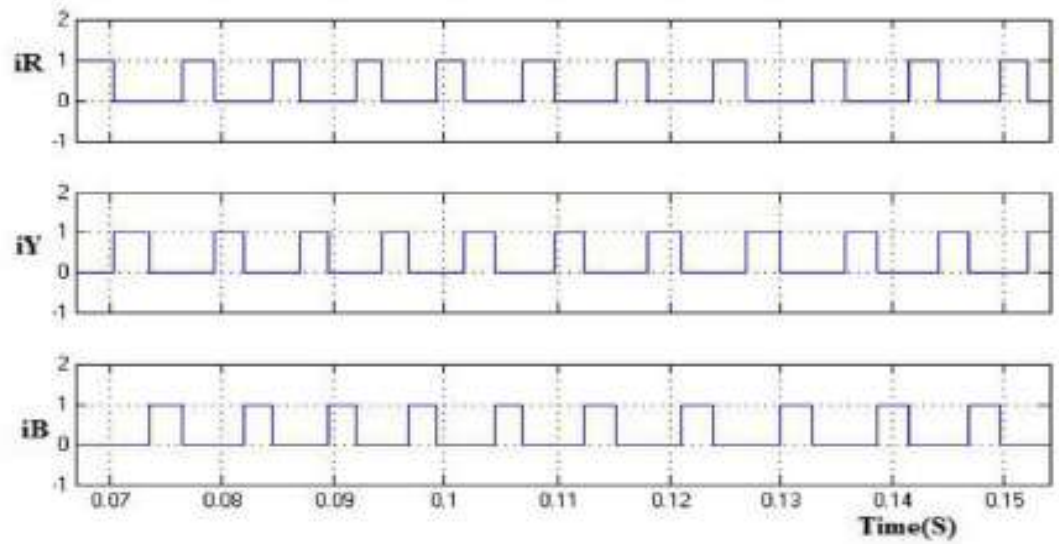

FIGURE 4.17 SWITCHING PULSES FOR THE BRIDGELESS CUK CONVERTER

The torque ripples are caused by the current ripples created by switching. Due to the time delay imposed by machine inductance, it is not possible to create optimal rectangular currents. As a result, the current form becomes more or less trapezoidal, resulting in a substantial commutation-torque ripple of roughly 10% of the rated torque. Moreover, due to considerable slot harmonics, the resultant emfs are not perfectly trapezoidal. These will, in turn, cause harmonic torque ripples, as seen in Figure 4.18. At time zero, the rotor is motionless. As seen in Figure 4.19, the speed then settles at the rated 800 rpm even before 0.4sec.

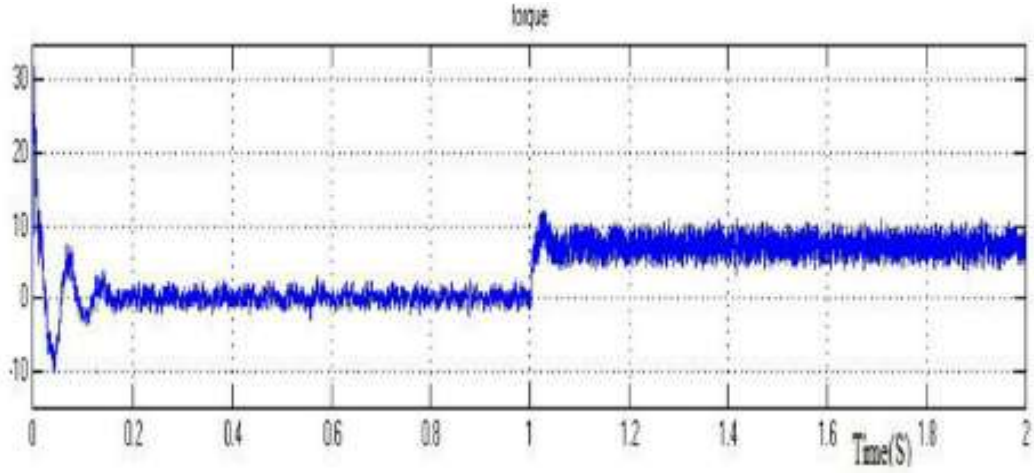

FIGURE 4.18 STEP CHANGE IN LOAD TORQUE APPLIED AT T=1 SEC

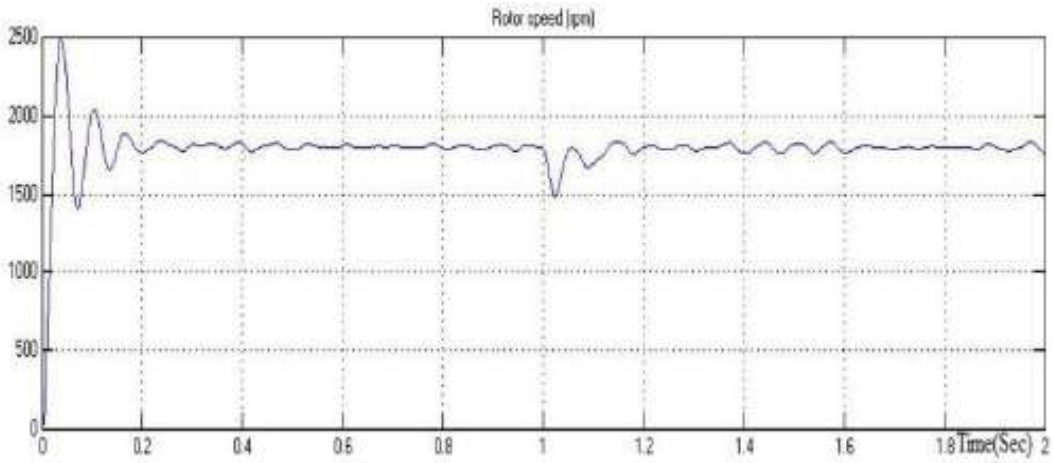

FIGURE 4.19 SPEED RESPONSE

The FFT analysis presented in Figure 4.20 shows, that the THD is only 0.73 % when a bridgeless Cuk converter is used as the PFC converter in a PMBLDC drive.

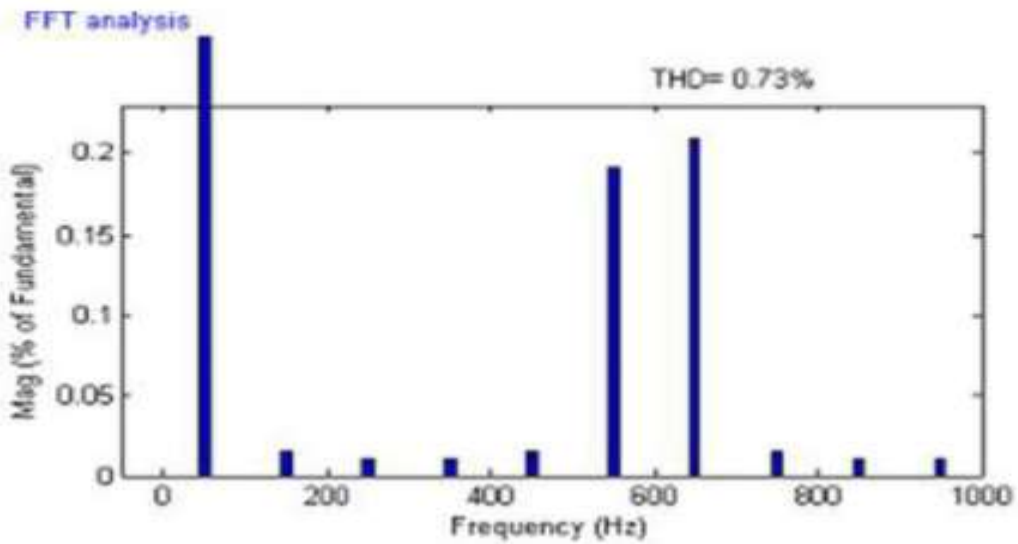

FIGURE 4.20 FFT ANALYSIS OF THE SOURCE CURRENT

4.4.3 EXPERIMENTAL RESULTS

A prototype Cuk-based PFC-fed PMBLDC motor drive was built and tested. Figure 4.21 depicts the experimental configuration. Figure 4.22 depicts the Cuk converter board individually. Figure 4.23 depicts the inverter and BLDC driver board. Figure 4.24 depicts the input voltage and current waveforms. Figure 4.25 depicts the Harmonic Spectrum of the source voltage. The driving system's technical parameters are as follows: Cin equals 2200 microfarad. The input voltage fed to PFC is 48V and output is 58V .Diode IN4007, Microcontroller AT89C2051, MOSFET IRF840, Driver IR2110, Voltage (0-500V) and Current 8A are used.

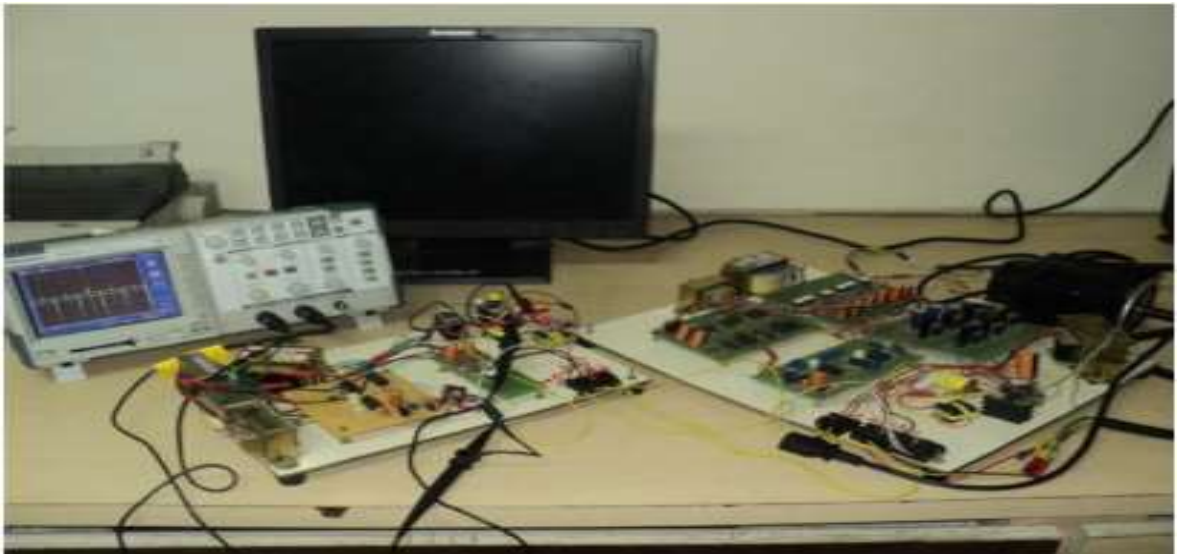

FIGURE 4.21 EXPERIMENTAL SETUP

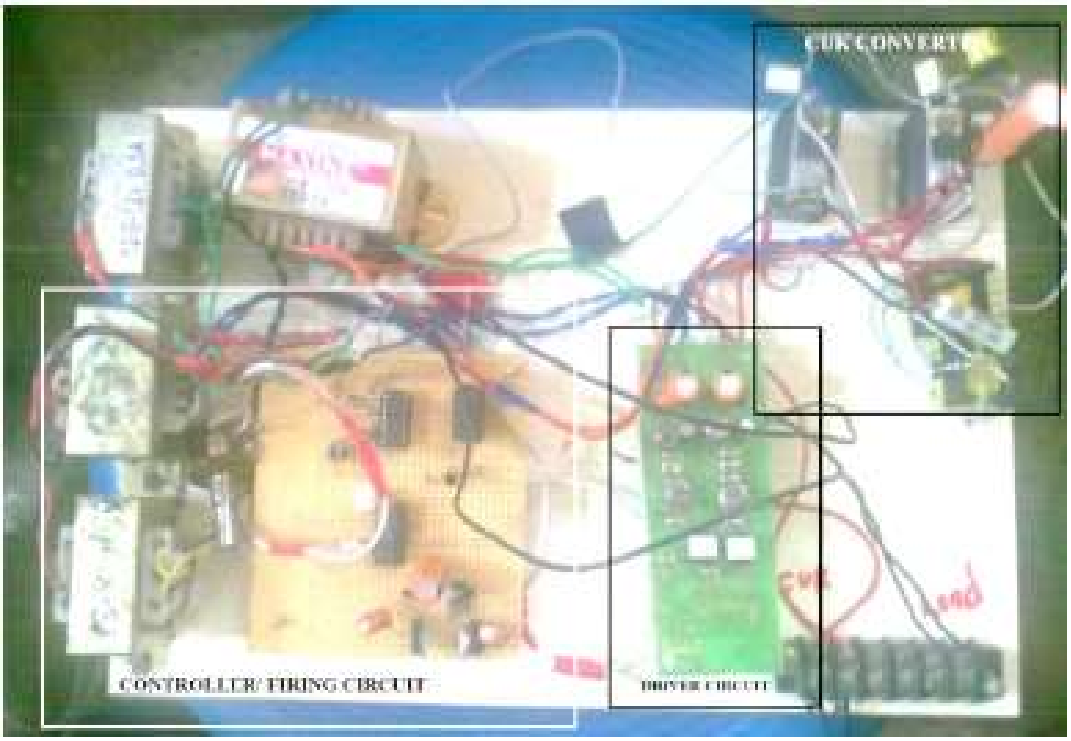

FIGURE 4.22 BRIDGELESS CUK CONVERTER BOARD

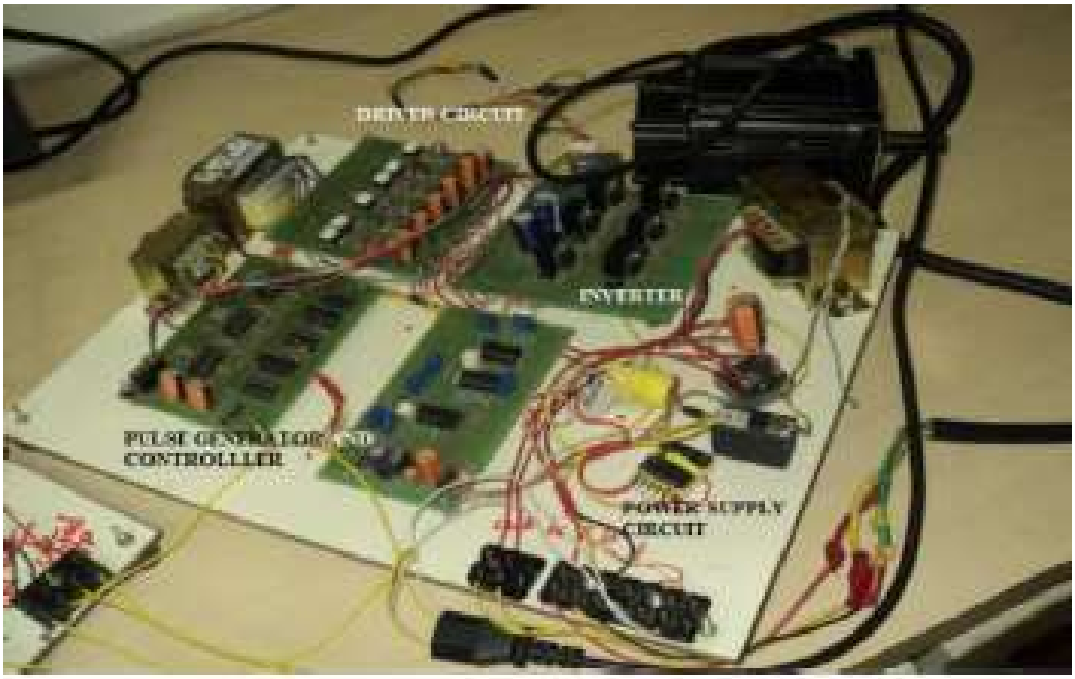

FIGURE 4.23 INVERTER AND BLDC DRIVE BOARD

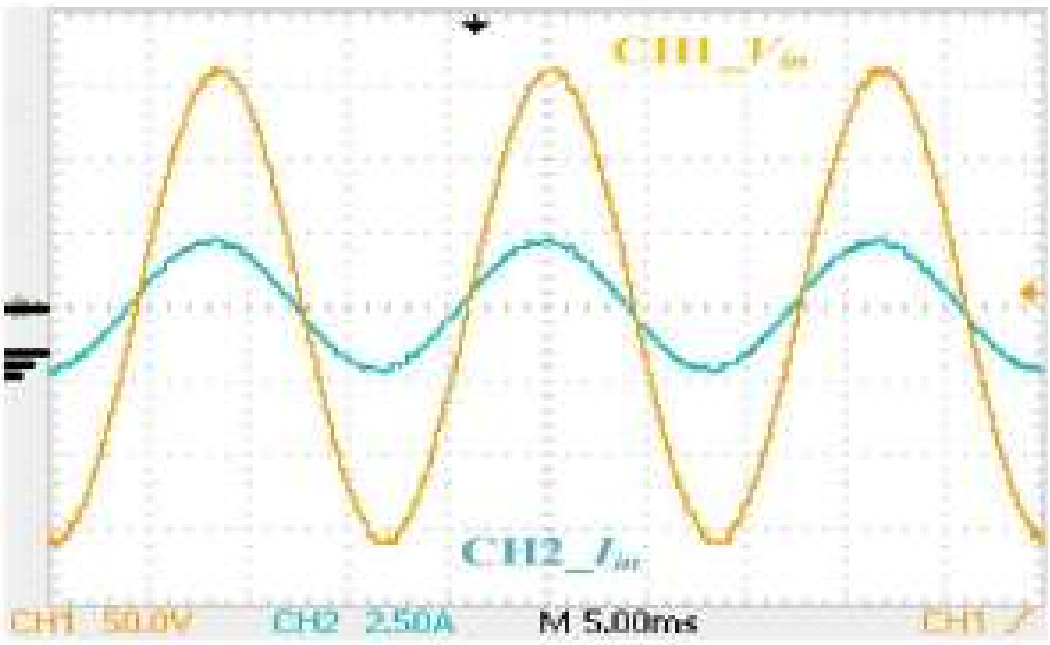

FIGURE 4.24 INPUT VOLTAGE AND INPUT CURRENT WAVEFORMS

FIGURE 4.25 HARMONIC SPECTRUM OF SOURCE VOLTAGE

By linking the two inductors, the switching frequency harmonics are considerably decreased, allowing the Cuk converter to operate as an automated current wave shaper with no current control. Because the inductance employed in the DCM is substantially lower, the lag effect in the input current at zero crossing is insignificant. High-frequency transformer isolation can be used to provide isolation. The transformer and two inductors can be combined into a single magnetic structure. This configuration allows both the output and input ripples to be transported to the transformer, where the AC ripple exists naturally as the transformer's magnetising current.

4.5 PFC SEPIC CONVERTER FOR THREE PHASE BLDC MOTOR WITH ELECTRONIC COMMUTATION

In general, natural language is the most effective means of transmitting information. Traditional mathematical approaches have not

completely exploited language's possibilities. Many physical processes are not linear, and modelling them requires a decent level of approximation. The mathematical formulae provide a clear description of the system behaviour for a basic system. Similarly, model-free approaches give strong methods to minimise ambiguity and uncertainty in increasingly complex systems with a large quantity of accessible data. Complicated systems with limited numerical data can be managed using fuzzy logic by employing an approximation input-output technique. The major strength of fuzzy logic is that it uses language variables to express imprecise facts rather than numerical variables.

4.5.1 BASIC SEPIC OPERATION

The basic SEPIC converts DC-DC voltages by exchanging energy between its coupling capacitor and switching inductors (Cin, L1 and L2). The switch regulates the quantity of energy exchanged between the capacitor and inductors. To maximise energy exchange efficiency and overall converter efficiency, this SEPIC design must be used in continuous conduction mode (CCM).

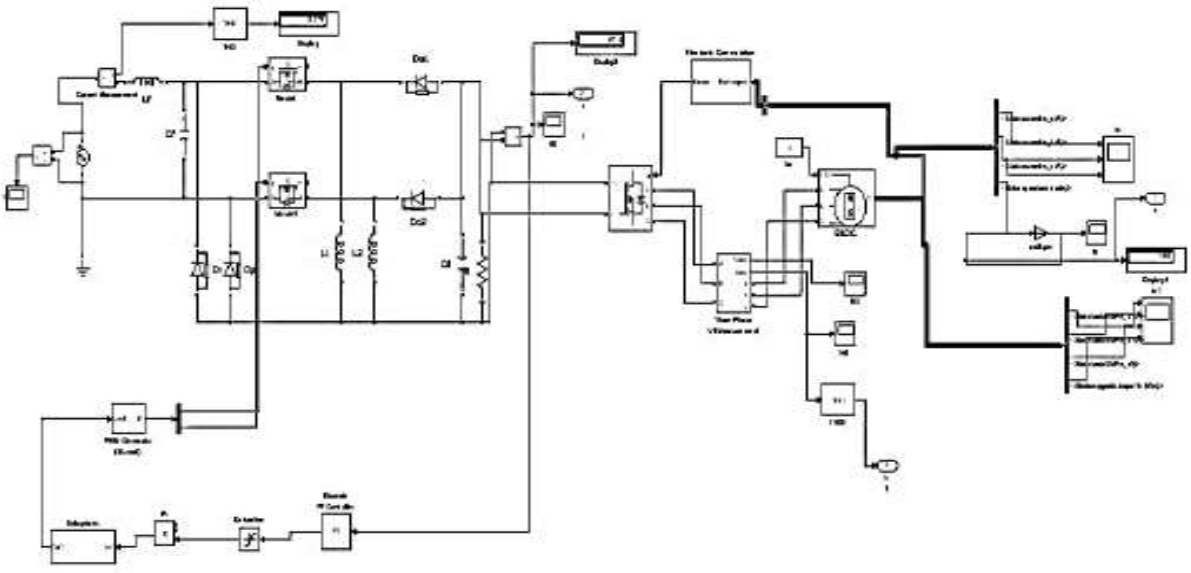

FIG 4.26 SIMULINK MODEL OF A SEPIC CONVERTER

Figure 4.26 depicts a Simulink model of a PMBLDC drive with a SEPIC converter PI controller closed loop control. To increase the power factor, the SEPIC converter was added on the input side. The AC input voltage and the current waveforms of the closed loop controlled PMBLDC drive, fed via a SEPIC converter are shown in figure 4.30.

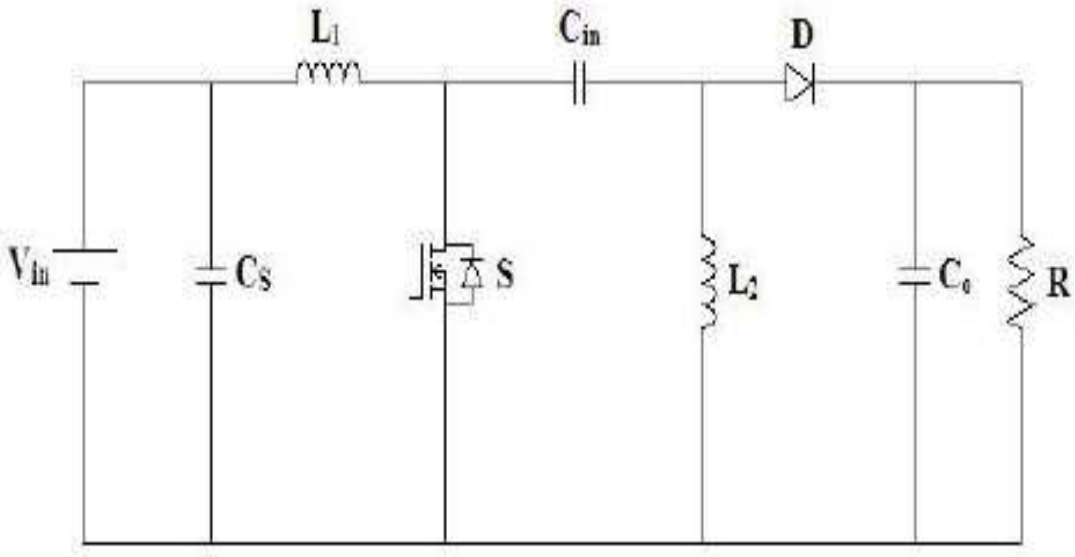

FIGURE 4.27 SEPIC CONVERTER

Figure 4.27 shows the circuit diagram of a SEPIC converter. There are two modes of operation in SEPIC. They are

1. Continuous Conduction Mode
2. Discontinuous Conduction Mode

4.5.1.1 CONTINUOUS CONDUCTION MODE

The inductor current will be continuous in continuous conduction mode and will never approach zero. That is, operating the SEPIC in CCM implies never allowing the currents through L1 and L2 to drop below 0A - that is, never allowing L1 and L2 to entirely discharge. When the SEPIC achieves steady-state functioning, the average voltage across Cin equals

Vin. Moreover, in steady-state, the average current through Cin is 0A. L2 is the only source of current to the output load when this steady-state occurrence occurs. As a result, L2's average current equals the output load and is independent of Vin.

The total of the average voltages across the SEPIC's energy storage devices (excluding the input and output filter capacitors Cs and Co) equals the SEPIC's input voltage specified below in CCM.

$$V_{in} = V_{L1} + V_{Cin} + V_{L2}$$

Since the average voltage across Cin equals that of Vin, VCin equals Vin, leading to

$$V_{L1} = V_{L2}$$

The SEPIC's functioning under CCM in steady-state is further divided into two modes: when switch S conducts and when it does not conduct. Understanding the SEPIC's whole operation in CCM necessitates examining it in both the conduction and non-conduction modes of switch S.

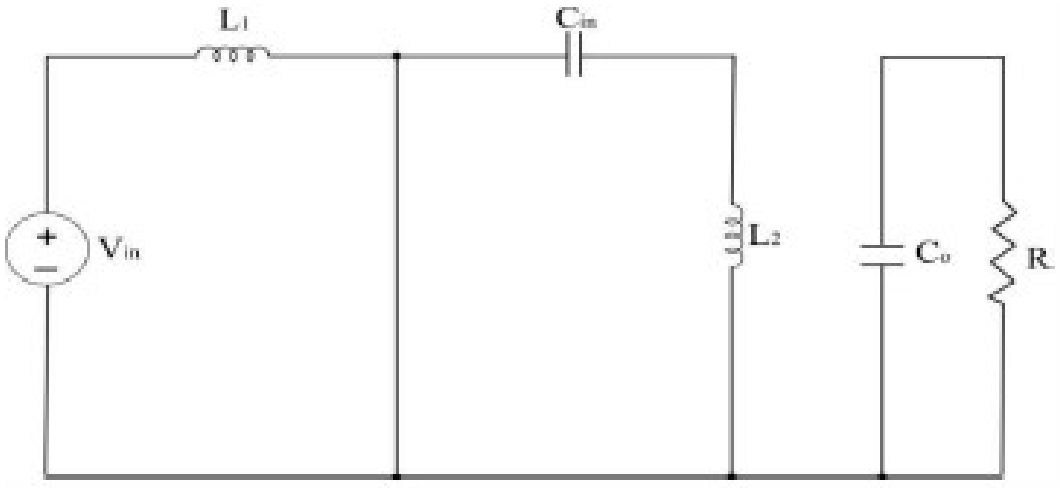

FIGURE 34.28 SWITCH ON CONDITION WHEN SWITCH IS CLOSED

Figure 4.28 depicts the SEPIC's functioning when switch S is turned on. Because the filter capacitors Cs and Co are considered to be in steady-state, no current passes through them until they discharge. Additionally, Cs and Co are believed to have sufficient capacitance that the SEPIC's input and output ripple voltages are almost zero.

When switch S is turned on during the first half-switching cycle, current through L1 grows in the positive direction, while current through L2 increases in the negative direction. As a result, L1 charges via Vin, whereas L2 discharges (acts as a source) via Cin. S stays closed for a brief amount of time, during which the instantaneous voltage across Cin equals Vin. Hence, the magnitudes of VL1 and VL2 are essentially equal to Vin.

When L2 is discharging, the only difference between the two voltages is that VL2's polarity is reversed (i.e. negative). Cin then discharges and feeds current to L2 to store energy in it, allowing L2 to deliver current to the output load during the following half-switching cycle when switch S no longer conducts. Diode D does not conduct over the full half-switching cycle, indicating that it is reverse-biased. While switch S is conducting, Co discharges and hence is the only component that helps sustain the output load current. Switch S is turned off during the second half-switching cycle.

4.5.1.2 WHEN SWITCH IS OPENED

When the switch is opened, the SEPIC operates as shown in Figure 4.29. Switch S is turned off at the conclusion of one half-switching cycle. The input current now travels via L1 and Cin. Inductor Currents do not change immediately because current cannot change instantly through an

inductor. As a result, the capacitor current Cin equals the L1 current. L2 continues to discharge, but during this half-switching cycle it discharges into Co, turning on D, making it forward biassed and delivering current to the output load.

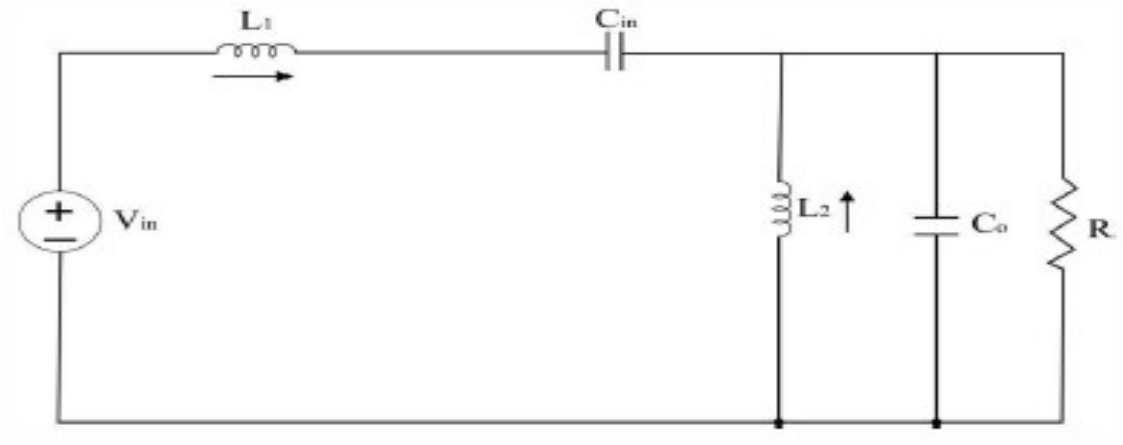

FIGURE 4.29 SWITCH OFF CONDITION

The direction of L2 current, on the other hand, leads it to add to the input current that is already flowing to the output load. When S is not conducting, both L1 and L2 provide current to the output load. Vin and L1 charge Cin (which discharged during the half-switching cycle when switch S conducted), and L2 discharges to the output load until switch S conducts again at the start of the next half-switching cycle (when Cin supplies current to charge L2).

4.5.1.3 DISCONTINUOUS CONDUCTION MODE

The inductor current reaches zero in the discontinuous conduction mode of operation. If the currents via L1 and L2 remain at 0A for any considerable time period relative to the switch switching period, the discontinuous conduction mode occurs. Running a SEPIC in DCM results in improved efficiency at lower current loads, but needs large current loads. As a result, running in CCM should result in higher overall converter

efficiency. The phase difference between the input voltage and current is seen in Figure 4.30.

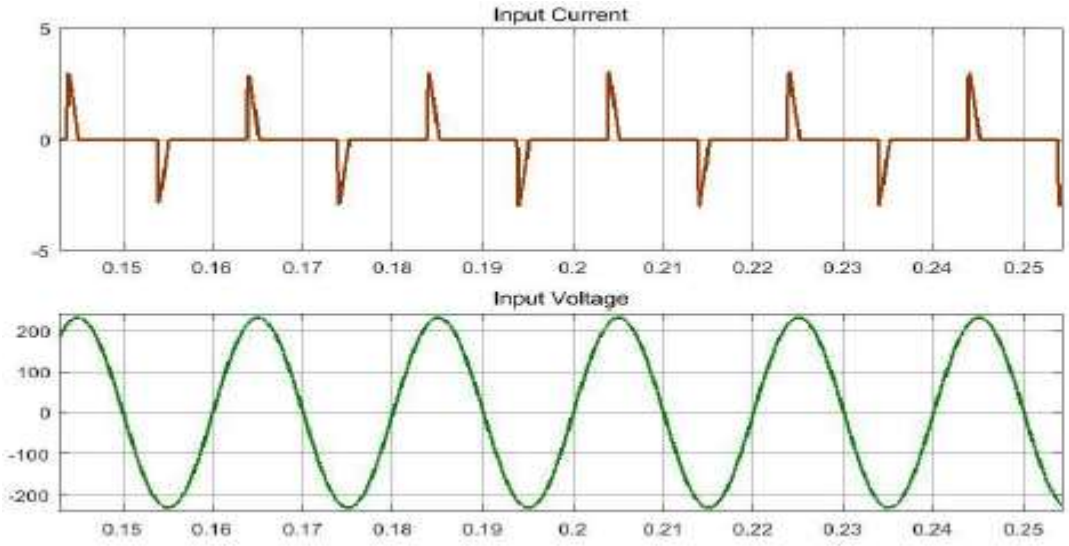

FIGURE 4.30 INPUT VOLTAGE AND INPUT CURRENT WAVEFORMS

Figure 4.31 shows the phase difference between the output voltage and current.

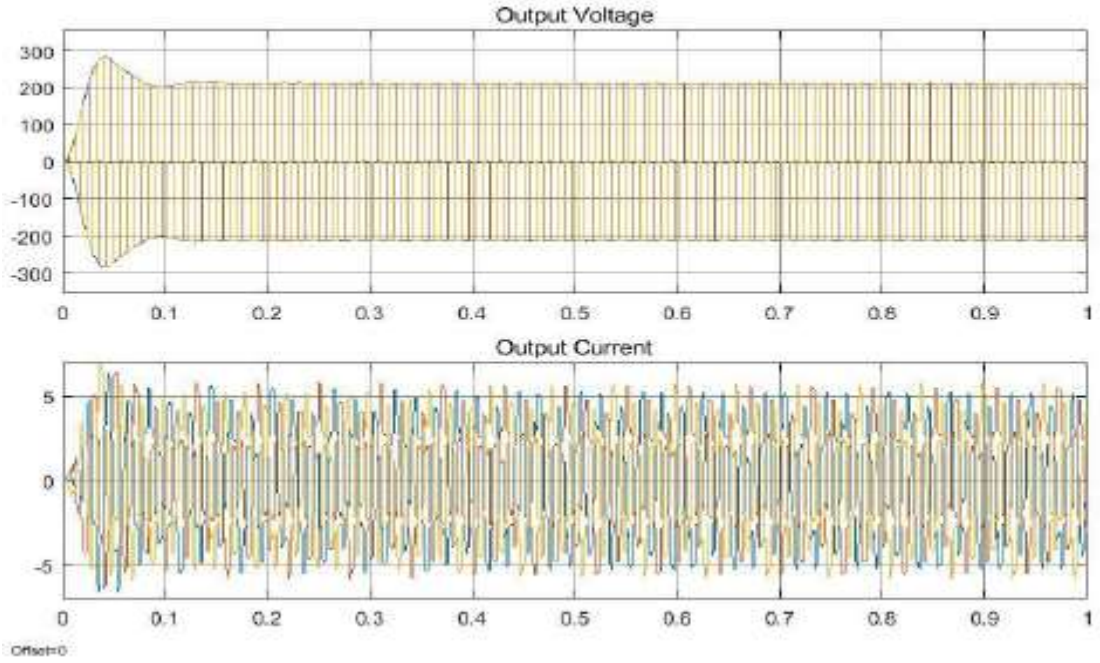

FIGURE 4.31 OUTPUT VOLTAGE AND CURRENT WAVEFORMS

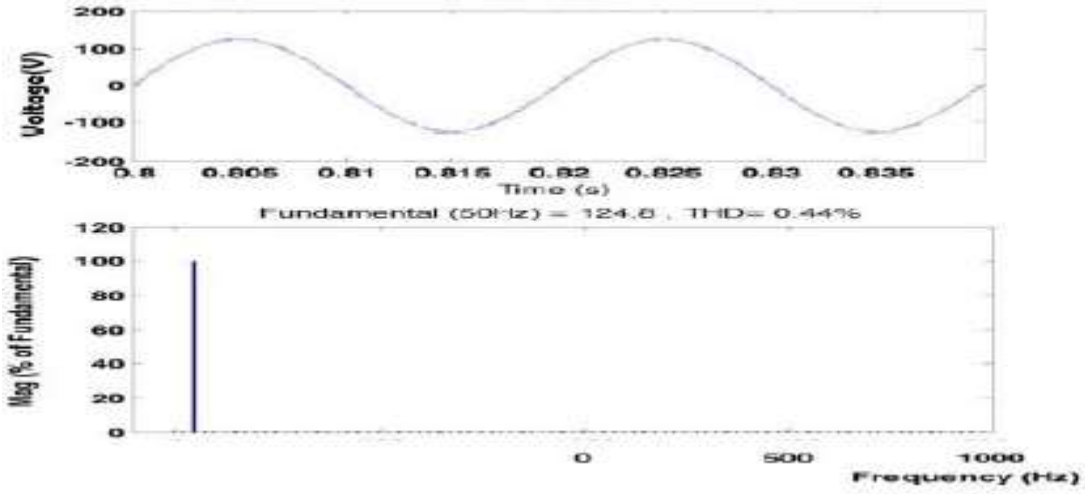

FIGURE 4.32 FFT OUTPUT OF SEPIC CONVERTER

The FFT analysis presented in Figure 4.32 shows, that the THD is only 0.44 % when a SEPIC converter is used as the PFC converter in a PMBLDC drive.

4.5.2 FUZZY LOGIC

4.5.2.1 FUZZY LOGIC CONTROL COMPONENTS

Fuzzy logic controller components characteristics and functionalities have been distinctly stated and presented in this section. Figure 4.33 shows that when input data is received by the fuzzy controller, it automatically translates the same into fuzzy form and the entire process is referred to as Fuzzification. Thereafter which fuzzy processing is carried out by the controller, entailing input information evaluation in line with the IF…THEN rules that are user generated through fuzzy control system programming and stages of the designing process.

Defuzzification begins once the fuzzy controller completes the rule-processing step and reaches the point of a result conclusion. The fuzzy controller turns the output inferences as "actual" output data at the last stage (e.g., analogue counts). Following that, the data is used as an output module interface for processing.

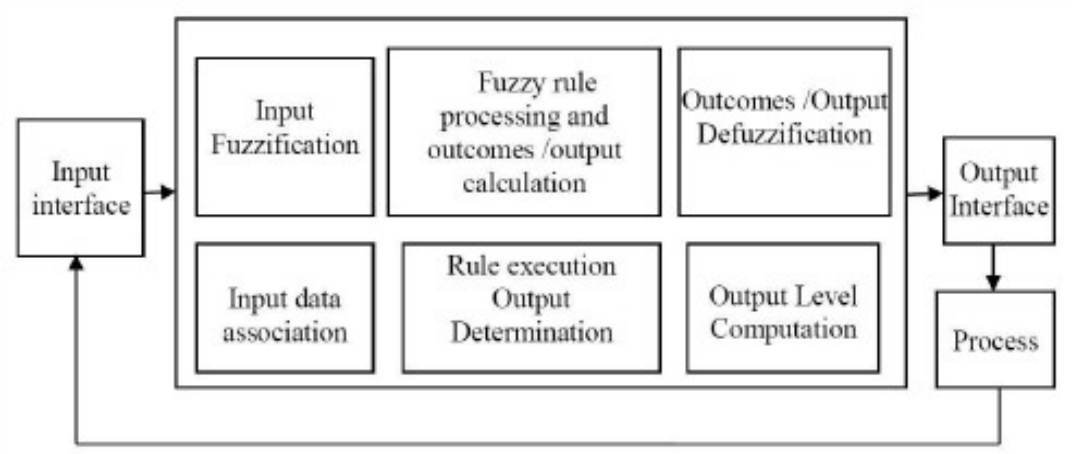

FIGURE 4.33 FUZZY LOGIC CONTROLLER OPERATIONS

In place of mathematical equations, fuzzy logic operational laws have been expressed using language phrases. Some systems are either too difficult to develop with precision or require mathematical equations that are intricate in terms of applicability; hence, applying typical approaches for such systems becomes essentially impossible. Yet, fuzzy logic linguistic concepts provide decisive approaches that are practicable and may be applied to improve system operational qualities. The fuzzy logic controller is a symbolic controller that belongs to a certain class.

The fuzzy logic controller carries out three operative functions as below:

- Fuzzification

- Fuzzy inference
- Defuzzification

4.5.2.2 FUZZIFICATION

The fuzzifier conducts input variable measurement (input signals, actual variables), scale mapping, and fuzzification (Transformation 1). As a result, all monitoring input signals are scaled, and measured signals (crisp input quantities with numerical values) are turned into fuzzy quantities via the fuzzification process. Membership functions are used to make this transition. With a traditional fuzzy logic controller, the user determines the number of membership functions and the forms. Membership functions can be piecewise linear or continuous, and the most widely used membership functions are sigmoid, bell-shaped, trapezoidal, gaussian, and triangular. A membership function contains values between 0 and 1, indicating the degree to which a quantity belongs to a fuzzy collection.

4.5.2.3 FUZZY INFERENCE

Fuzzy inference is the use of fuzzy logic to create a mapping output from a given input. As a result, the mapping process provides a foundation for decision making or pattern recognition. Two types of fuzzy inference systems may be created using the Fuzzy Logic Toolbox. The Mamdani is the first type, while the Sugeno is the second. Both categories have distinct properties, particularly in terms of output determination.

Several applications of fuzzy inference systems have been successful, including computer vision, automated control, decision analysis, data categorization, and expert systems. These systems are multidisciplinary in nature and are known by a variety of names, including fuzzy-rule-based systems, fuzzy modelling, fuzzy expert systems, fuzzy

logic controllers, fuzzy associative memory, and simply (and ambiguously) fuzzy Mamdani's fuzzy inference method, which is one of the most popular fuzzy methodologies.

Mamdani's approach is regarded as one of the earliest control systems developed using fuzzy set theory. These are the deliberate and purposeful efforts made to manage both the steam engine and boiler combination by fusing language control rules and acquiring human operators who were familiar with and had prior expertise in the same. Mamdani's paradigm in fuzzy algorithms is used for complicated systems that need decision making.

The fuzzy inference phase of the fuzzy logic controller's second phase has both a knowledge base and decision making logic. The knowledge base contains both the rule and the data base. The description of input and output variables is included in the database. The control rules are analysed by the decision making logic. Control-rule bases are further developed to facilitate the link between output action and controller inputs.

4.5.2.4 DEFUZZIFICATION

The inference mechanism output generates fuzzy output variables. The fuzzy logic controller is necessary to transform the internal fuzzy output variables into crisp values, allowing the real system to utilise such variables. Defuzzification is the collective term for the conversion process. There are several methods for carrying out this surgery. The most frequent defuzzification strategy is the max criterion approach, abbreviated as max. The Max criteria identifies the membership function in which the fuzzy control action achieves the highest value.

4.5.3 PROPOSED FUZZY BASED CONTROLLER IN BLDC MOTOR

The fuzzy controller has been proposed in this chapter for the control of a BLDC motor. This fuzzy controller substitutes a traditional PI controller to increase the control scheme's performance. The FLC is a strong tool in all sorts of real-time applications, and it outperforms traditional control methods. The primary goal of a fuzzy controller is to minimise rising time discrepancies and settling time differences in both DC-link voltage and motor speed. Figure 4.34 shows the second proposed speed control scheme with fuzzy logic controller based on the control of the reference DC-link voltage. Similar to previous chapter, the rotor position signals of the BLDC motor are obtained by Hall-effect sensors and it is used by an electronic commutator to generate the switching pulses for the VSI feeding the BLDC motor.

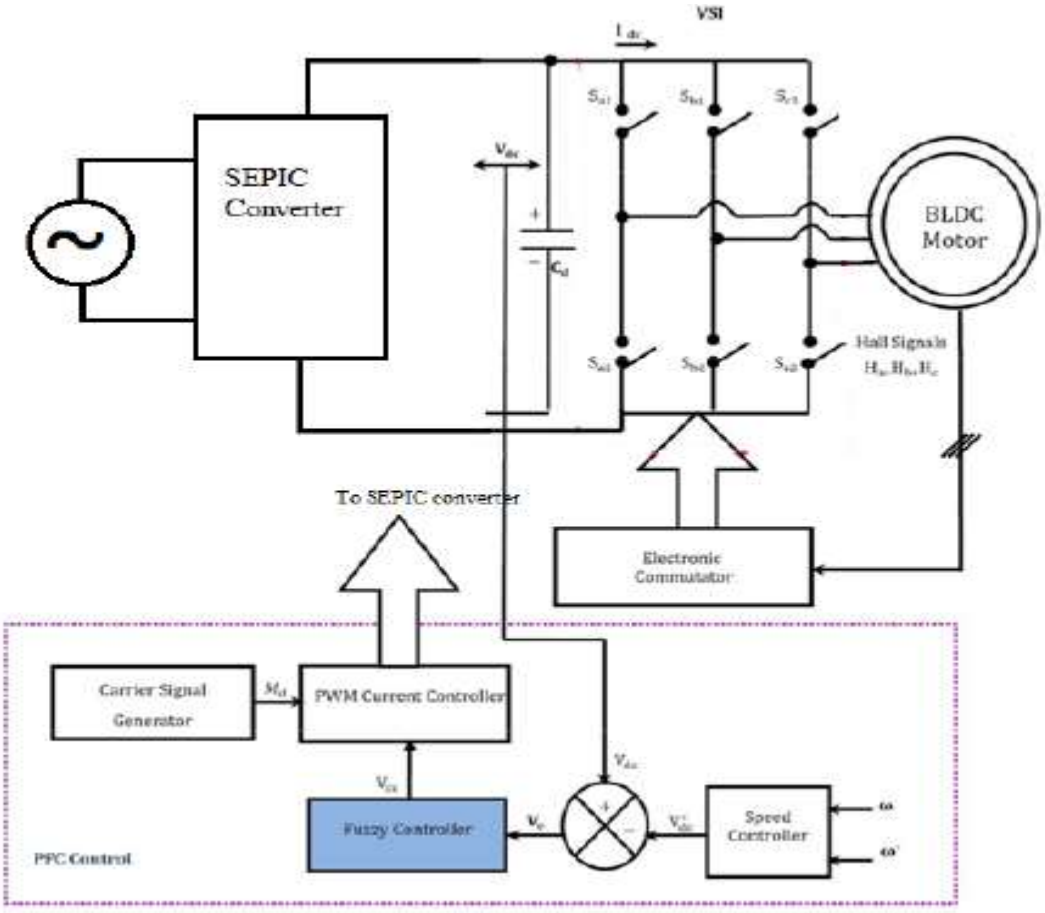

FIGURE 4.34 FUZZY BASED PROPOSED SEPIC CONVERTER DESIGN WITH BLDC MOTOR

The measured speed () and reference speed () are processed by the speed controller (PI controller) in Figure 4.35 to generate the corresponding reference DC-link voltage. Equation gives the equation for the DC-link voltage (5.4)

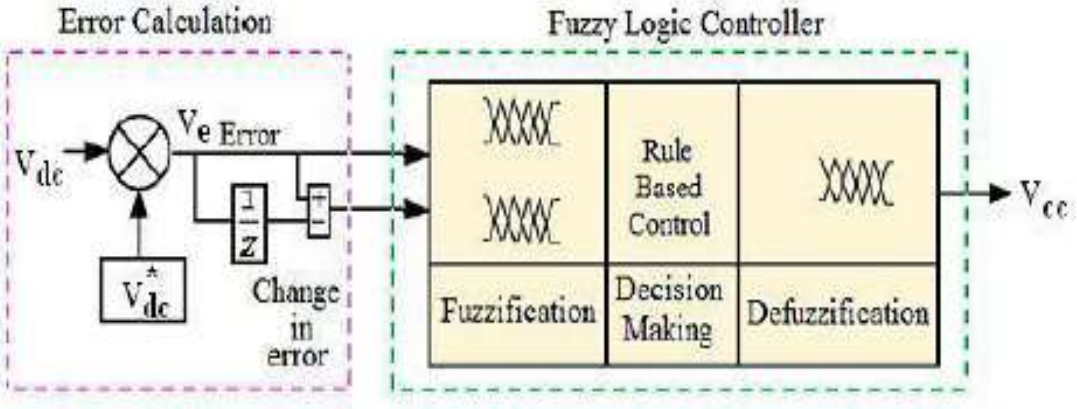

FIGURE 4.35 STRUCTURE OF FUZZY LOGIC CONTROLLER AT DC BUS VOLTAGE

Figure 6.6 depicts the FLC structure at DC-link voltage for providing the switching pulse to the proposed PFC SEPIC converter. The difference between the reference DC bus voltage and the detected DC bus voltage is the error (Ve).

The fuzzy controller developed is based on standard Mamdani type fuzzy logic with two inputs and one output. The error voltage (Ve) and change in error voltage (e) are the two inputs and the output of the FLC is Vcc which is further processed to the PWM current controller to generate the switching pulse to the proposed PFC SEPIC converter.

4.5.3.1.1 MEMBERSHIP FUNCTIONS AND RULE BASE

The membership functions of a fuzzy set define its fuzziness. The membership functions normalise the degree of fuzziness into the normalised interval (0, 1), where the boundary values 0 and 1 correspond to crisp set membership degrees. For the error (e) and change in error (e) inputs, the FLC utilised at the DC bus voltage controller with five membership functions was chosen. The main objective of FLC in DC voltage controller is to decrease the rising time and settling time discrepancy in both DC-link voltage and speed error. The triangle membership function was chosen because it is the most widely recognised and balanced choice in many applications.

The five input and output membership functions are labelled NB (Negative Big), NS (Negative Small), ZE (Zero), PS (Positive Small), and PB (Positive Big). Figure 4.36 depicts the fuzzy membership functions for the input and output. The goal of a fuzzy controller is to make human-like

judgements while regulating a target system. This is accomplished through the use of appropriate fuzzy rules that comprise a fuzzy rule basis. The fuzzy rules are created using IF-THEN rules. Table 4.1 shows the rule table, which has 25 rules. The fuzzy control rules' structure for the two inputs and one output may be stated as IF (e is NS ande is NS) THEN output is NB. Membership functions fuzzify and express the two input variables (e and e) in fuzzy set notations. The linguistic variables are produced by the defined 'if.... and then....' rules.

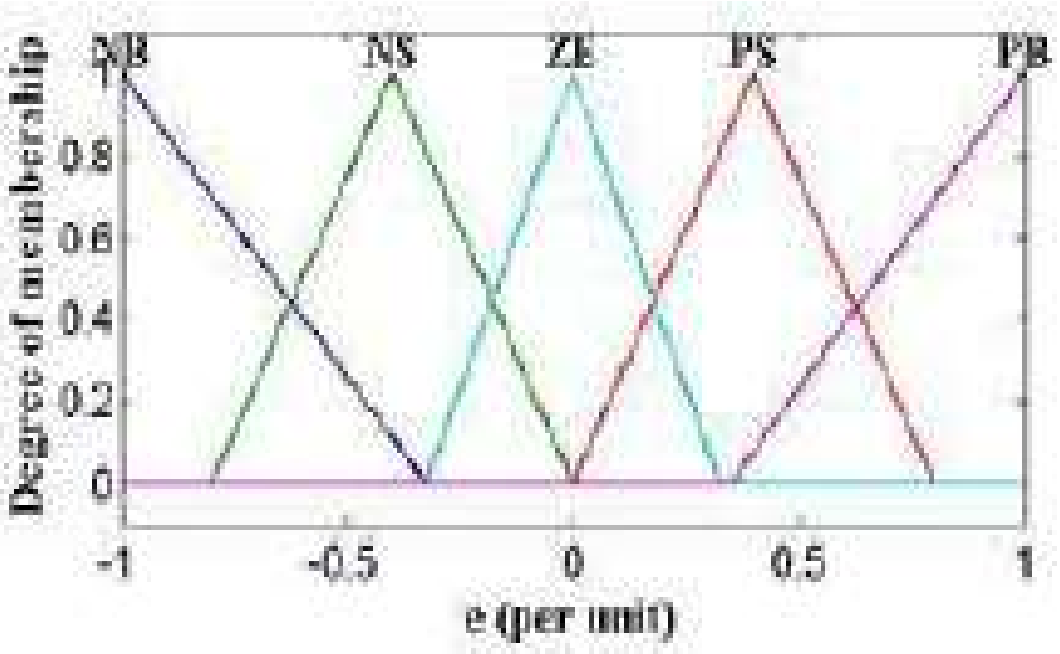

(A) ERROR (E)

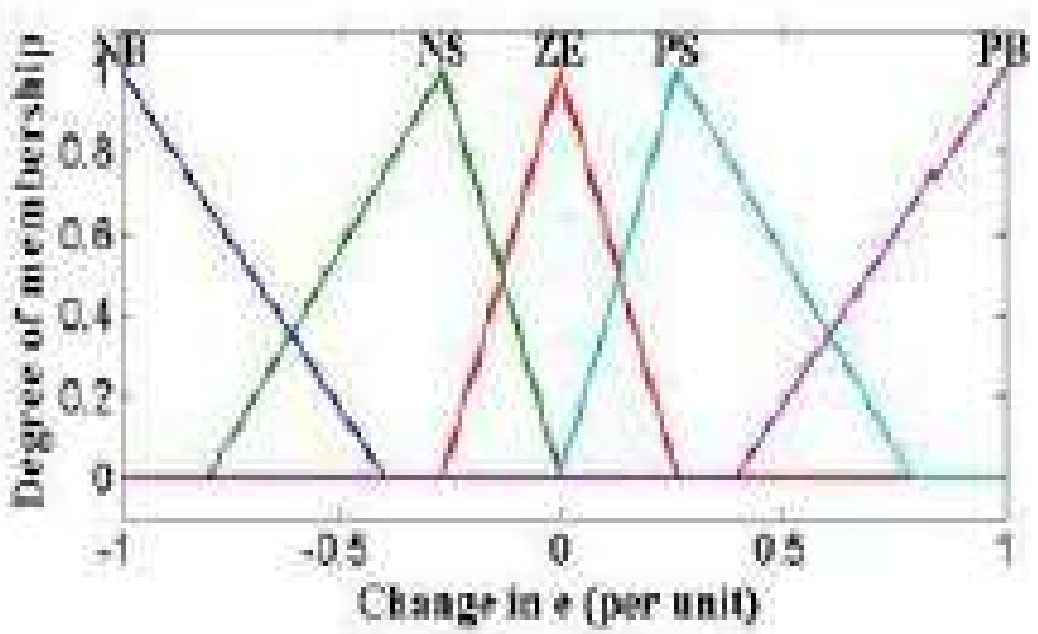

(A) CHANGE IN ERROR (ΔE)

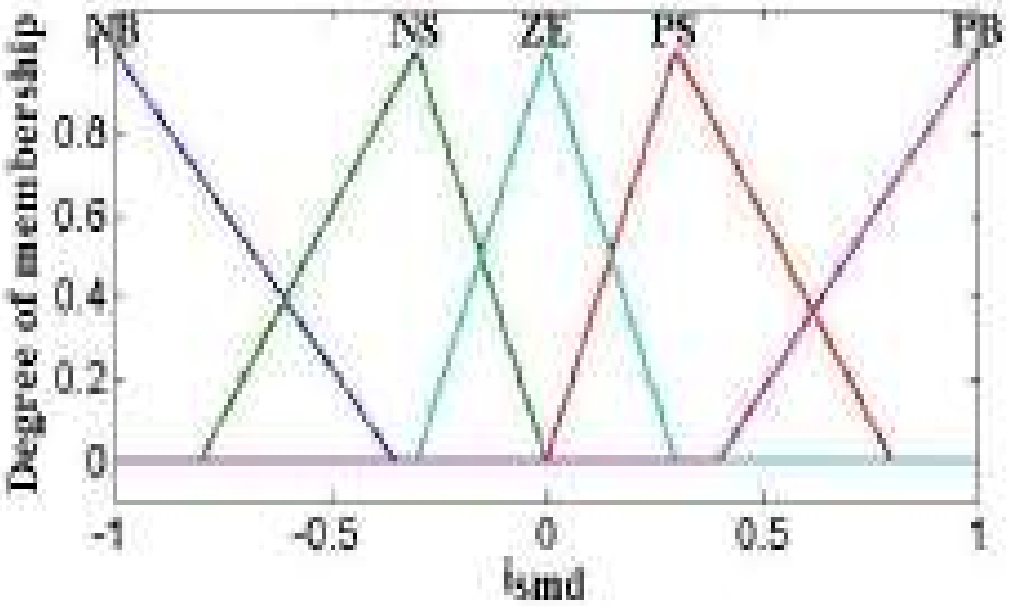

(A)OUTPUT FUZZY MEMBERSHIP FUNCTIONS

FIGURE 4.36 INPUT AND OUTPUT MEMBERSHIP FUNCTIONS OF FLC

TABLE 4.1 FUZZY CONTROL RULE TABLE

E \ Δ E		ΔE				
		NB	**NS**	**ZE**	**PS**	**PB**
	NB	NB	NB	NB	NS	ZE
	NS	NB	NB	NS	ZE	PS
	ZE	NB	NS	ZE	PS	PB
	PS	NS	ZE	PS	PB	PB
	PB	ZE	PS	PB	PB	PB

These variables are defuzzified into a control signal, which is compared to a carrier signal (Md) to form a PWM gating pulse for the proposed PFC SEPIC converter.

4.5.4 RESULTS AND DISCUSSION

The simulation results for the proposed PFC SEPIC converter fed VSI driven BLDC motor with suggested FLC utilised for speed control are provided in this part. In order to verify the controller's performance, the SEPIC converter design with the proposed controller is also modelled using MATLAB software. The simulation results show that the suggested FLC is effective for BLDC motor speed control and power factor enhancement.

To evaluate the overall performance of the proposed PFC SEPIC converter with BLDC motor, five case studies are investigated. The first four case studies deal with varied BLDC motor speeds, whereas the fifth instance is primarily for BLDC motors under dynamic load situations. All of the case studies are based on variances in rising time and settling time in both DC-link voltage and motor speed.

4.5.4.1 CASE 1: BLDC MOTOR UNDER 1500 RPM

The FLC-based speed control method is analysed with the motor speed set at 1500 rpm. A single phase 230 V supply powers the planned BL PFC SEPIC converter.

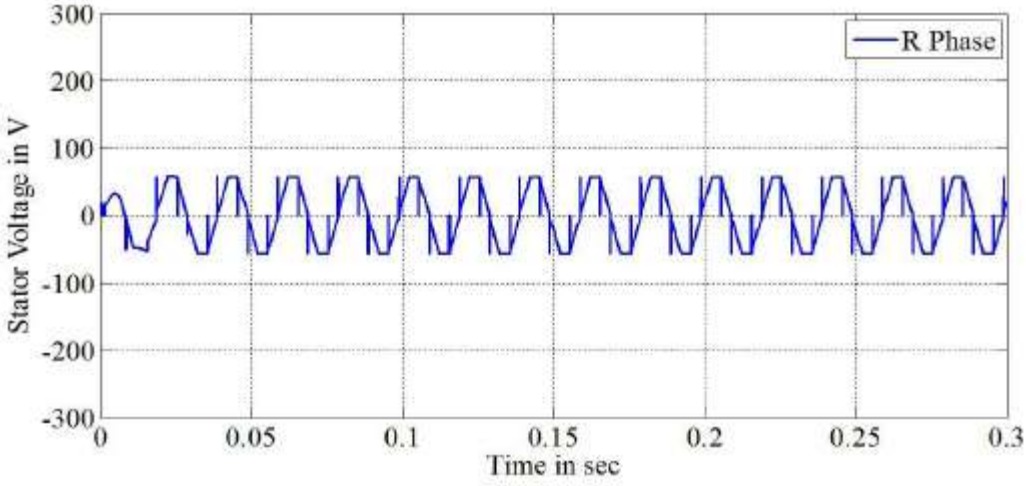

(A) STATOR VOLTAGE FOR R PHASE

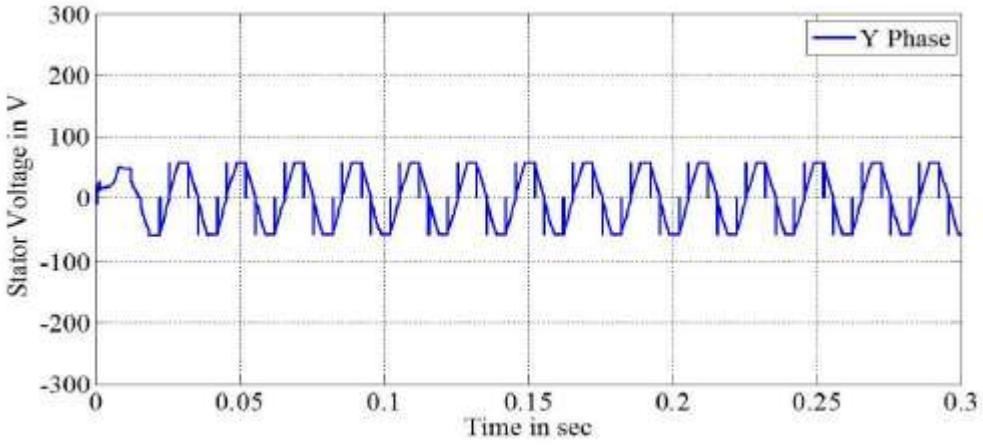

(B) STATOR VOLTAGE FOR Y PHASE

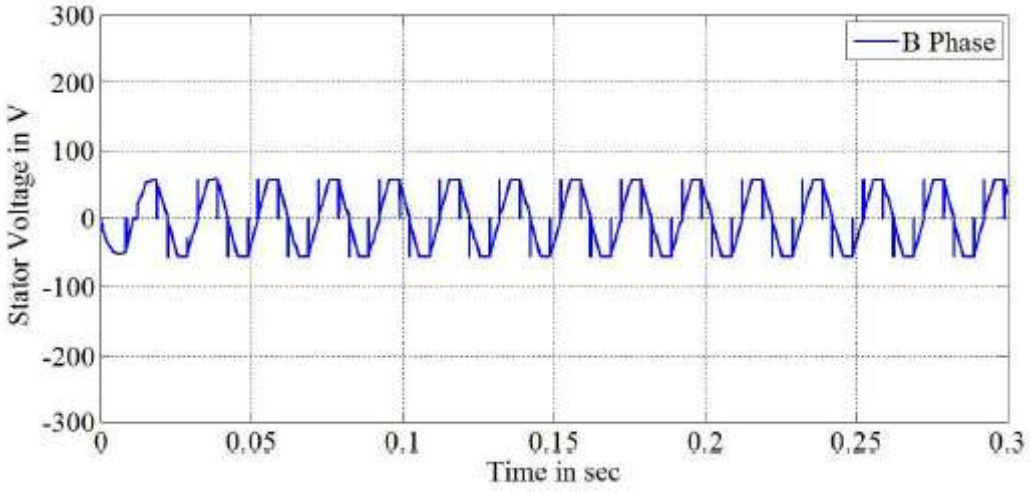

(C) STATOR VOLTAGE FOR B PHASE

FIGURE 4.37 BLDC MOTOR STATOR VOLTAGE FOR ALL THE THREE PHASES FOR CASE 1

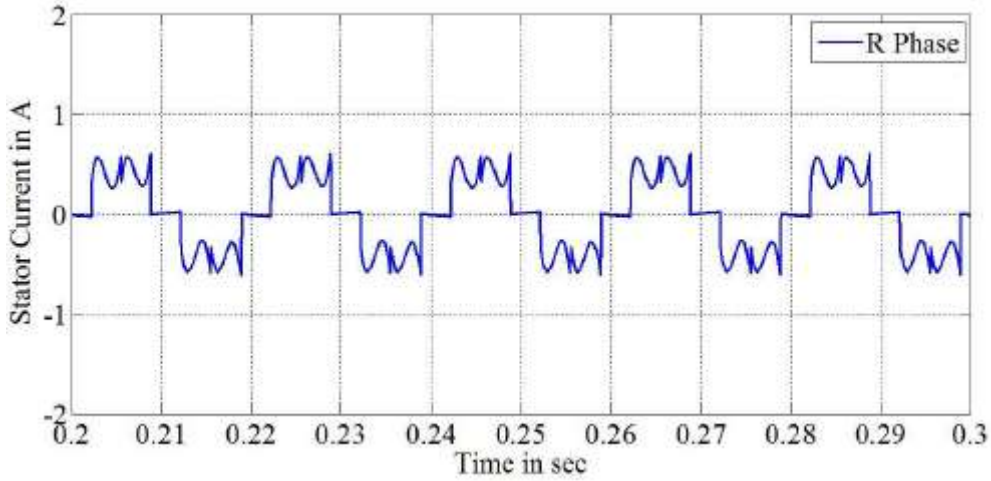

(A) STATOR CURRENT FOR R PHASE

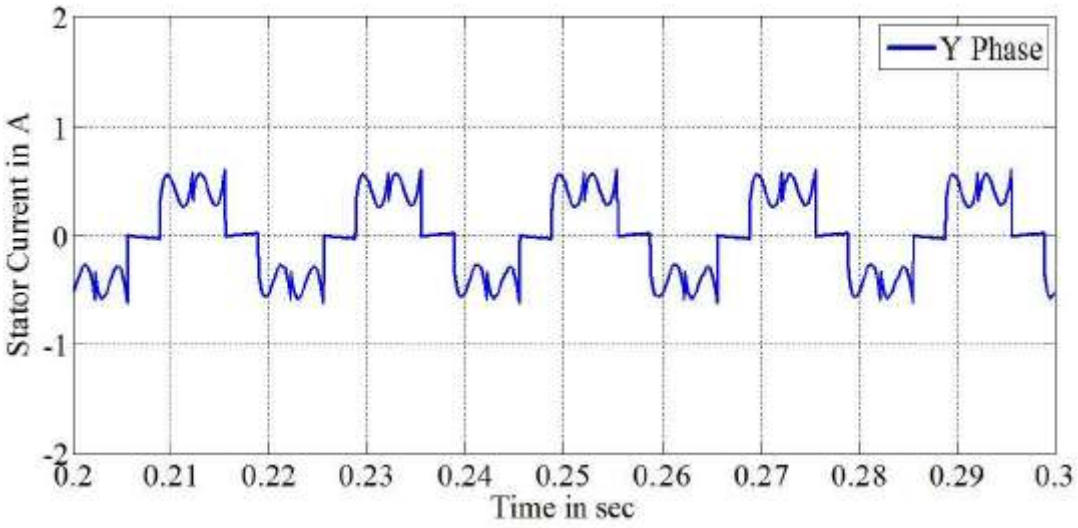

(B) STATOR CURRENT FOR Y PHASE

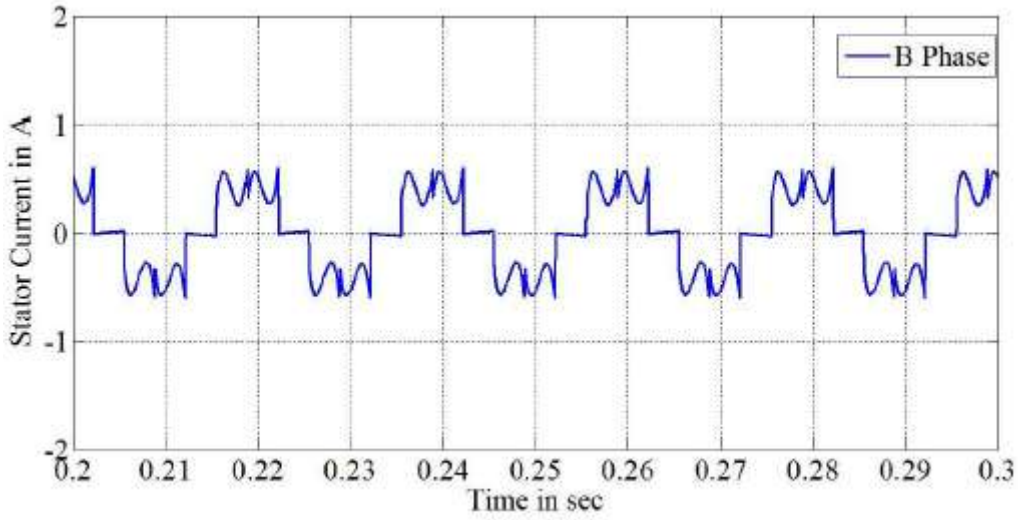

(C) STATOR CURRENT FOR B PHASE

FIGURE 4.38 BLDC MOTOR STATOR CURRENT FOR ALL THE THREE PHASES IN CASE 1

The suggested converter's output is the three-leg VSI's DC bus (DC-link) voltage. The BLDC motor's speed is proportional to the DC-link voltage of the three-leg VSI. As a result, the suggested SEPIC converter is primarily employed to keep the DC-link capacitor voltage stable. The suggested FLC-based speed control technique lowers DC-link voltage and speed error rise time variances and settling time differences. To drive the motor at the specified speed, the three-leg VSI is linked to the stator of the

BLDC motor. The three phase stator voltage and current waveforms are shown in Figures 4.37 and 4.38, respectively.

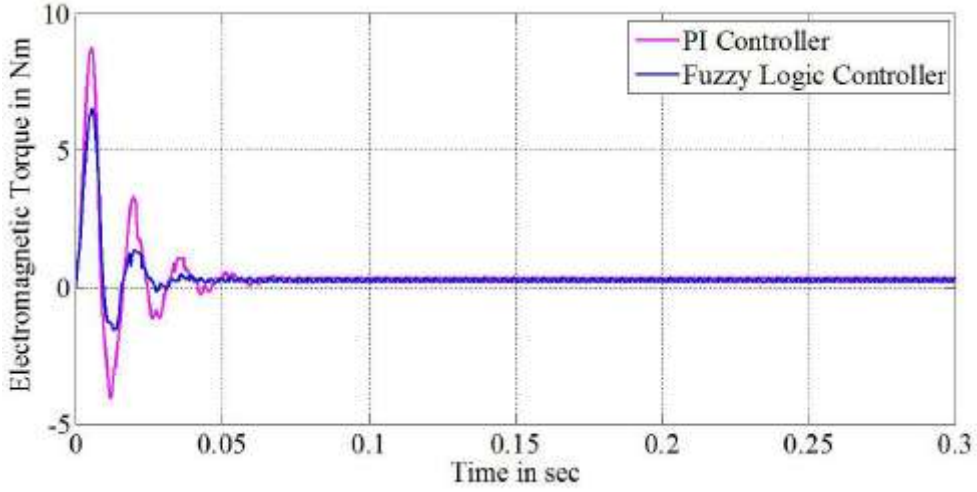

FIGURE 4.39 ELECTROMAGNETIC TORQUE OF THE BLDC MOTOR FOR CASE 1

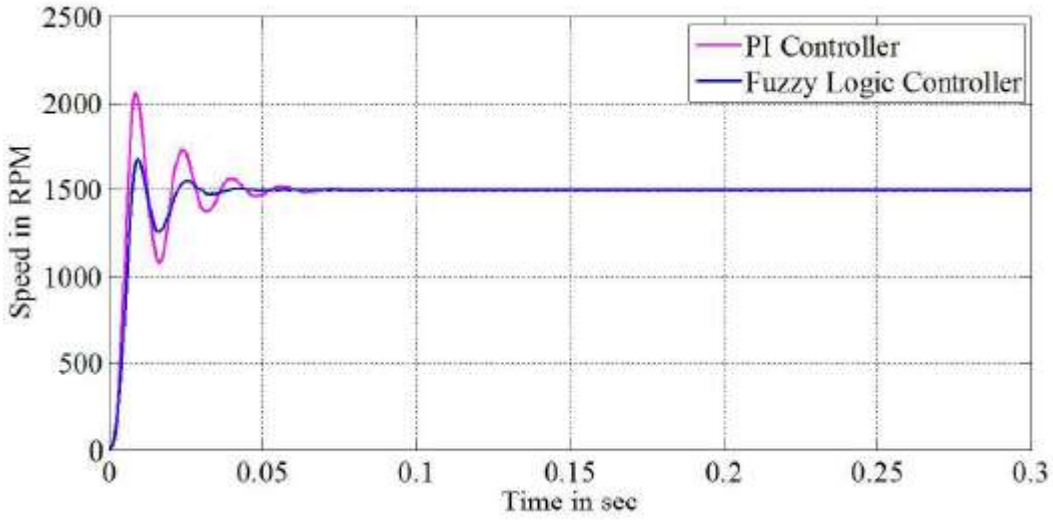

FIGURE 4.40 SPEED OF THE BLDC MOTOR FOR CASE 1

For simulation times ranging from 0 to 0.3 seconds, the stator voltage waveforms for the three phases R, Y, and B are derived. Similarly, for simulation times ranging from 0.2 to 0.3 seconds, the stator current waveforms for the three phases R, Y, and B are shown. Figure 4.39 depicts the electromagnetic torque waveforms of the PI used DC voltage controller and the FLC used DC voltage controller. According to Figure 4.40, the

peak overshoot of the torque has been minimised in FLC when compared to traditional PI controller.

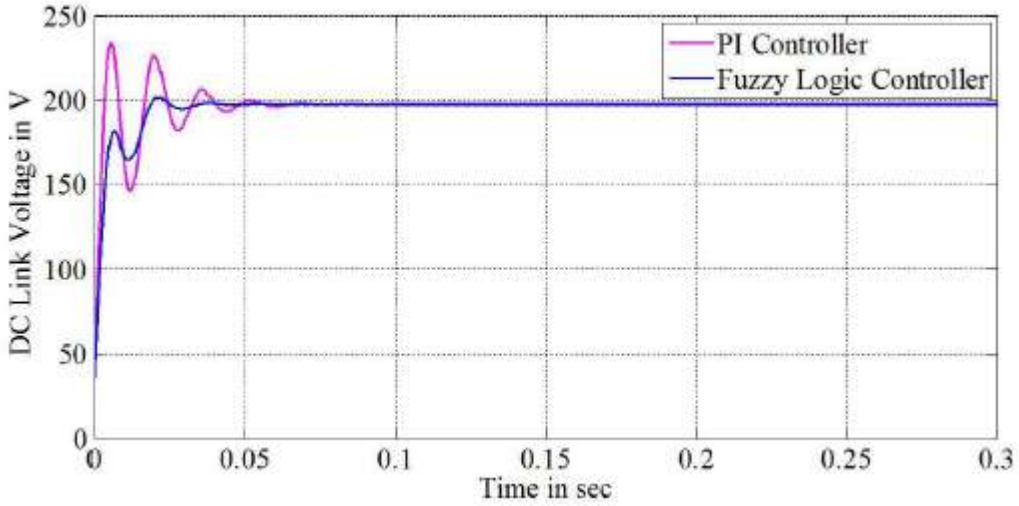

FIGURE 4.41 DC-LINK VOLTAGE OF THE VSI FOR CASE 1

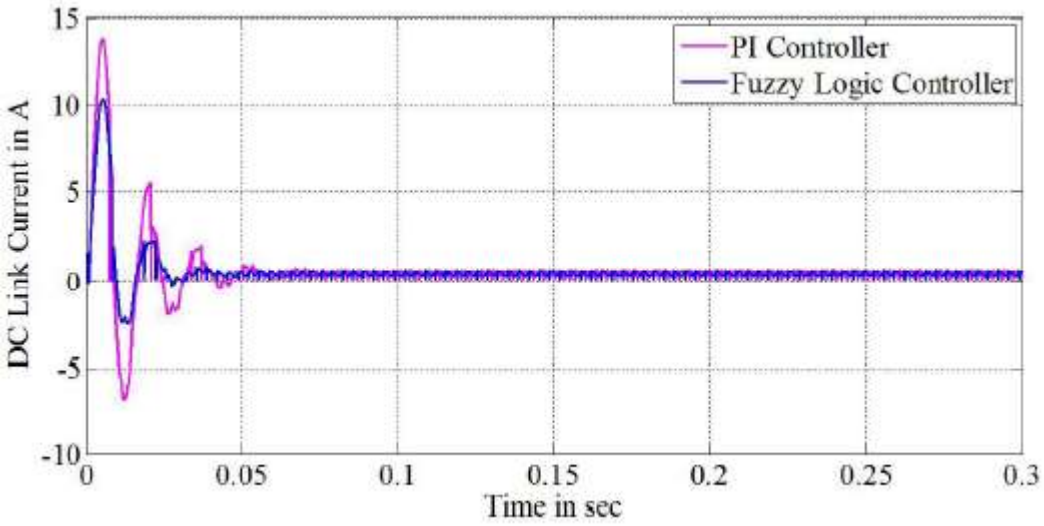

FIGURE 4.42 DC-LINK CURRENT OF THE VSI FOR CASE 1

Figure 4.41 depicts the BLDC motor speed under standard PI and the suggested fuzzy based control technique. This figure shows that the speed of the motor is settled at 0.06 sec for the traditional controller and 0.03 sec for the fuzzy controller. After settling, it maintains the same speed of 1500 rpm for the duration of the 0.3-second simulation. Figure 4.40

depicts the DC-link voltage of the three-leg VSI for traditional PI and the suggested fuzzy-based control system for simulation times ranging from 0 to 0.3 sec. The figure shows that the DC-link voltage is settled at 0.07 sec for the PI controller and 0.03 sec for the fuzzy controller.

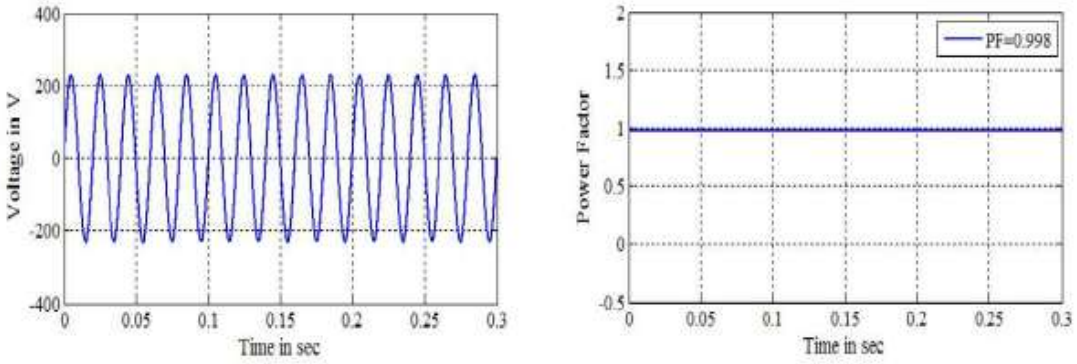

(A) SOURCE VOLTAGE C) POWER FACTOR OF INPUT AC SOURCE

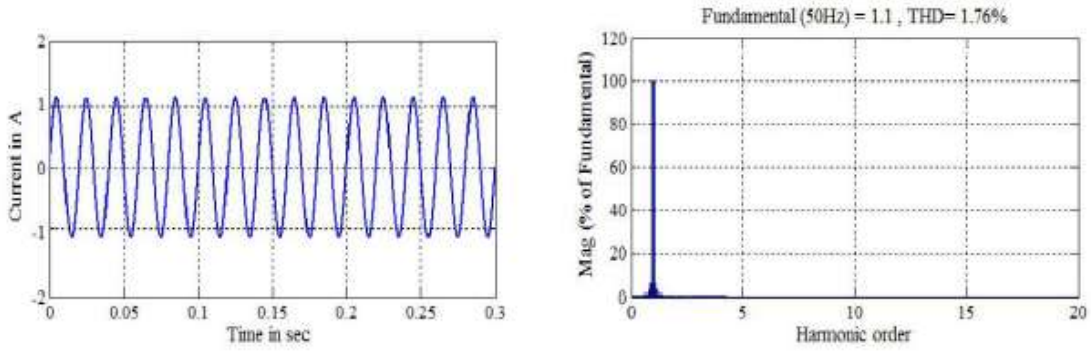

(B) SOURCE CURRENT (D) CURRENT THD OF THE AC SOURCE

FIGURE 4.43 SOURCE VOLTAGE, CURRENT, POWER FACTOR AND CURRENT THD OF THE AC SOURCE IN CASE 1

To keep the motor running at the required speed, a DC-link voltage of 200 V is maintained at the three-leg VSI. Figure 4.42 depicts the DC-link current for traditional PI and the suggested fuzzy based control

technique. The figure shows that the rising time in current has been lowered in the FLC when compared to the standard PI controller. Hence, when comparing the fuzzy control system to the standard PI controller, the rising time deviations and settling time difference in both DC-link voltage and motor speed have been greatly decreased. Figures 4.43 (a) through (d) depict the source voltage, source current, power factor of the input AC source, and current THD of the AC source, in that order.

4.5.4.2 CASE 2: BLDC MOTOR UNDER 2000 RPM

Moreover, the FLC-based speed control system is investigated using a motor speed of 2000 rpm. To maintain the DC-link voltage, the front-end suggested SEPIC converter is regulated using a fuzzy based speed control mechanism, as previously mentioned. As a result, the speed control system creates the appropriate PWM pulse for the proposed SEPIC converter, allowing the motor to run at the specified speed. Figures 4.44 and 4.45 show the stator voltage and current waveforms for the three phases R, Y, and B, respectively. The stator voltage waveforms for the three phases are produced for simulation times ranging from 0 to 0.3 seconds. Similarly, for this scenario, the stator current waveforms of all three phases R, Y, and B are reported for simulation times ranging from 0.2 to 0.3 seconds.

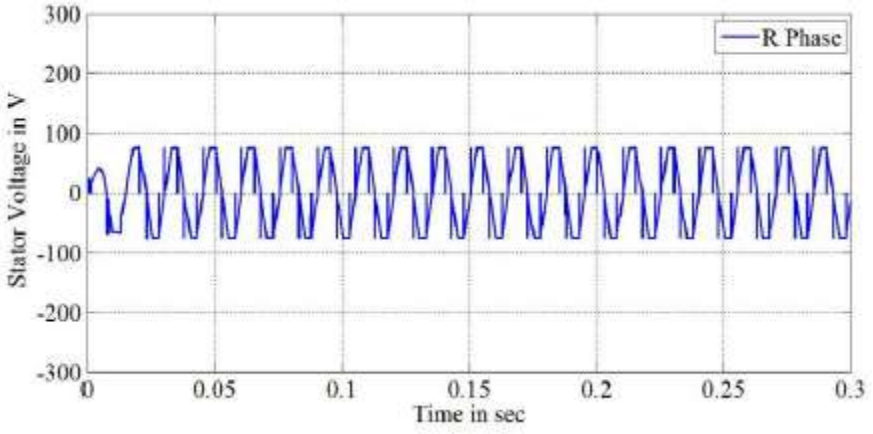

(A) STATOR VOLTAGE FOR R PHASE

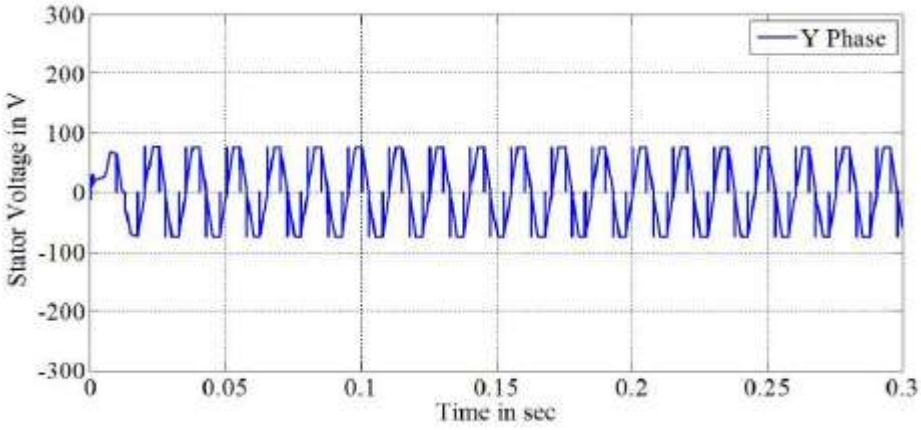

(B) STATOR VOLTAGE FOR Y PHASE

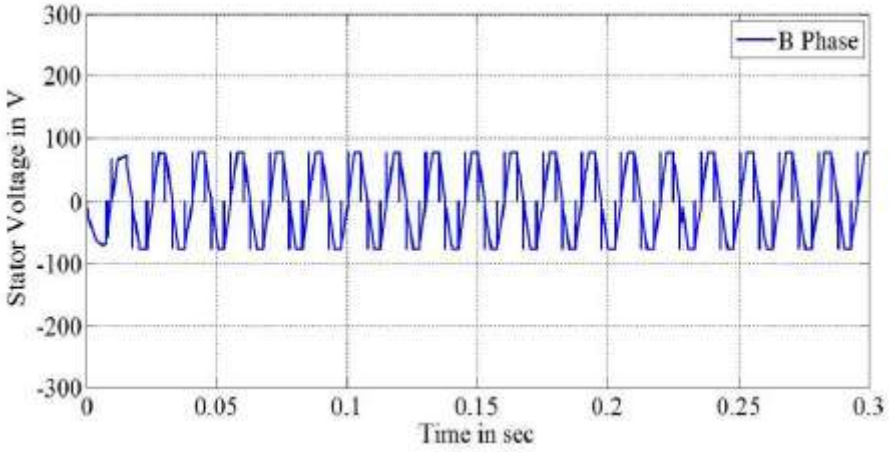

(C) STATOR VOLTAGE FOR B PHASE

FIGURE 4.44 BLDC MOTOR STATOR VOLTAGE FOR ALL THE THREE PHASES IN CASE 2

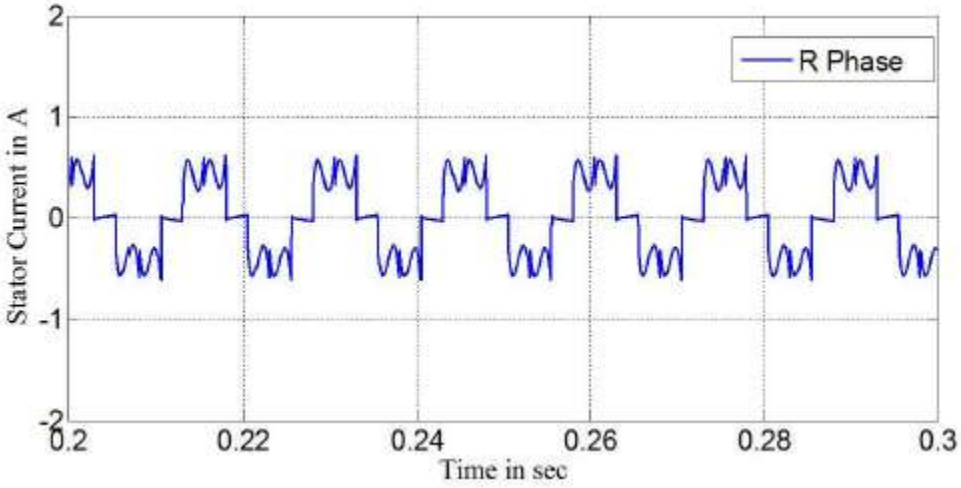

(A) STATOR CURRENT FOR R PHASE

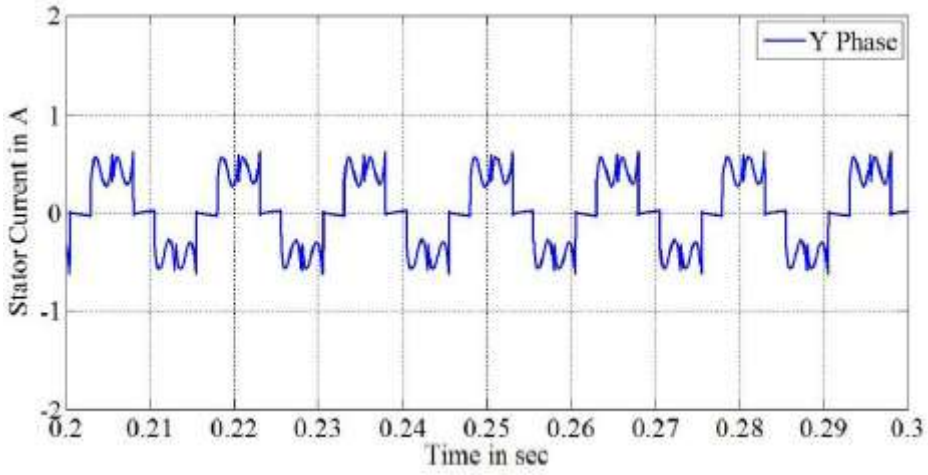

(B) STATOR CURRENT FOR Y PHASE

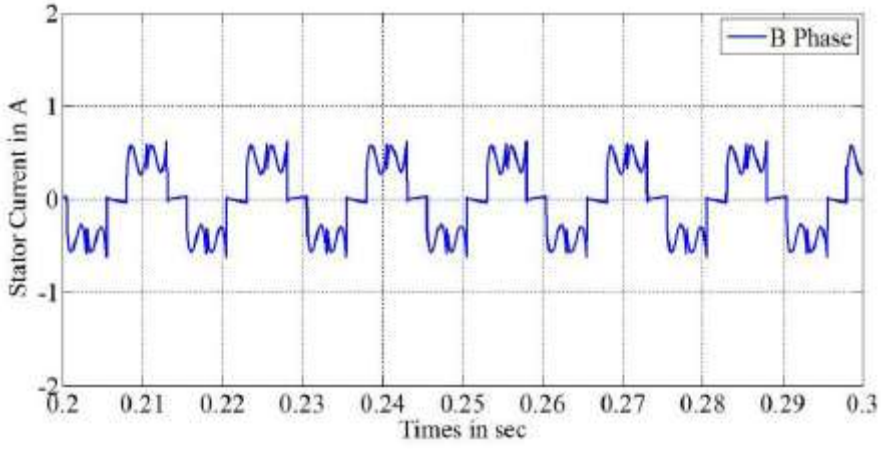

(C) STATOR CURRENT FOR B PHASE

FIGURE 4.45 BLDC MOTOR STATOR CURRENT FOR ALL THE THREE PHASES IN CASE 2

Figure 4.46 depicts the electromagnetic torque of the BLDC motor for PI and fuzzy controller. Figure 4.46 shows that the rising time in torque has been significantly decreased in FLC when compared to PI controller. Figure 4.47 depicts the BLDC motor speed under standard PI and the suggested fuzzy based speed control approach. According to Figure 4.47, the conventional controller settles the motor speed at 0.05 sec, whereas the fuzzy controller settles at 0.04 sec. After 0.04 sec, the speed remains steady at 2000 rpm for the duration of the 0. 3sec simulation.

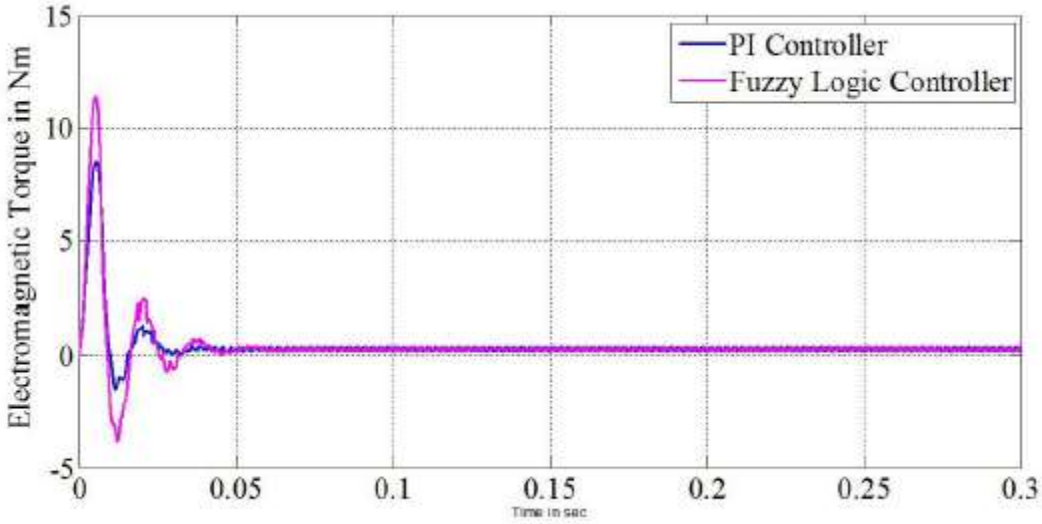

FIGURE 4.46 ELECTROMAGNETIC TORQUE OF THE BLDC MOTOR FOR CASE 2

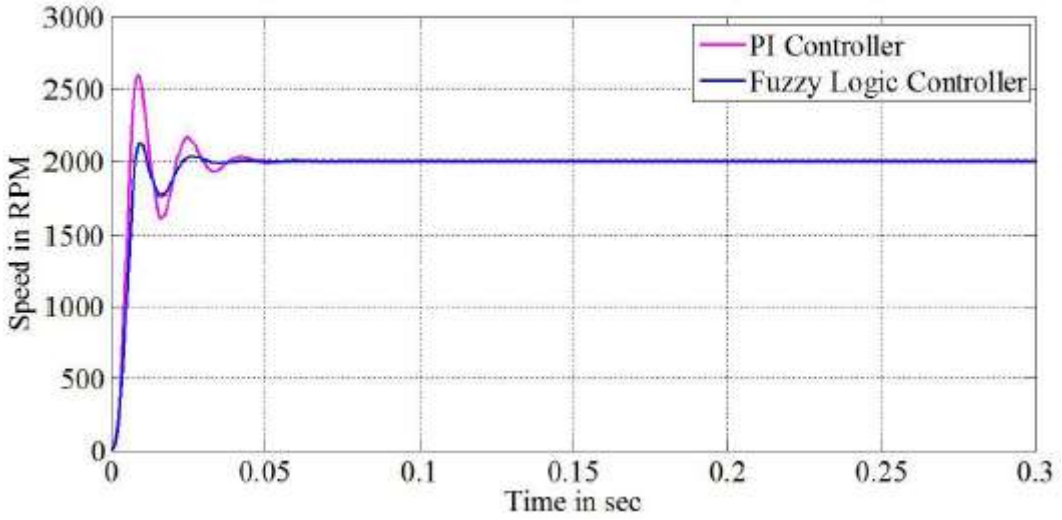

FIGURE 4.47 SPEED OF THE BLDC MOTOR FOR CASE 2

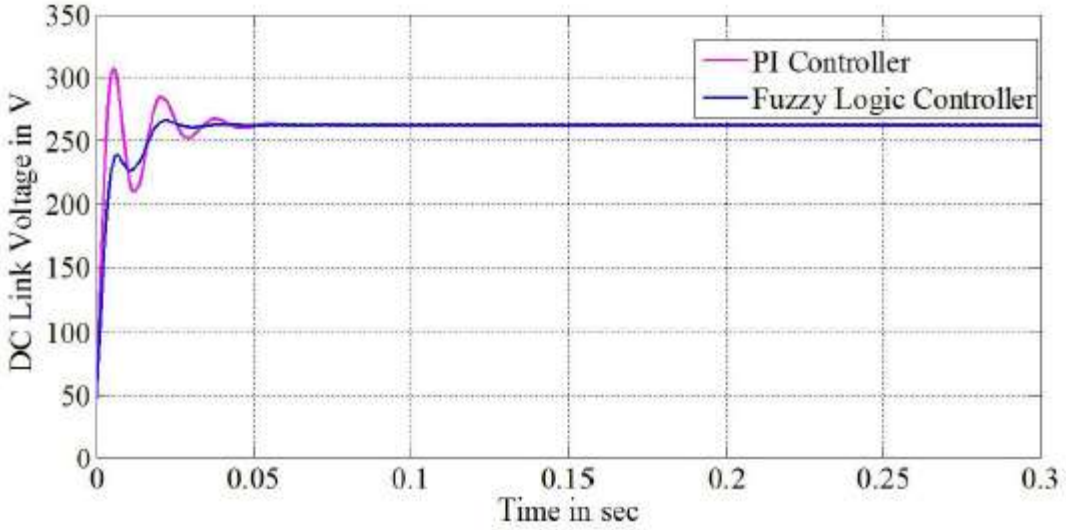

FIGURE 4.48 DC-LINK VOLTAGE OF THE VSI FOR CASE 2

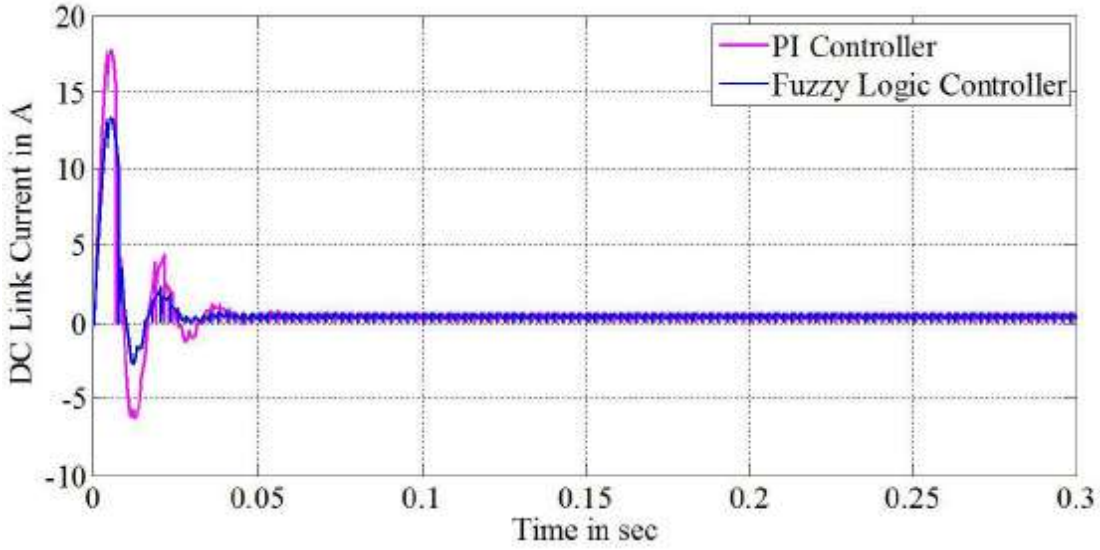

FIGURE 4.49 DC-LINK CURRENT OF THE VSI FOR CASE 2

Figure 4.48 shows the DC-link voltage of the three-leg VSI for traditional PI and the suggested fuzzy based speed control system for simulation times ranging from 0 sec to 0.3 sec. According to the graph, the DC-link voltage settles at 0.05 sec for the PI controller and 0.028 sec for the fuzzy controller. To keep the motor running at the correct speed, a DC-link voltage of 271.33 V is maintained at the three-leg VSI. Figure 4.49 depicts the DC-link current for both the standard PI and the suggested fuzzy controller. The increase time in current has been lowered in FLC when compared to traditional PI controller, as seen in the figure. As compared to the typical PI controller, FLC significantly reduced the rising time deviations and settling time difference in both DC-link voltage and motor speed. Figure 4.50 (a) - (d) depict the source voltage, source current, power factor of the input AC source, and current THD of the AC source, in that order.

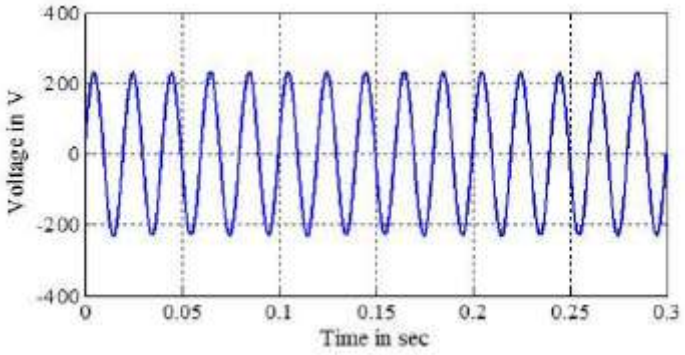

(A) SOURCE VOLTAGE

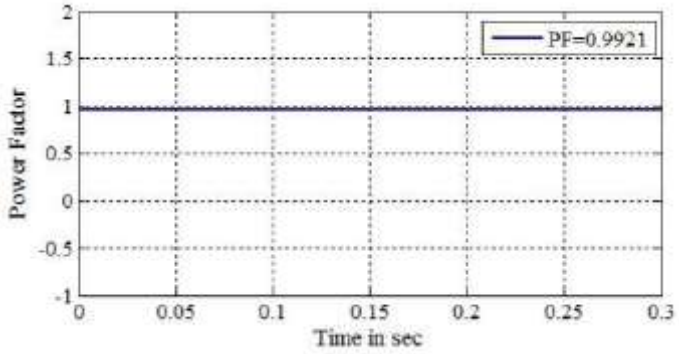

(C) POWER FACTOR OF INPUT AC SOURCE

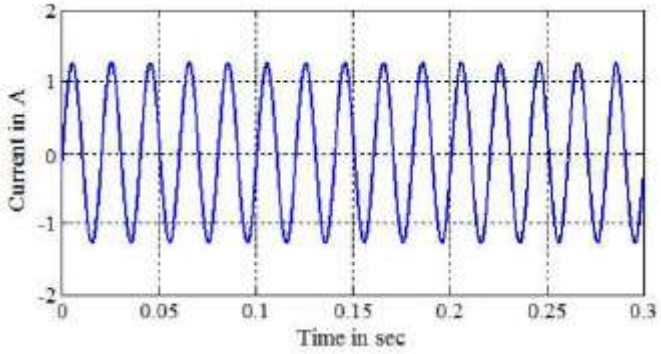

(B) SOURCE CURRENT

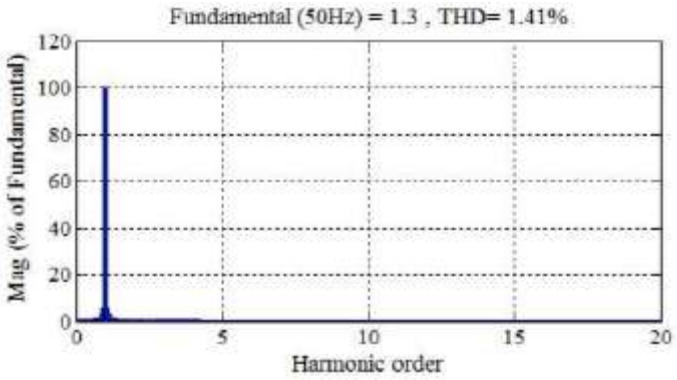

(D) CURRENT THD OF THE AC SOURCE

FIGURE 4.50 SOURCE VOLTAGE, CURRENT, POWER FACTOR AND CURRENT THD OF THE AC SOURCE IN CASE 2

4.5.4.3 CASE 3: BLDC MOTOR UNDER 2500 RPM

The analysis is also carried out by setting the motor speed as 2500 rpm. The fuzzy based speed control scheme is employed to change the PWM pulse for the proposed SEPIC converter. Thus, it helps to maintain necessary voltage at the DC-link capacitor of the three-leg VSI to run the motor at the desired speed. Figure 4.51 and Figure 4.52 are the stator voltage and stator current waveforms for the three phases (R, Y and B) respectively. The three phase stator voltage waveforms are observed for simulation times ranging from 0 to 0.3 seconds. Similarly, for this scenario, the three phase stator current waveforms (R, Y, and B) are produced for simulation times ranging from 0.2 to 0.3 sec.

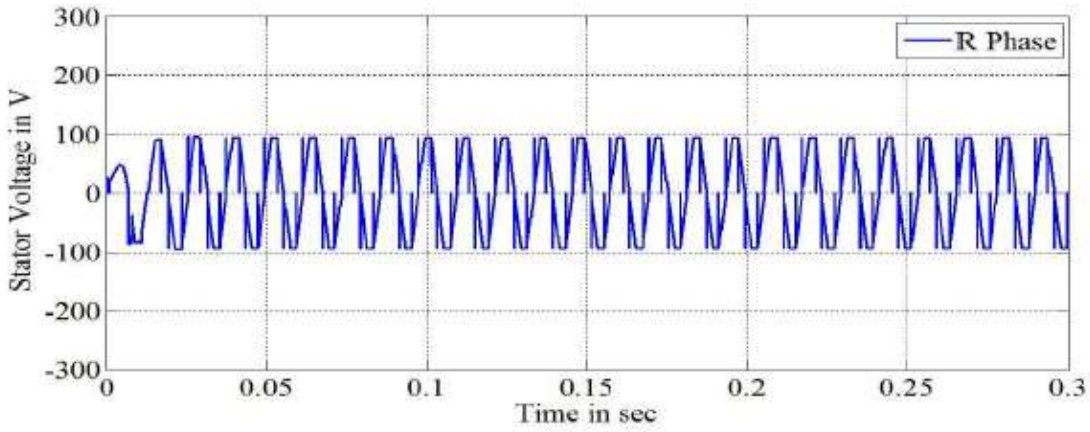

(A) STATOR VOLTAGE FOR R PHASE

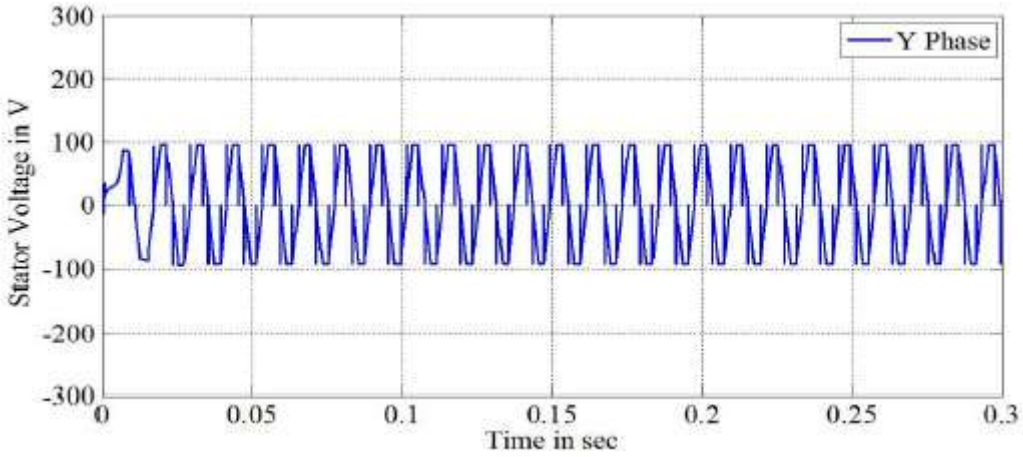

(B) STATOR VOLTAGE FOR Y PHASE

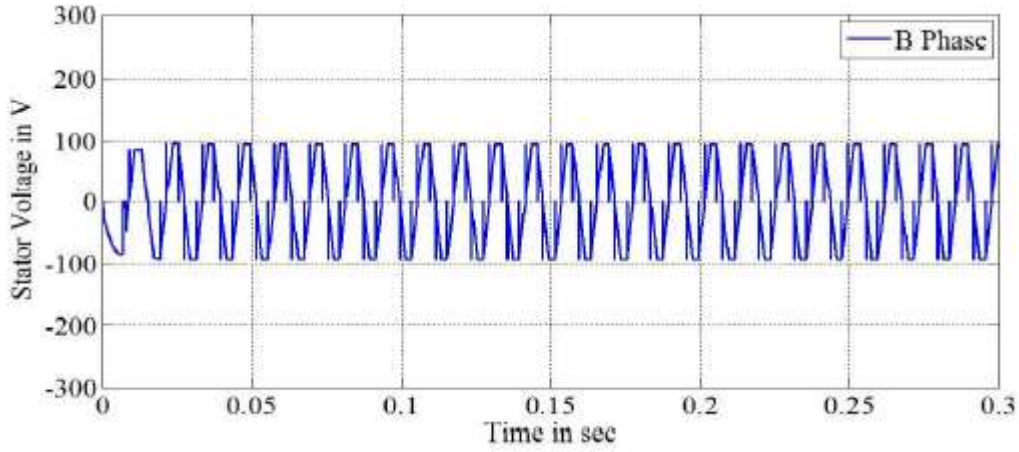

(C) STATOR VOLTAGE FOR B PHASE

FIGURE 4.51 BLDC MOTOR STATOR VOLTAGE FOR ALL THE THREE PHASES IN CASE 3

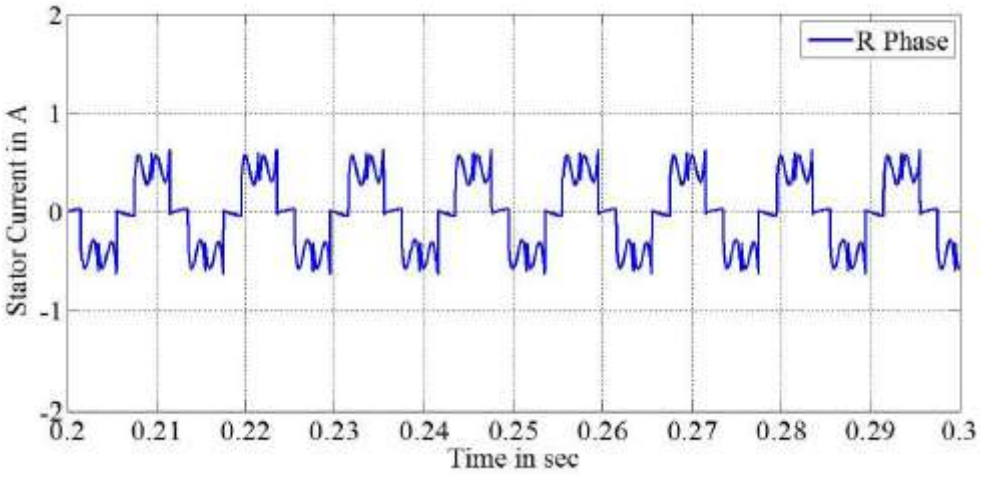

(A) STATOR CURRENT FOR R PHASE

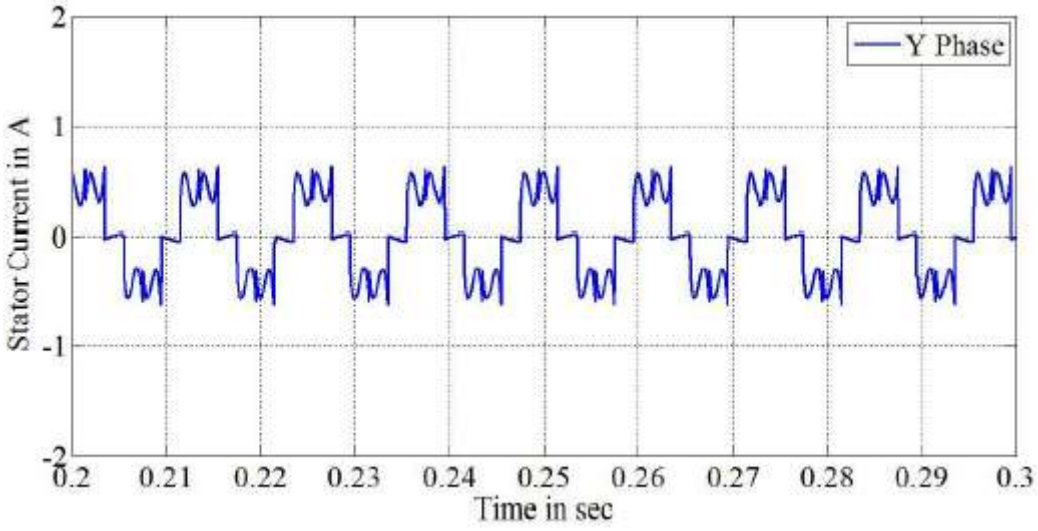

(B) STATOR CURRENT FOR Y PHASE

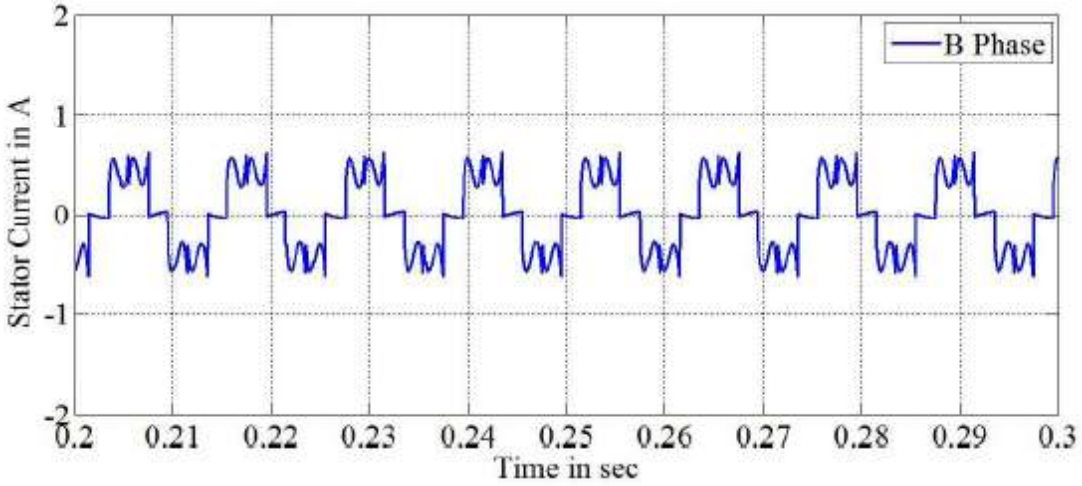

(C) STATOR CURRENT FOR B PHASE

FIGURE 4.52 BLDC MOTOR STATOR CURRENT FOR ALL THE THREE PHASES IN CASE 3

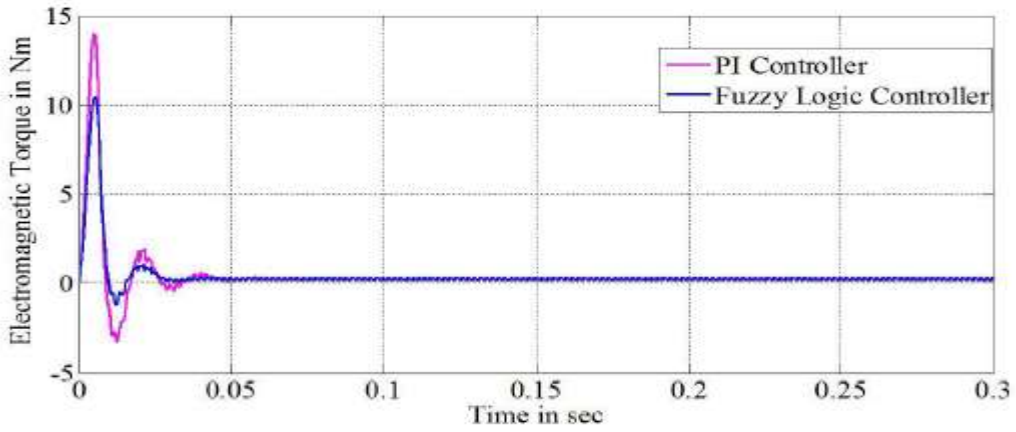

FIGURE 4.53 ELECTROMAGNETIC TORQUE OF THE BLDC MOTOR FOR CASE 3

The electromagnetic torque of the BLDC motor for PI and fuzzy controller is shown in Figure 4.53. Figure 4.53 shows that the torque rising time in FLC has been significantly decreased when compared to PI controller. Figure 4.54 depicts the typical PI BLDC motor speed and the suggested fuzzy based speed control approach. According to Figure 4.54, the conventional controller settles the motor speed at 0.040 sec, but the fuzzy controller settles at 0.025 sec. After 0.025 seconds, the speed remains steady at 2500 rpm for the duration of the 0.3-second simulation.

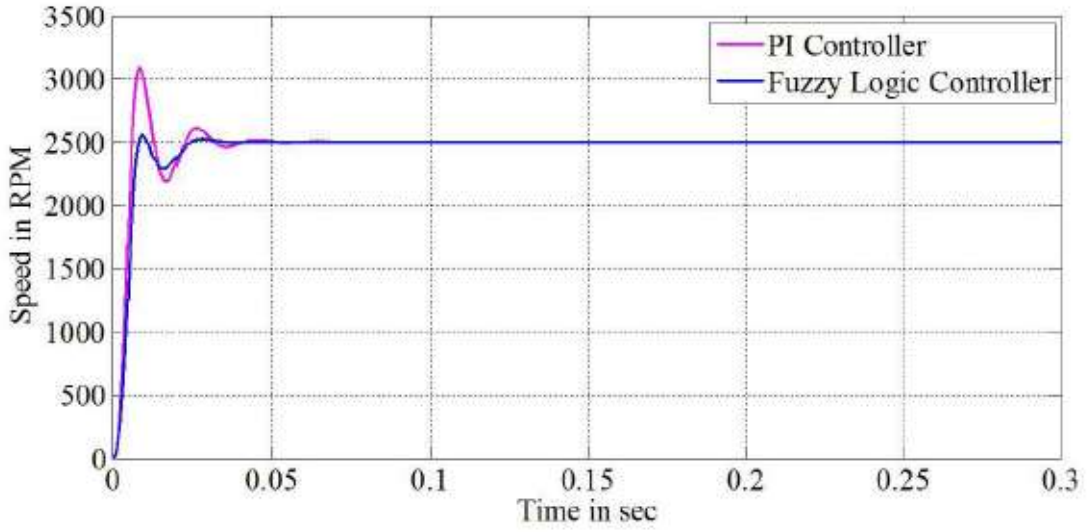

FIGURE 4.54 SPEED OF THE BLDC MOTOR FOR CASE 3

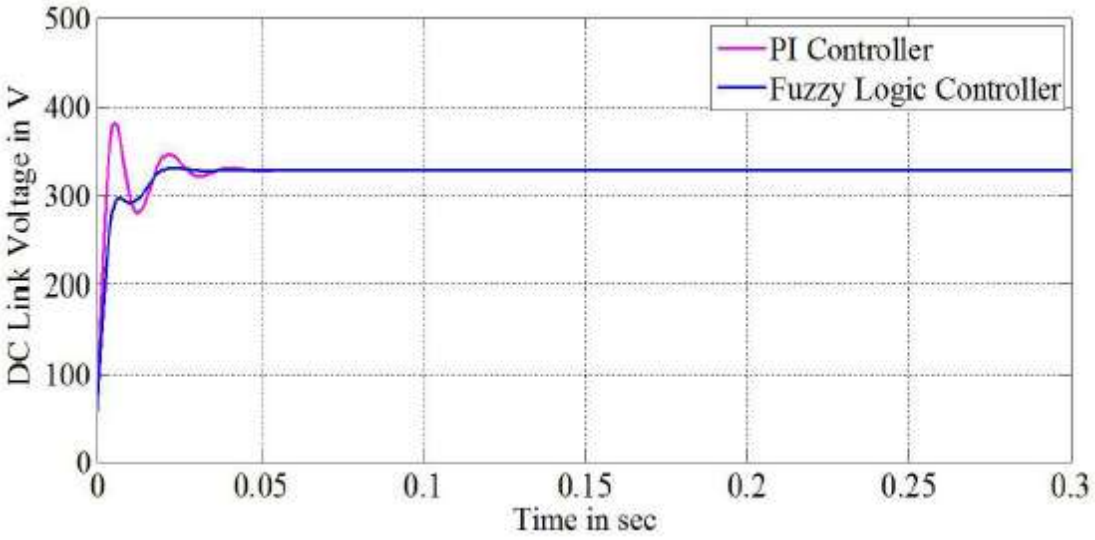

FIGURE 4.55 DC-LINK VOLTAGE OF THE VSI FOR CASE 3

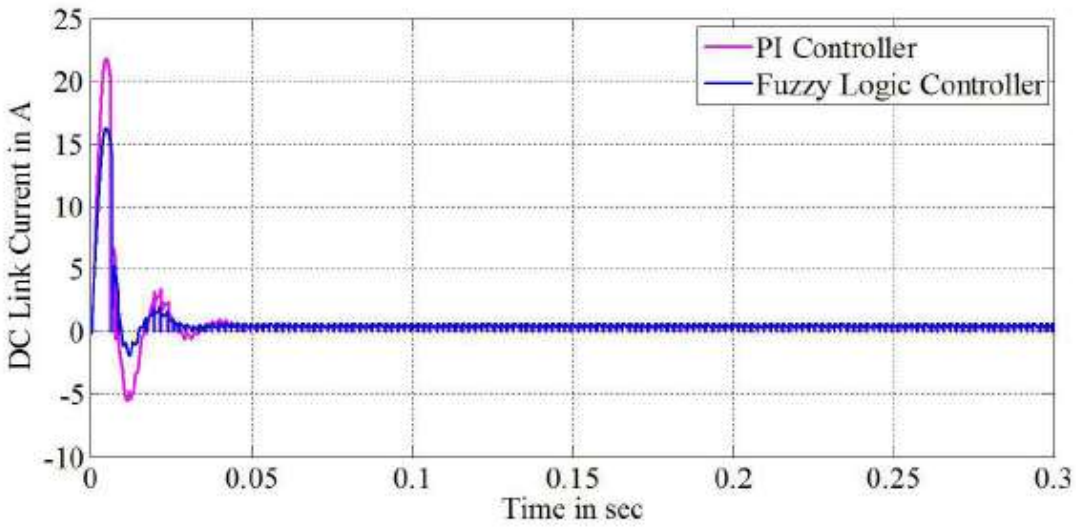

FIGURE 4.56 DC-LINK CURRENT OF THE VSI FOR CASE 3

The DC-link voltage of the three-leg VSI for traditional PI and suggested fuzzy controller is determined for simulation times ranging from 0 sec to 0.3 sec in Figure 4.55. According to Figure 4.55, the DC-link voltage is established at 0.04 sec for the PI controller and 0.025 sec for the fuzzy controller. The DC-link voltage of 332.89 V is maintained at the three-leg VSI to keep the motor running at the required speed.

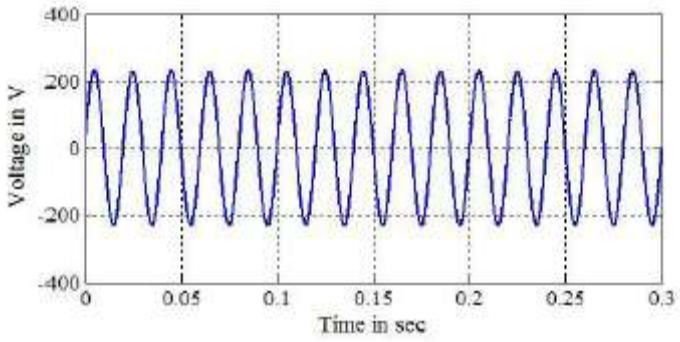

(A) SOURCE VOLTAGE

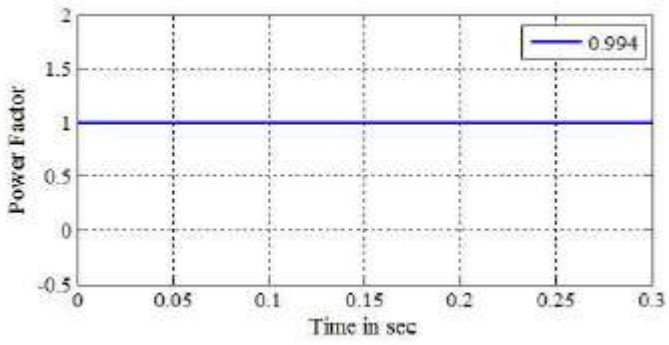

(C) POWER FACTOR OF INPUT AC SOURCE

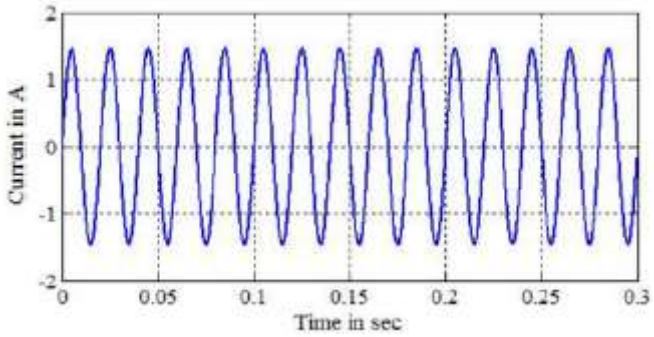

(B) SOURCE CURRENT

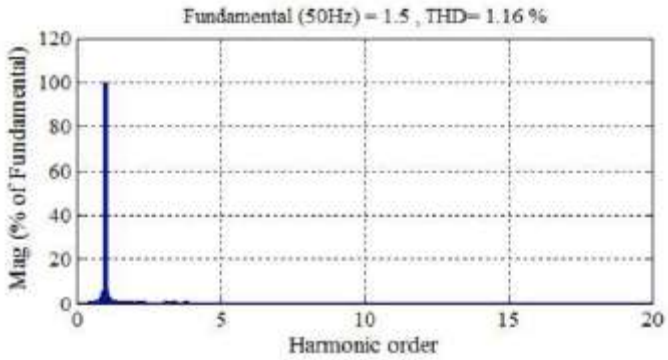

(D) CURRENT THD OF THE AC SOURCE

FIGURE 4.57 SOURCE VOLTAGE, CURRENT, POWER FACTOR AND CURRENT THD OF THE AC SOURCE IN CASE 3

Figure 4.56 depicts the DC-link current waveforms for traditional PI and the suggested fuzzy controller. By comparing the fuzzy control method to the typical PI controller, it is clear from the figure that the rising time in

current has been greatly decreased. The comparison shows that the fuzzy-based speed control system responds faster than the PI controller in terms of rising time deviations and settling time difference in both DC-link voltage and motor speed. Figure 4.57 (a) - (d) depict the source voltage, source current, power factor of the input AC source, and current THD of the AC source, in that order.

4.5.4.4 CASES 4: BLDC MOTOR UNDER 3000 RPM

The proposed system is also tested by setting the motor speed as 3000 rpm.

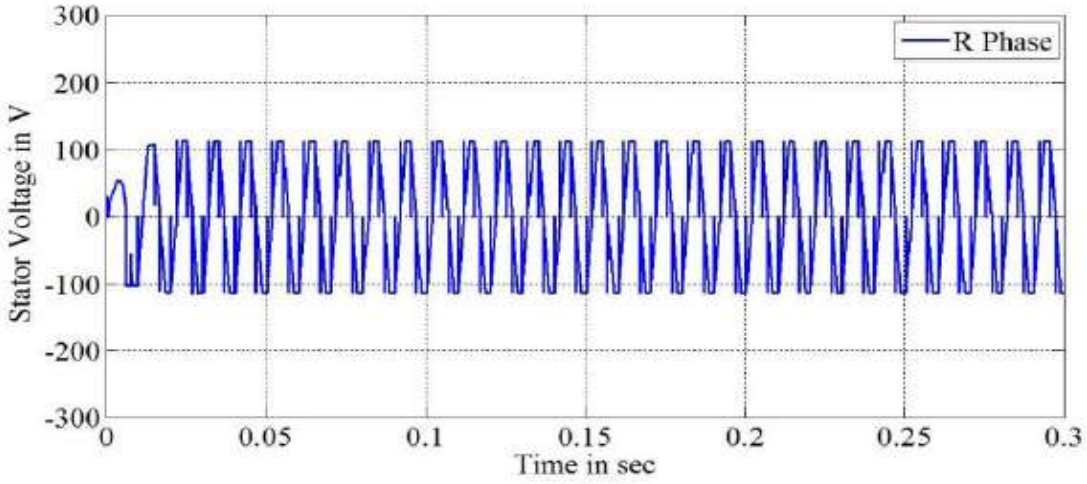

(A) STATOR VOLTAGE FOR R PHASE

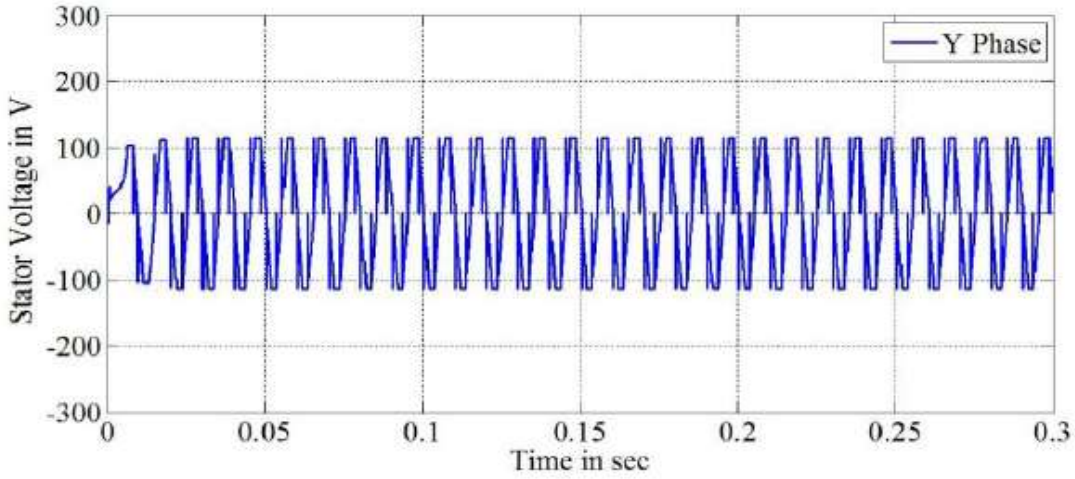

(B) STATOR VOLTAGE FOR Y PHASE

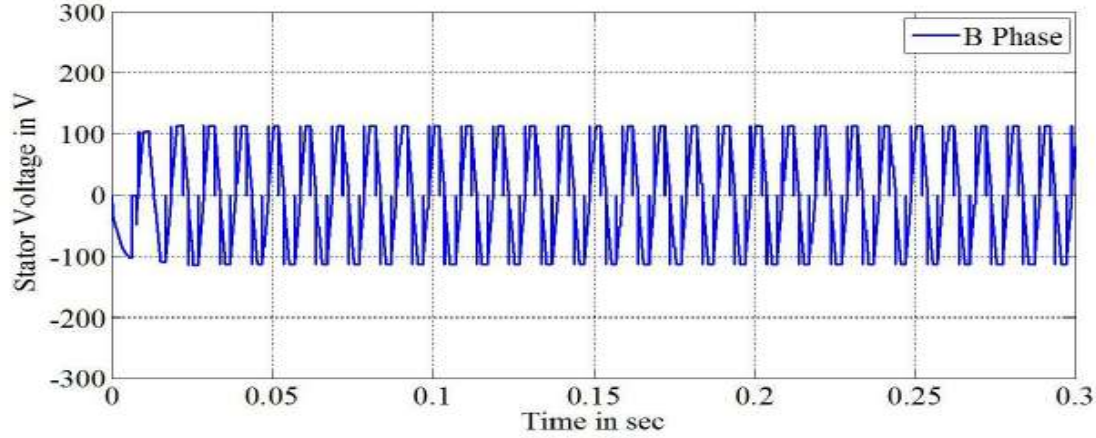

(C) STATOR VOLTAGE FOR B PHASE

FIGURE 4.58 BLDC MOTOR STATOR VOLTAGE FOR ALL THE THREE PHASES IN CASE 4

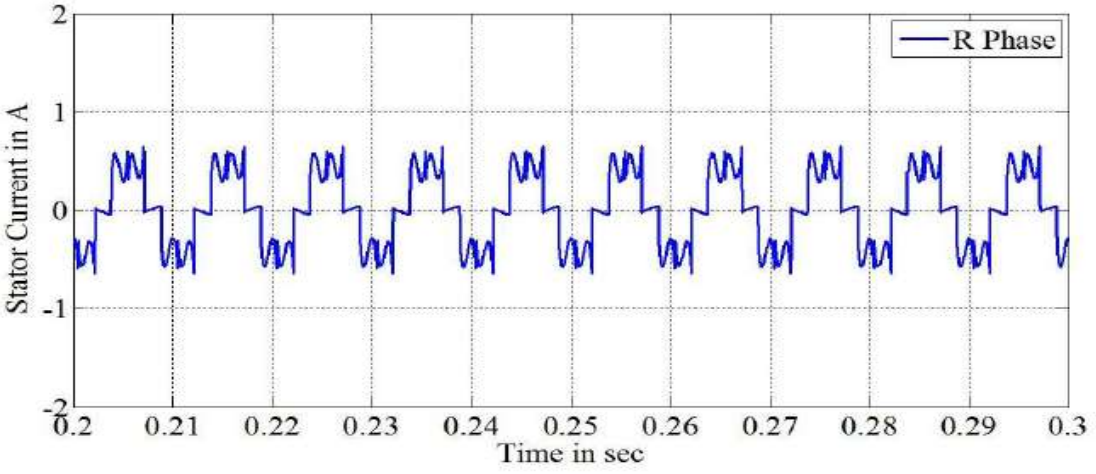

(A) STATOR CURRENT FOR R PHASE

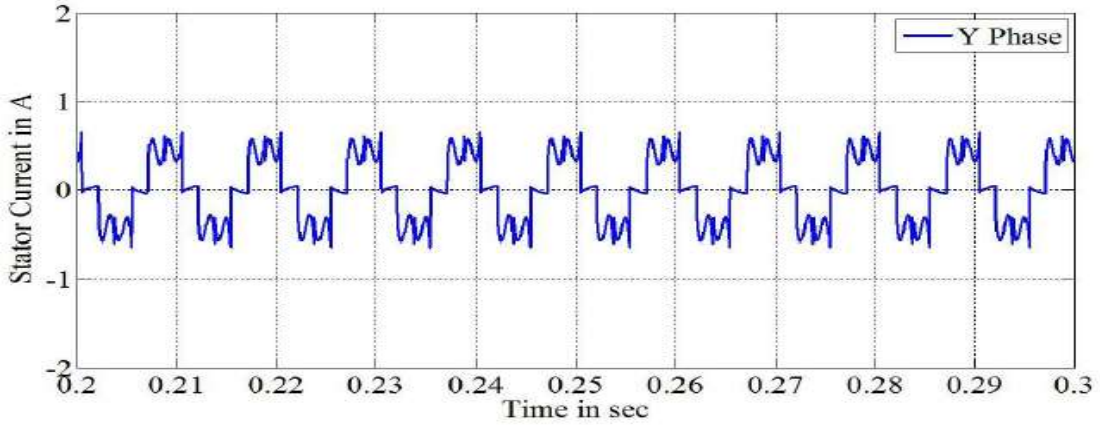

(B) STATOR CURRENT FOR Y PHASE

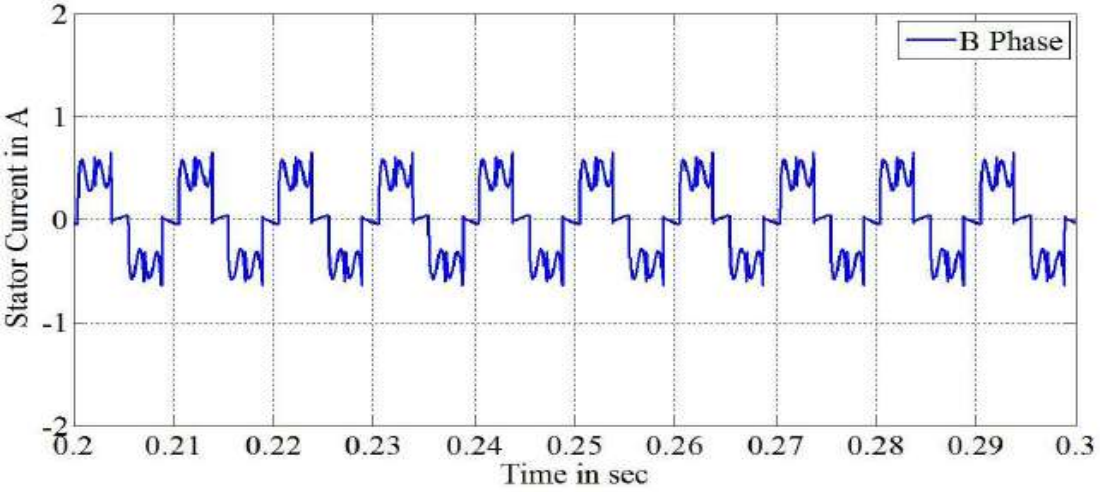

(C) STATOR CURRENT FOR B PHASE

FIGURE 4.59 BLDC MOTOR STATOR CURRENT FOR ALL THE THREE PHASES IN CASE 4

Figures 4.58 and 4.59 depict the stator voltage and current waveforms for the three phases (R, Y, and B). For the simulation duration of 0 sec to 0.3 sec, the stator voltage of the three phases is recorded. Similarly, for this scenario, the three phase stator current waveforms (R, Y, and B) are produced for simulation times ranging from 0.2 to 0.3 sec. Figure 4.60 depicts the electromagnetic torque waveform of the BLDC motor for PI and fuzzy controller. The torque increase time in the fuzzy

controller has been significantly lowered when compared to the PI controller, as shown in Figure 4.60. Figure 4.61 shows the BLDC motor speed for the standard PI and the suggested fuzzy-based speed control system.

According to Figure 4.61, the traditional controller strategy settles the motor speed at 0.035 sec, but the fuzzy controller approach settles at 0.025 sec. After 0.025 seconds, the speed remains steady at 3000 rpm for the duration of the 0.3-second simulation.

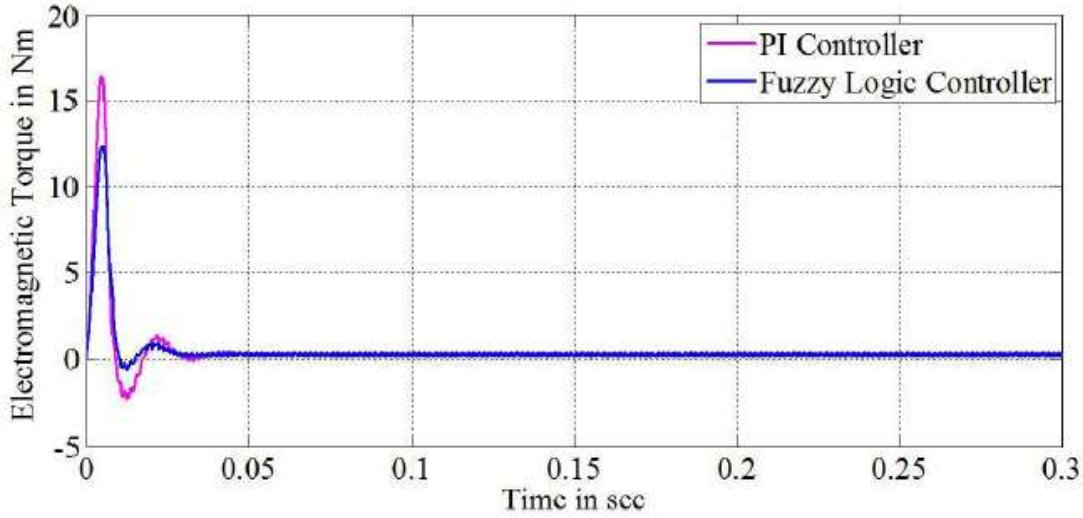

FIGURE 4.60 ELECTROMAGNETIC TORQUE OF THE BLDC MOTOR FOR CASE 4

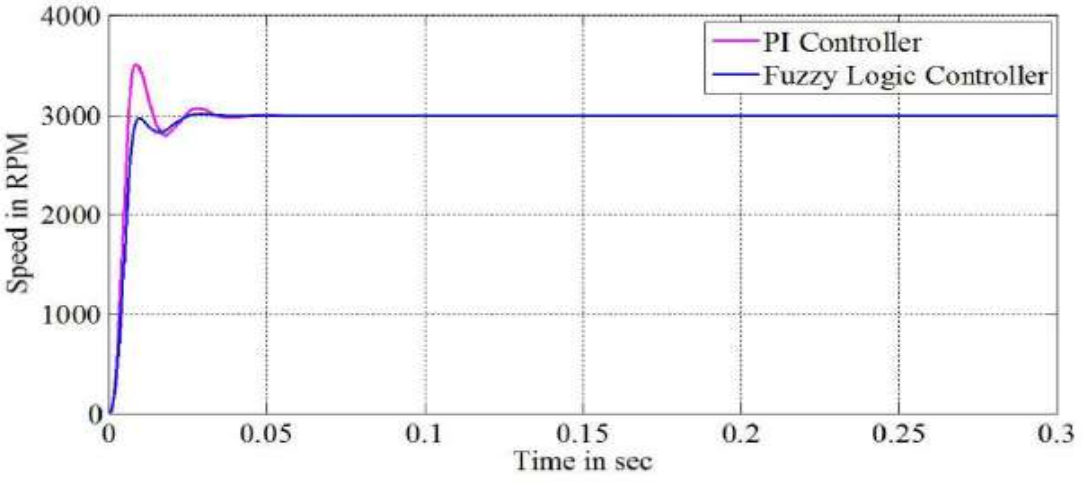

FIGURE 4.61 SPEED OF THE BLDC MOTOR FOR CASE 4

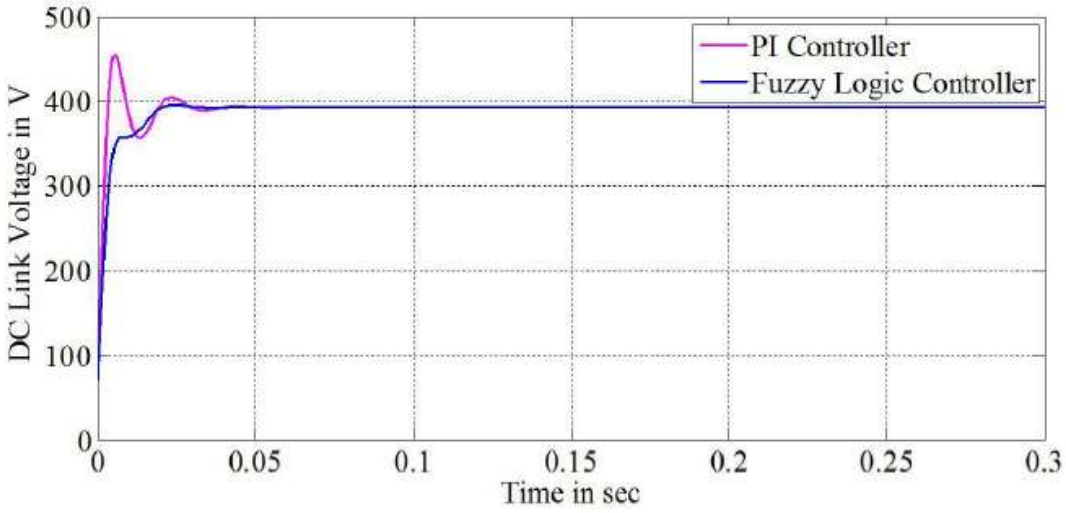

FIGURE 4.62 DC-LINK VOLTAGE OF THE VSI FOR CASE 4

Figure 4.62 depicts the DC-link voltage of a three-leg VSI for traditional PI and the suggested fuzzy controller for simulation times ranging from 0 to 0.3 seconds. According to Figure 4.62, the DC-link voltage is established at 0.035 sec for the PI controller and 0.025 sec for the fuzzy controller. The three-leg VSI maintains the DC-link voltage of 392.38 V. Figure 4.63 depicts the DC-link current waveforms for traditional PI and the suggested fuzzy controller. When comparing the fuzzy control method to the PI controller, it is clear from the figure that the current rise time has been greatly decreased.

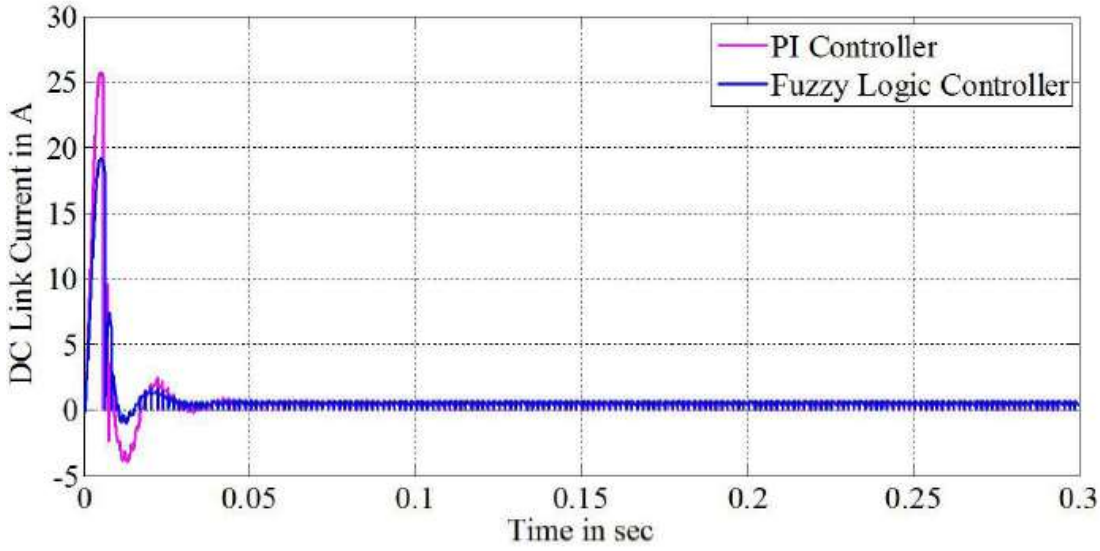

FIGURE 4.63 DC-LINK CURRENT OF THE VSI FOR CASE 4

According to the comparison, the fuzzy control system reacts faster than the PI controller in terms of rising time deviations and settling time difference in both DC-link voltage and motor speed. Figure 4.64 (a) to (d) depict the source voltage, source current, power factor of the input AC source, and current THD of the AC source.

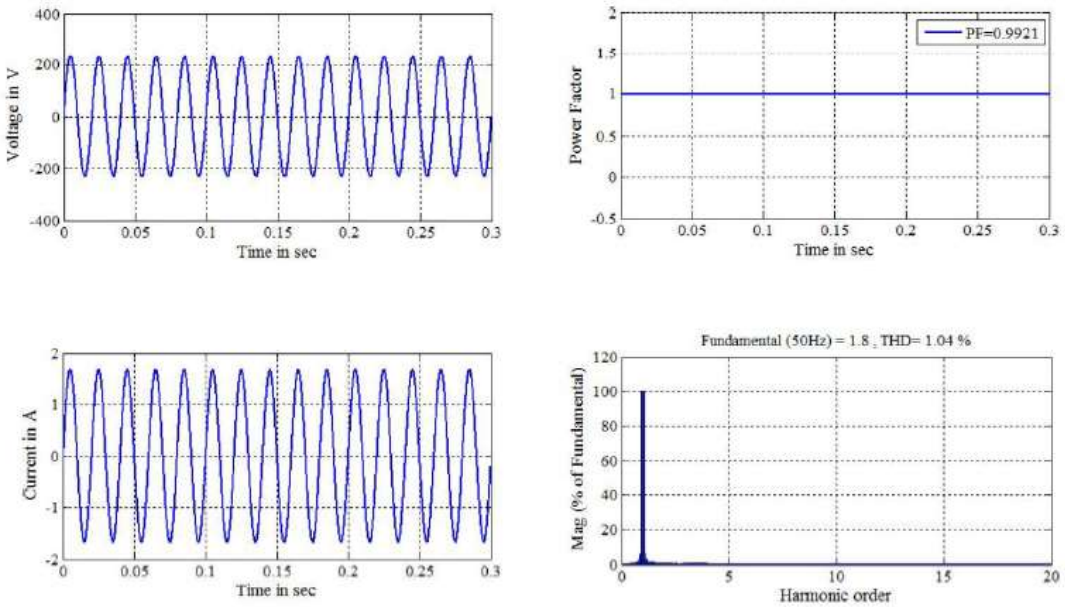

FIGURE 4.64 SOURCE VOLTAGE, CURRENT, POWER FACTOR AND CURRENT THD OF THE AC SOURCE IN CASE 5

4.5.4.5 CASE 5: BLDC MOTOR WITH FUZZY CONTROLLER UNDER DYNAMIC LOAD CONDITIONS

The final study is performed to demonstrate the performance of the BLDC motor with fuzzy control under dynamic load conditions. The motor speed is set to 3000 rpm for this analysis. This section examines the motor's performance under load by altering the DC-link voltage and current of the three-leg VSI.

The suggested PFC SEPIC converter's firing pulse is created by a speed control strategy combined with the proposed fuzzy control approach. This section also compares the performance of the standard PI controller with the suggested fuzzy control method.

As previously stated, the BLDC motor's speed is exactly proportional to the DC-link voltage of the three-leg VSI. Figure 4.65 shows the stator voltage waveforms for the three phases R, Y, and B for simulation times ranging from 0 to 0.3 seconds. The graphic shows that a load of 1.5 Nm was given to the BLDC motor at 0.15 sec. As a result, the magnitude of the stator voltage has been slightly raised in all three phases to allow the motor to run at the intended speed of 3000 rpm.

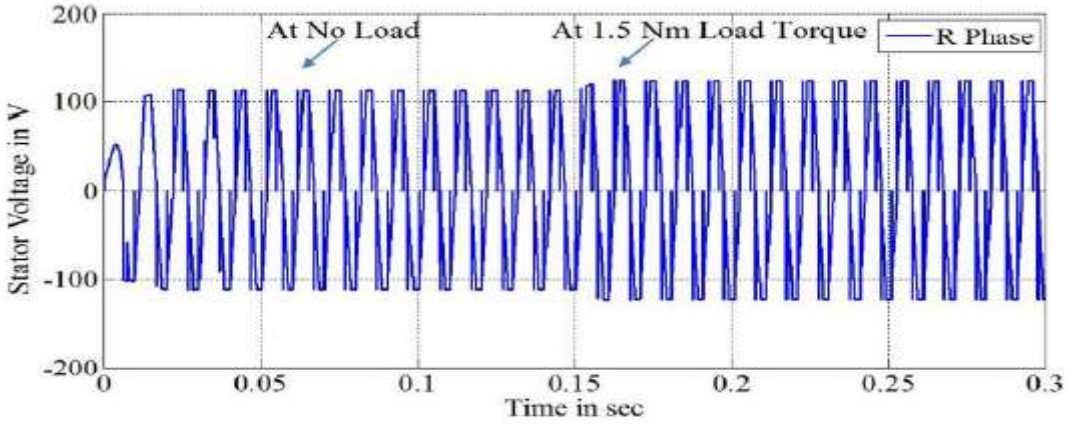

(A) STATOR VOLTAGE FOR R PHASE

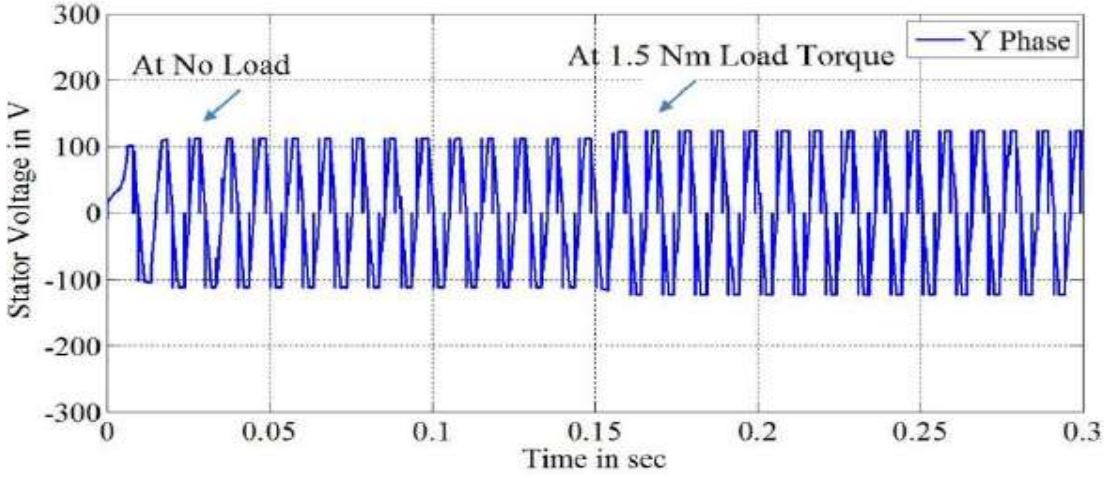

(B) STATOR VOLTAGE FOR Y PHASE

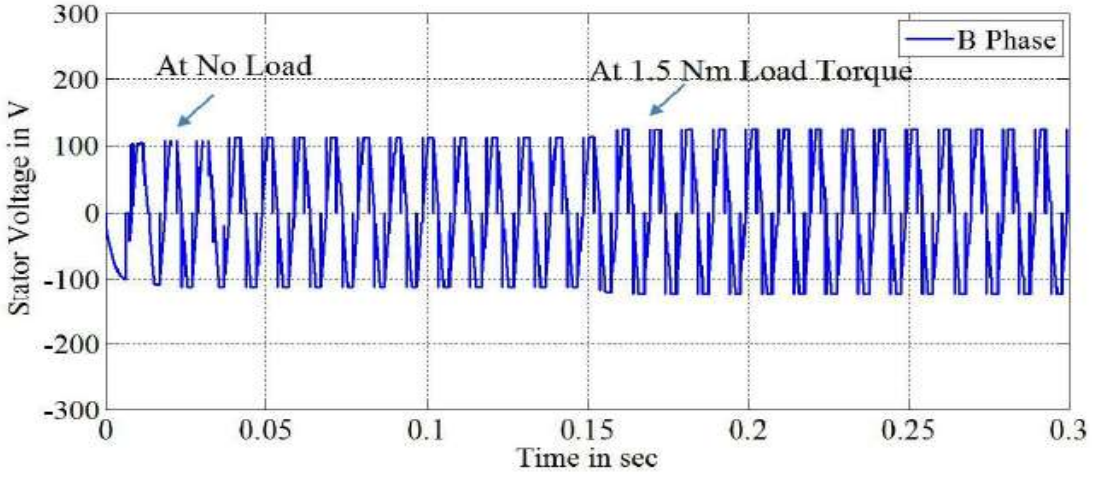

(C) STATOR VOLTAGE FOR B PHASE

FIGURE 4.65 BLDC MOTOR STATOR VOLTAGE FOR ALL THE THREE PHASES FOR CASE 5

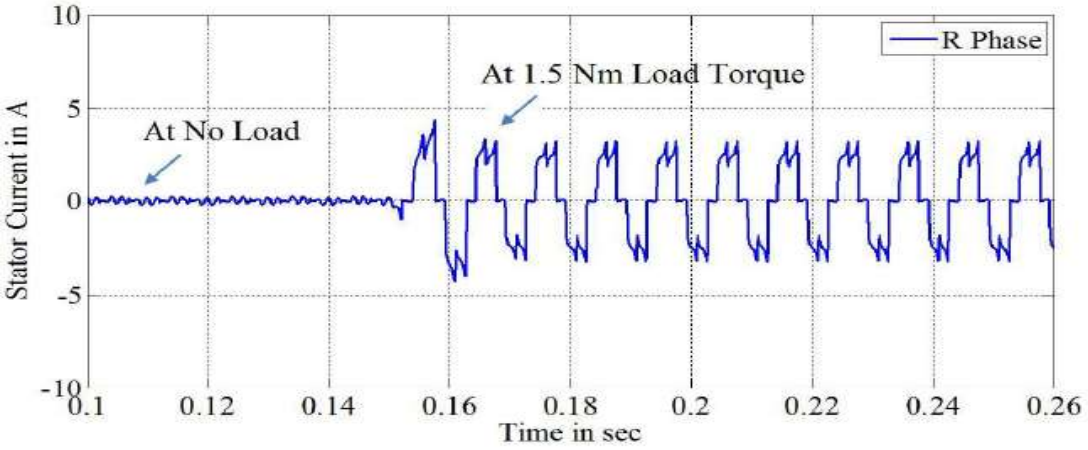

(A) STATOR CURRENT FOR R PHASE

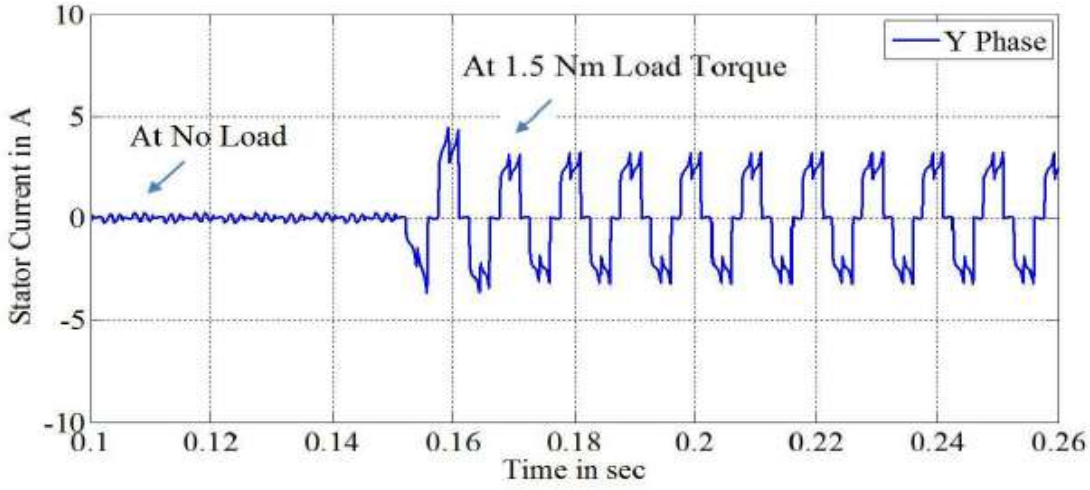

(B) STATOR CURRENT FOR Y PHASE

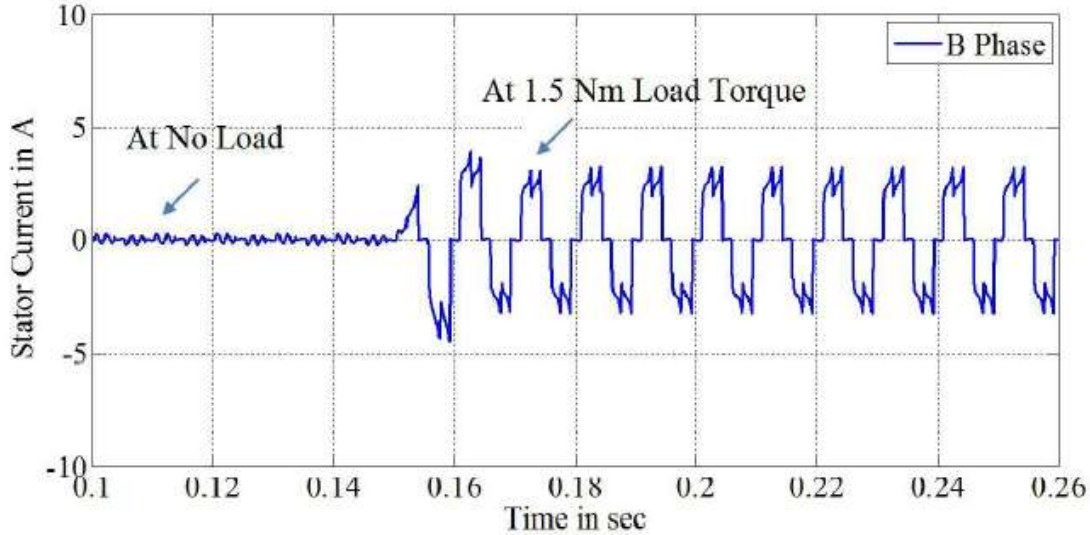

(C) STATOR CURRENT FOR B PHASE

FIGURE 4.66 BLDC MOTOR STATOR CURRENT FOR ALL THE THREE PHASES FOR CASE 5

This is accomplished by adjusting the DC-link voltage of the three-leg VSI. Similarly, the stator current waveforms for the three phases R, Y, and B are presented in Figure 4.66 for simulation times ranging from 0.1 sec to 0.26 sec. According to the current waveforms, the magnitude of stator currents in all three phases rose at 0.15 sec due to a shift in load.

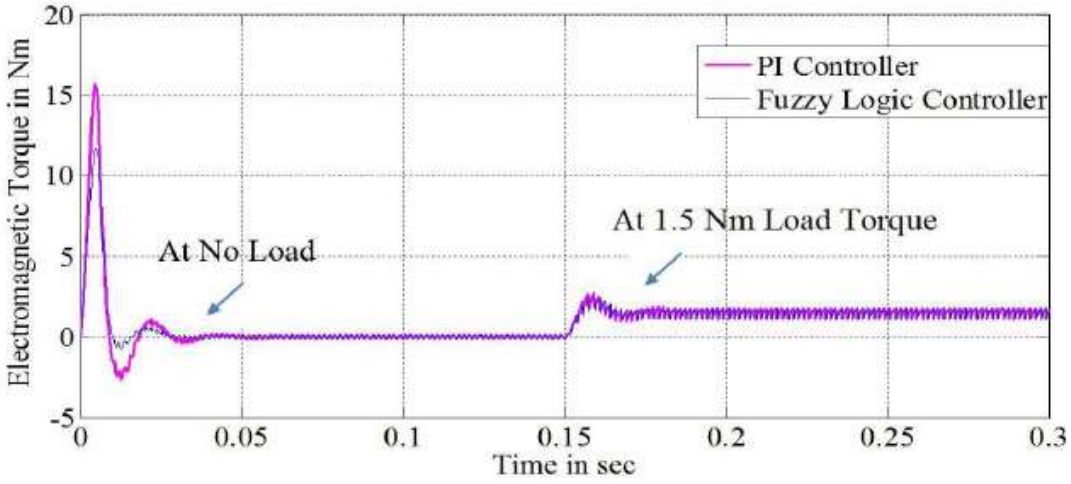

FIGURE 4.67 ELECTROMAGNETIC TORQUE OF THE BLDC MOTOR FOR CASE 5

Figure 4.67 depicts the electromagnetic torque waveform obtained for the BLDC motor using the standard PI controller and the suggested fuzzy controller. Figure 4.67 shows that the rising time in the torque waveform has been greatly decreased in the fuzzy controller when compared to the PI controller. The motor torque rose at 0.15 sec due to external load and remains constant at this level until the simulation duration of 0.3 sec to keep the motor speed at 3000 rpm.

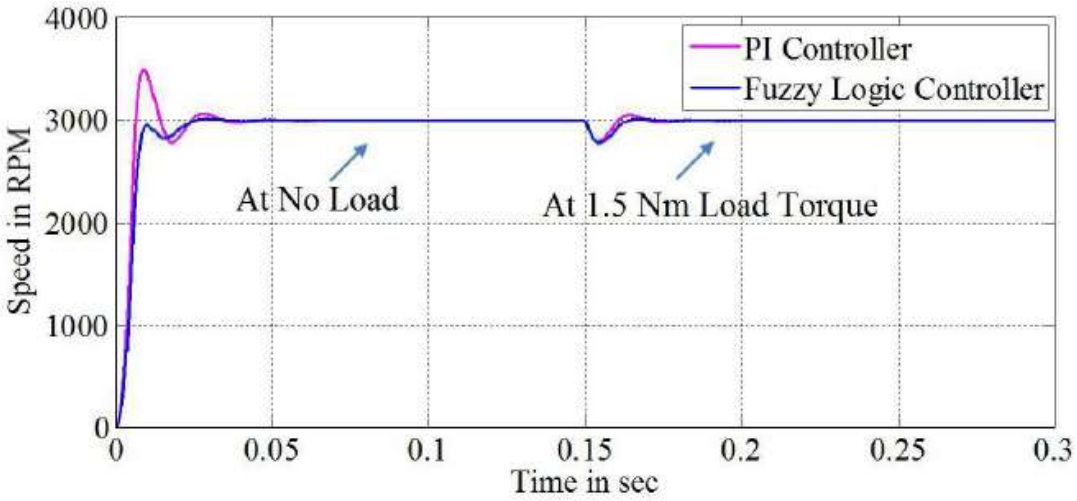

FIGURE 4.68 SPEED OF THE BLDC MOTOR FOR CASE 5

Figure 6.68 depicts the BLDC motor speed curves for traditional PI and the suggested fuzzy based speed control technique. According to Figure 6.68, the traditional controller strategy settles the motor speed at 0.04 sec, but the fuzzy controller approach settles at 0.025 sec. The same graphic also shows that the speed curve becomes unstable around 0.15 sec owing to the external stress. The speed is then stabilised after 0.17 seconds for the standard PI controller and 0.16 seconds for the fuzzy technique. As a result of the above explanation, it is clear that the fuzzy control strategy outperforms the standard PI controller.

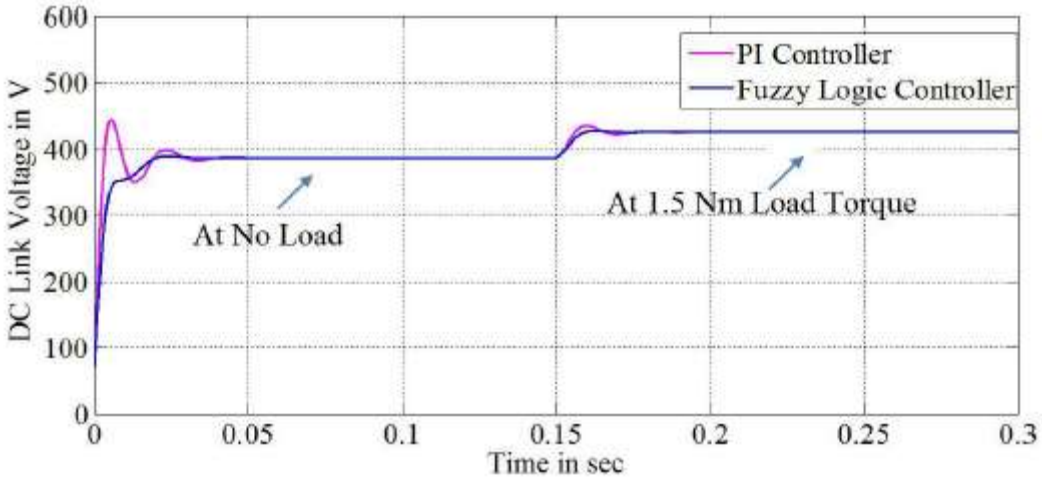

FIGURE 4.69 DC-LINK VOLTAGE OF THE VSI FOR CASE 5

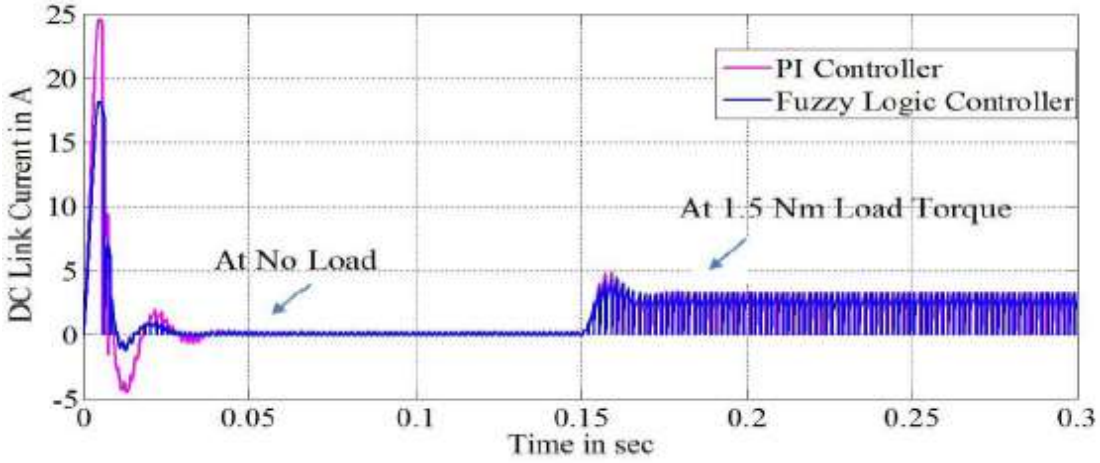

FIGURE 4.70 DC-LINK CURRENT OF THE VSI FOR CASE 5

The DC-link voltage and DC-link current waveforms of the three-leg VSI for the traditional PI controller and suggested fuzzy controller are shown in Figures 6.69 and 6.70 for simulation times ranging from 0 to 0.3 seconds. According to the voltage waveform, the DC-link voltage settles at 0.04 sec for the standard PI controller and at 0.02 sec for the fuzzy control technique. The DC-link voltage was raised at 0.15 sec due to load torque and remained at 425 V throughout the simulation duration of 0.3 sec.

Table 4.2 summarises the various parameter values obtained under various speed and loading situations for performance comparison of the PI controller and FL controller based SEPIC converter supplied BLDC motor. By comparing FLC to PI controller for motor speeds ranging from 1500 to 2000 rpm, the rising time in torque has been greatly decreased. The motor speed is set at 0.05 sec for the standard PI controller and 0.04 sec for the fuzzy controller. Throughout the simulation duration of 0.3sec, the speed remains constant at 2000 rpm after 0.04 sec. The DC-link voltage is established at 0.05 sec for the PI controller and 0.028 sec for the fuzzy controller. To keep the motor running at the correct speed, the DC-link

voltage is kept constant at 271.33 V. When compared to the PI controller, the FLC controller offers a faster rise time in current.

TABLE 4.2 COMPARISON BETWEEN PI CONTROLLER AND FL CONTROLLER BASED SEPIC CONVERTER FED BLDC MOTOR

PI CONTROLLER										
Speed (rpm)			Stator Voltage (V)			Stator current (A)			T H D %	
1500									2.83	
2000									2.52	
2									2	

500									.32	
3000									2.18	
FUZZY LOGIC CONTROLLER										
Speed (rpm)			Stator Voltage (V)			Stator current (A)			THD %	
1500									1.76	
200									1.4	

0								1	
2 5 0 0								1 . 1 6	
3 0 0 0								1 . 0 4	

SETTLING TIME OF SPEED IN SEC

Speed (rpm)	PI controller	Fuzzy Controller
1 5 0 0	0 . 0 7	0 . 0 3
2 0 0 0	0 . 0 5	0 . 0 2 8

The analysis is also carried out by raising the motor speed from 2000 to 2500 revolutions per minute. The torque increase time in FLC is significantly shorter than in PI controller, and the speed is established at 0.040 sec for PI and 0.025 sec for fuzzy controller. The DC-link voltage

settles at 0.04 sec for the PI controller and 0.025 sec for the fuzzy controller, with the DC-link voltage remaining constant at 332.89 V. Similarly, the rising time in current has been greatly reduced in fuzzy control when compared to PI controller. The fuzzy-based speed control responds instantaneously in terms of rising time and settling time in both DC-link voltage and motor speed.

The suggested method is also tested with the motor speed set to 3000 rpm. When comparing the fuzzy controller to the PI controller, the torque increase time has been lowered, and the motor speed for the PI controller is set at 0.035 sec, whilst the fuzzy controller is set at 0.025 sec. Throughout the 0.3-second scenario, the speed remains constant at 3000 rpm. The DC-link voltage is established at 0.035 sec for the PI controller and 0.025 sec for the fuzzy controller, with a constant DC-link voltage of 392.38 V. Similarly, the current rise time in the fuzzy control system has been lowered when compared to the PI controller. The table shows that the Fuzzy Logic Controller (FLC) based SEPIC converter fed BLDC motor drive outperforms the PI Controller based BLDC drive in terms of THD, power factor, speed increase and settling time, and DC link voltage.

FIGURE 4.71 HARDWARE PROTOTYPE

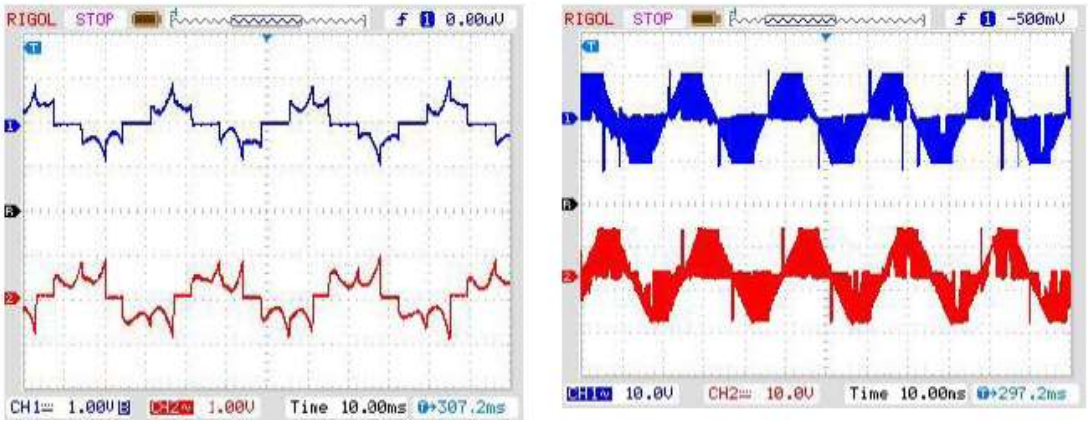

FIGURE 4.72 (A) & (B) CURRENT AND VOLTAGE OF THE BLDC MOTOR

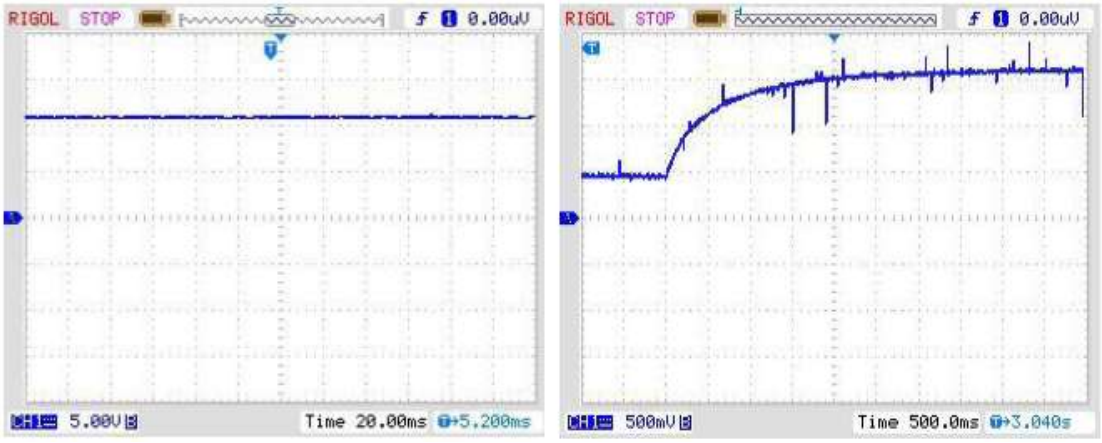

FIGURE 4.73 (A) & (B) DC LINK VOLTAGE AND TRANSIENT VOLTAGE WAVEFORM

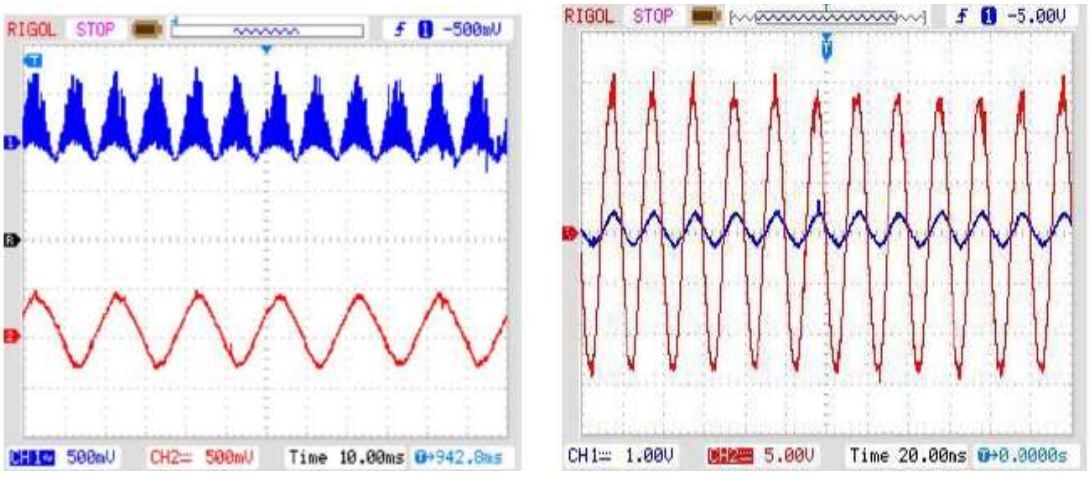

FIGURE 4.74 A) SOURCE CURRENT INDUCTOR CURRENT B) SOURCE VOLTAGE AND CURRENT

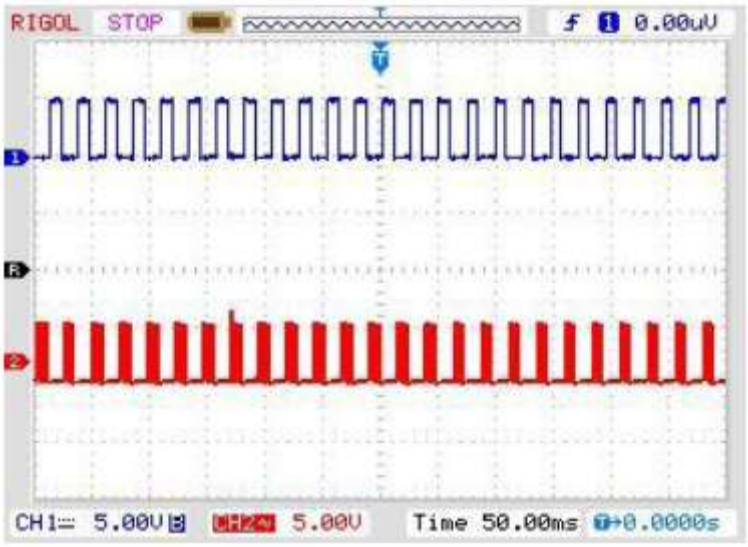

FIGURE 4.75 PWM PULSES

Figure 4.71 depicts the experimental prototype of the suggested BLDC drive using the Microcontroller AT89C2051. The PIC microcontroller controls the BLDC drive as well as the SEPIC converter. Figure.4.72 depicts the BLDC motor stator voltage and current. Figure 4.73 depicts the DC link voltage and its transient. Figure 4.74 (a) depicts the inductor current and source voltage (b). The PWM pulse is seen in Fig. 4.75.

CHAPTER 5
CONCLUSION

5.1 CONCLUSION

In this thesis, the induction motor and BLDC motor drives were examined using different converters such as boost converters, buck boost converters, cuk converters, and SEPIC converters, which were simulated and implemented in hardware prototypes.

Matlab/simulink was used to model the boost converter with compound active clamping and FSTPI fed induction motor driving. To reduce the resonance in winding inductance and junction capacitance, the boost converter with compound active clamping supplied IM drive requires an extra diode and inductor. The planned converter was executed with an FSTPI fed induction motor, and results were obtained.

The simulation of a PFC buck-boost converter-based PMBLDC motor drive is compared to the experimental findings. Using a PI controller, the driving signals for the inverter switches are obtained from the feedback signals from the PMBLDC motor, which indicate the speed and position. The hardware was made and tested. The use of the buck-boost converter has raised the power factor, resulting in increased efficiency. In Chapter 5, a Cuk PFC fed PMBLDC drive was simulated using Matlab Simulink. Feedback signals indicating speed and position from the PMBLDC motor were used to generate driving signals for the inverter switches through a PI controller. The power factor has been observed to improve with the usage of the Cuk converter. The increase in the power factor has boosted efficiency. The Cuk converter's PFC function provided a power factor close to unity. Because of the enhanced power factor, the

Cuk Converter fed PMBLDC motor is recommended over the other methods.

The performance of the suggested PFC SEPIC converter design with BLDC motor is clearly analysed using a fuzzy logic controlling approach. The significance of combining a fuzzy logic controller with the proposed PFC SEPIC converter architecture is explored in detail. The suggested fuzzy controller's performance is confirmed by lowering the peak overshoot and settling time difference in both DC-link voltage and motor speed. As compared to the PI controller, the simulation results show that the fuzzy logic controller offers a greater reduction in settling time and speed error.

By analysing the various converter-fed drives, it is possible to infer that the BLDC drive fed by SEPIC converter controlled by fuzzy based control has a low power factor and THD, reducing losses. As a result, the SEPIC fed BLDC drive is more efficient than the other drives presented in this thesis.

5.2 SCOPE FOR FUTURE WORK

1. The current study work's performance might be improved further by using alternative intelligent controllers, such as neuro-fuzzy controllers.
2. AI methods like as GA, PSO, and others can be used to optimise the PI gain settings.
3. Another potential improvement of this study is to integrate the battery with the converter design and store the power during the motor's regenerative cycle.

4. Using a bridgeless PFC SEPIC converter fed drive, a steady state study with diverse loads and components may be performed.